NTNU

Norwegian University of
Science and Technology

Thermomechanical processing of an AA6082 - IF steel cold roll bonded composite material

Harald Solhaug

Materials Science and Engineering
Submission date: June 2017
Supervisor: Ida Westermann, IMA
Co-supervisor: Bjørn Holmedal, IMT
Siri Marthe Arbo, IMT

Norwegian University of Science and Technology
Department of Materials Science and Engineering

Preface

This master's thesis was submitted in partial fulfillment of the degree of Master of Science. The thesis was produced at the department of Materials Science and Engineering, at the Norwegian University of Science and Technology (NTNU), during the spring of 2017.

The work reported in this thesis was based on activities within Centres for Research-based Innovation, SFI Manufacturing in Norway, and is partially funded by the Research Council of Norway under contract number 237900.

Trondheim, June 2017

Harald Solhaug

Abstract

The work carried out in this thesis was conducted to investigate thermomechanical aspects of a steel-aluminum cold roll bonded material. The objective was to study different production parameters related to ageing of an AA6082 aluminum alloy, combined with IF steel, through a cold roll bonding process. Three different sequences of solutionizing, ageing, and cold roll bonding of the materials were tested.

Sheets of steel and aluminum, measuring 30 x 120 mm, were used to produce the samples. Each sheet measured roughly 1 mm in thickness, and were stacked together to form a three layered composite, with aluminum in the middle and steel on either side. The sheets were prepared by scratch brushing, and were roll bonded at pre-heat temperatures of 150, 200, & 300 ^{o}C. Three different sequences were used for heat treating the aluminum; The BSA samples were roll bonded, followed by solutionizing and ageing to T6. The SBA samples were solutionized, roll bonded, and then aged to T6. The SAB samples were solutionized and aged to T6, followed by roll bonding. The three sequences were meant to determine the optimal way of producing a precipitation hardened structure in the aluminum, while still achieving a good bond to the steel.

The cold roll bonded samples were cut into sections and studied through several microstructural and mechanical characterization methods. Optical and scanning electron microscopes were used to study the aluminum grain structure, and the roll bonded interface. A peel testing rig was designed and built to allow for peel testing of the composites with at 90 degree peeling direction. Energy-dispersive X-ray spectroscopy was used to study the resulting fracture surfaces, to determine the amount of residual material left on each surface.

In summary, the SAB samples were found to produce the greatest bond strengths, followed by the SBA samples, and the BSA samples. The achieved bond strength values were overall fairly low compared to what others have achieved. The solutionizing step caused the aluminum in all samples to recrystallize, and the BSA samples, which were solutionized after roll bonding, developed an intermetallic layer roughly 1 μm thick. This layer was found to severely impact the bond strength of the composite. No intermetallic layers were found for the two other sample sequences. Roll bonding after solutionizing was not found to have any negative effects on the ageing potential. The bonding mechanism was found to be consistent with the film theory.

Sammendrag

Arbeidet utført i denne oppgaven ble gjort for å undersøke termomekaniske aspekter ved et stål-aluminium kaldsveiset materiale. Oppgaven gikk ut på å studere ulike produksjonsparametere for herding av en AA6082 aluminiumslegering, kombinert med IF-stål ved kaldsveising. Tre ulike sekvenser for innherding, utherding, og kaldvalsing, ble undersøkt.

Plater av stål og aluminium, på 30 x 120 mm, ble brukt til å produsere prøvene. Hver plate var ca. 1 mm tykke, og ble stablet til en trelags kompositt, med aluminium i midten og stål på hver side. Platene ble preparert med stålbørsting, og ble kaldvalset etter å ha blitt forhåndsvarmet til 150, 200 & 300 ^{o}C. Tre forskjellige sekvenser av herding ble brukt; BSA-prøvene ble kaldvalset, etterfulgt av innherding og utherding til T6. SBA-prøvene ble innherding, kaldvalset, og så utherdet til T6. SAB-prøvene ble innherdet, utherdet til T6, og så kaldvalset. De tre sekvensene ble undersøkt for å finne den optimale måten å produsere kompositttmaterialet med aluminium i T6, samtidig som båndet mellom stål og aluminium ble best mulig.

De kaldvalsede prøvene ble kappet i biter og studert ved flere forskjellige analytiske metoder for å studere mikrostruktur og mekaniske egenskaper. Optisk og elektronmikroskop ble brukt til å studere mikrostrukturen i aluminiumet, i tillegg til båndet mellom stål og aluminium. En peeltestrigg ble designet og bygget for å teste båndstyrken med en 90 graders peelretning. Kvantitativ røntgenmikroanalyse ble brukt til å studere bruddflatene, for å undersøke hva slags materiale som ble sittende fast på hver bruddflate.

Det ble konkludert med at SAB-prøvene oppnådde den beste båndstyrken, etterfulgt av SBA og BSA -prøvene. Båndstyrkene som ble oppnådd var likevel forholdsvis lave, sammenlignet med andre studier. Innherdingsprosedyren førte til at aluminiumet i alle prøvene ble rekrystallisert, og BSA-prøvene, som ble innherdet etter valsing, fikk et intermetallisk lag, ca. 1 μm tykt, i overgangen mellom stål og aluminium. Dette laget hadde sterkt negativ innvirkning på båndstyrken til BSA-prøvene. Ingen intermetalliske faser ble funnet på de to andre prøvesekvensene. Ingen negative effekter for utherdingspotensialet ble funnet ved valsing etter innherding. Mekanismen bak kaldsveisingen stemte overens med filmteorien.

Contents

1 Introduction

Hybrid materials have received an increasing amount of attention in recent years, as they offer interesting properties and characteristics that are hard to match by traditional materials. Combinations of different metals in layered composites are of particular interest, as the resulting materials can be designed with unique engineering properties [1].

Cold roll bonding (CRB) is a way of producing metal composites, that has experienced rapid development in recent years. It offers several advantages over other, similar techniques, as it is performed at relatively low temperatures. The potential for undesirable phases or microstructures to form is thus reduced, as well as issues related to differences in thermal expansion. Furthermore, CRB tends to yield high quality surfaces, and it is a relatively inexpensive and fast production method. Products commonly produced by cold roll bonding includes cooking utensils, heat exchangers, electrical components, electrodes, and automotive trims and exhaust systems [2].

Steel-aluminum materials are of particular interest as these are the two most common engineering metals. They both have desirable and undesirable properties, few of which are overlapping. By combining them, the best attributes from each metal can be extracted to produce a material with several great qualities. For instance, the low cost, and the high strength and stiffness of steel, can be combined with the corrosion resistance and low weight of aluminum. This of interest to many industries, particularly the automotive and transportation industries, where low weight and high strength are desirable traits.

The AA6082 alloy has been extensively used in the automotive industry, due to its high strength, good formability, and corrosion resistance. AA6082 is a precipitation hardenable alloy, and proper heat treatment parameters have to be applied if these properties are to be achieved. When combined with steel through a cold roll bonding process, these same heat treatment procedures pose many challenges. Both the roll bonding procedure itself, and the resulting bond interface, are strongly affected by temperatures and mechanical properties of the metals. When producing the composite, there are several different orders in which the roll bonding and heat treatment of the aluminum can be conducted. Finding the best sequence of production steps is thus vital to produce a material with the best properties possible. Three different sequences were tested to determine the optimal way of producing a precipitation hardened structure in the aluminum, while still achieving a good bond to the steel.

This thesis will first provide a theoretical background to hybrid materials, cold roll bonding, and aluminum alloys. Next, the experimental work conducted is described. This work revolved around the thermomechanical production, and characterization, of different cold roll bonding procedures. IF steel and AA6082 aluminum were combined to a three layered composite material, and different parameters of heat

treatment were conducted before and after the cold rolling procedure, to age the aluminum to T6 condition. Three different production sequences were tested, each of which produced with several different pre-heat temperatures. The resulting microstructure and bond interfaces were studied by microscope, and the mechanical properties, in terms of hardness and bond strength, were investigated.

2 Theoretical background

2.1 Hybrid materials

Hybrid materials combine the properties of two or more materials into one. These combinations generally receive attributes from each individual material, some of which are beneficial, and some of which may be detrimental. Improvements in the form of strength, toughness, weight, and corrosion resistance are commonly found, but often at a higher cost than for traditional materials. An overview of some of these materials are provided in Figure 1.

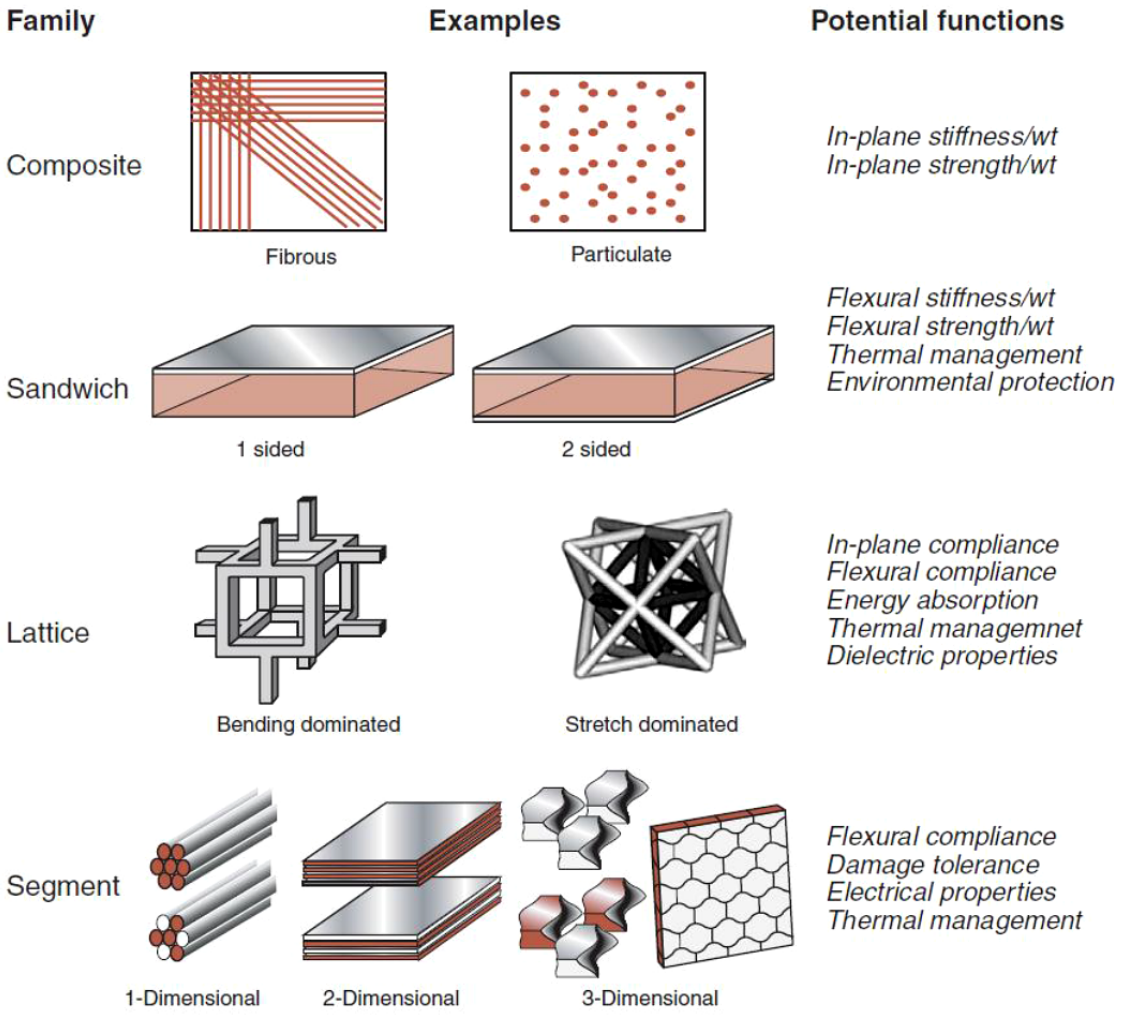

Figure 1: Types of hybrid materials and their functions [1].

Hybrid materials can generally be divided into four main categories, composites, sandwiches, cellular structures, and segmented structures. Composites consist of a matrix and a particle or fiber reinforcement phase. These materials behave as one homogeneous material on a large scale relative to its components. Sandwiches commonly utilize a lightweight core, supporting a stiff outer skin. Cellular structures, or lattice structures, combine materials and internal space, such as in honeycomb

structures. Segmented structures have material properties that are divided into one, two, or three dimensions, such as layered composites [1]. In addition to these four main categories, many variations can be obtained by combining materials in new ways through advanced processing techniques. The material demands in engineering can usually be met by traditional materials, but when engineering requirements are especially demanding, hybrid materials are often the best solution.

2.1.1 Laminated metal composites

Laminated metal composites (LMCs), consist of alternating layers of metals, that are bonded together with discrete interfaces. These materials should be distinguished from other composites, such as graded materials which have diffuse interfaces, and layered composites in general. Layered composites can consist of several different materials, such as metal/metal, metal/ceramics, ceramics/ceramics, or intermetallic/ceramic combinations.

Laminated metal composites offer many improved properties over traditional metals, including fracture toughness, fatigue properties, impact behavior, wear, corrosion, and damping capacity. They also allow for improved formability and ductility properties of otherwise brittle materials. One of the main features is the ability to create LMCs with accurately prescribed properties, combining different metals to meet an exact engineering requirement [3].

There are three main ways in which the LMCs may be produced; bonding, deposition, and spray forming. These main categories cover several different techniques and variations available. Bonding techniques involve sheets of metal that are solid state bonded, usually by applying pressure and heat. Deposition techniques utilize atomic or molecular level transportation of material to a substrate surface. Spray forming techniques directly deposit molten material on the component surface to form the laminate [3].

2.1.2 Steel-aluminum hybrid materials

One problem when combining different metals is the formation of intermetallic phases. Reducing the formation of these phases is an important aspect in improving strength in the interface between steel and aluminum, such as in welds, diffusion bonds and hot dip coatings. These phases may occur both when the metals are in their molten and their solid states, but formation generally increase with higher temperatures. During the roll bonding process, significant strain and shearing is introduced in the metals, resulting in high temperatures due to friction [4]. When combined with the already elevated temperatures of warm roll bonding, intermetallic phases may form. When heat treatments such as solutionizing of aluminum is done after roll bonding, the potential for intermetallic phases to form are even greater, due to the high temperatures applied.

For steel and aluminum, several intermetallic phases of the type Fe_xAl_y can form, five of which are indicated in Figure 2. These phases have complex atomic arrangements which hinders dislocation movement. Reduced dislocation movement results in both increased hardness and significant brittleness in intermetallic phases [5].

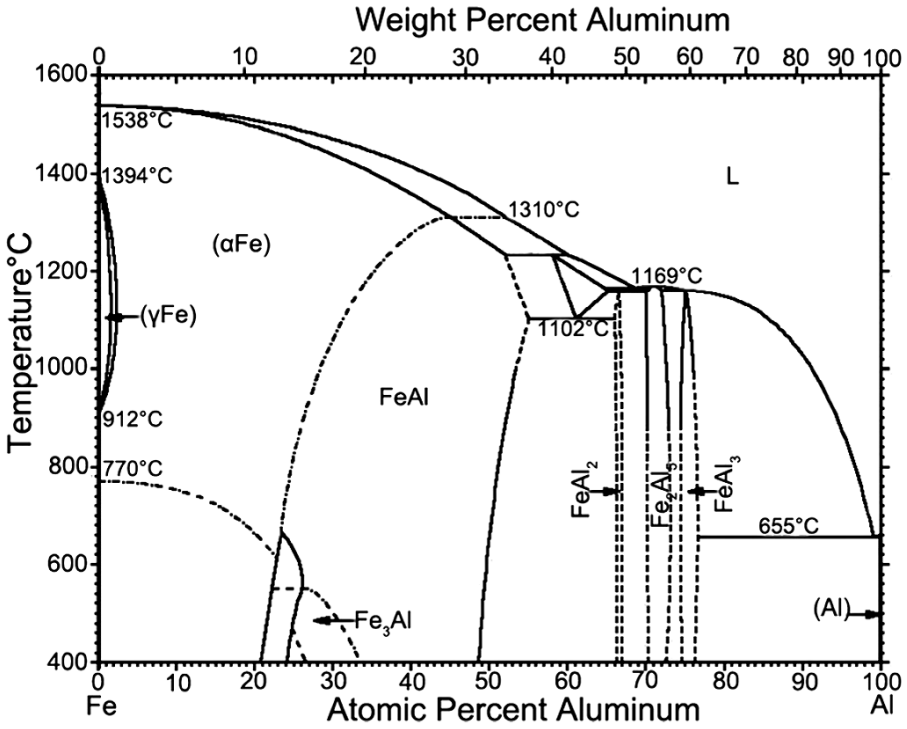

Figure 2: A phase diagram showing the iron-aluminum system, including common intermetallic phases [6].

$FeAl_3$ and Fe_2Al_5 are the most common intermetallic phases forming through diffusion at temperatures below the melting point of aluminum. The diffusion of iron atoms into aluminum is what causes the initial formation of $FeAl_3$, and Fe_2Al_5 will form in the interface between $FeAl_3$ and the steel. Steel has a higher diffusion rate in aluminum than that of aluminum in steel, though the former has a smaller possible temperature range. This cause the tendency of steel to diffuse into aluminum, and not the other way around [4].

Intermetallic phases are expected to occur as a thin layer in the interface between the two metals. The thickness of this layer has proven to have great influence on the mechanical properties of the bond. For the bond to be sufficiently strong, it should surpass the strength of the weaker metal, aluminum. An intermetallic layer of up to 10 micron has shown to still produce a sufficiently strong bond. Layers with a thickness of up to 25 micron were studied, and a significant reduction in bond strength was found with increasing thickness [5].

2.2 Cold roll bonding

Cold roll bonding (CRB), is a process in which two or more layers of metals are stacked together and fed through a roller at relatively low temperatures, as seen in Figure 3. The rolling process needs to apply sufficient pressure for cold bonding to take place between the sheets. Substantial plastic deformation is usually required for bonding, with thickness reductions commonly exceeding 50 percent. One of the main advantages with this process is the ability to join together metals with different properties, creating hybrid materials. Additionally, metals that are hard to join by traditional methods often respond well to cold roll bonding [2].

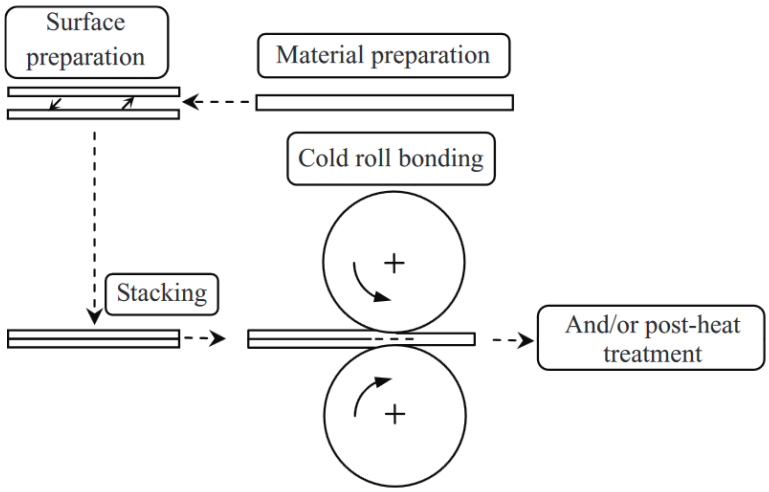

Figure 3: Schematic illustration of the cold roll bonding process [2].

The basic principle of cold roll bonding, is to plastically deform the metal surfaces sufficiently to crack the surface oxide layers. This allows virgin material to be extruded through the cracks by the pressure of the rolling mill. Contact between opposing virgin material is the mechanism that allows for cold bonding to take place, as interatomic forces in the interface is what causes the actual bond to form [7]. Several theories have been suggested to explain the cold bonding mechanism, the most prominent being the film theory, energy barrier theory, diffusion bonding theory and recrystallization theory. The film theory has generally been considered the most important among these. [2, 8] This theory proposes that a bond will spontaneously form if two clean metal surfaces are brought into intimate contact. The apparent resistance of metals to form the bond, is attributed to the relative hardness of the bulk metal and its oxide film. The degree of fragmentation of the oxide film controls the initiation of bonding [9]

A large span of different metals can be cold roll bonded together, and thereby numerous techniques and variations to the CRB process have been developed. One of the fundamental parameters in CRB is the degree of deformation, as seen in Equation 1. This is normally expressed as the degree of surface expansion, X, or surface exposure, Y, where A_0 is the initial and A_1 is the final interface area [7].

$$\mathbf{X} = \frac{\mathbf{A_1} - \mathbf{A_0}}{\mathbf{A_0}} \qquad \mathbf{Y} = \frac{\mathbf{A_1} - \mathbf{A_0}}{\mathbf{A_1}} \tag{1}$$

Bonding can not occur until a threshold surface exposure is reached, after which the bond strength increases rapidly. The thickness reduction will reach a level corresponding to the strength of the weaker metal. The threshold surface exposure for a certain combination of metals, is dependent upon the applied forming process and its parameters [7]. The threshold reduction, Rt, expresses the minimum percentage deformation required to consistently form a bond. [2]

2.2.1 Applicable metals

Most common engineering metals can be cold roll bonded to some degree. Figure 4 shows a map of various metals and their ability to successfully bond with other metals. These are divided into groups based on crystal structure and hardness of the metals at room temperature, with the hardest metals being found to the left or the bottom of each category. The map shows that FCC metals are generally the best suited for CRB processing, likely due to the low degree of work hardening they experience during reduction [2].

HCP metals have far inferior bonding qualities, though they can form many successful bonds with FCC metals. Hexagonal structures require both higher deformations and produce lower bond strengths than cubic lattice structures [10]. One suggested reason for this is that oxide layers on two opposing hexagonal surfaces form less coherent fractures than those formed on cubic metals. Thus more of the interface is covered by oxides, smaller areas of virgin material surfaces get in contact, and the bond strength is reduced [2].

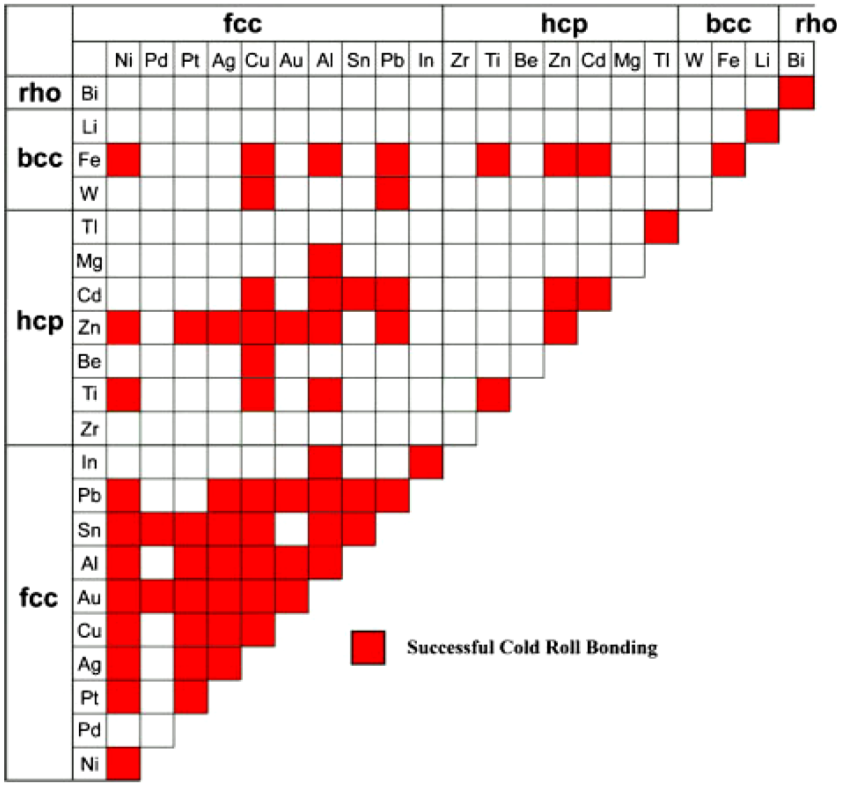

Figure 4: Various metals, ordered by structure and hardness, and their ability to form successful cold bonds. As seen, steel and aluminum are able to bond by CRB [10].

2.2.2 Surface preparation

Surface preparation prior to cold rolling has a significant effect on both bond strength of the final laminate, and on required deformation for bonding to take place. It is essential to remove surface oxide layers and contaminants to achieve a strong bond. Degreasing the oxide layers, followed by scratching and deforming the surface, has proven to be an effective way of preparation to achieve a good bond. Furthermore, the order in which the degreasing and deformation steps are taken, are of great importance. Degreasing prior to wire brushing, was found to produced significantly better results than when the procedure was reversed [2].

These steps are done not only to clean the surface, but to create a rougher and more deformed interface. The surface will experience work hardening and localized shear deformation, which promotes brittleness and fracture at the interface during the CRB process. If the surfaces are not sufficiently deformed prior to CRB, they will resist bonding, as was clearly shown when electropolishing was tested for use in CRB. These highly polished surfaces were unable to bond even at 80 percent deformation [2]. Figure 5 shows the required deformation and resulting bond strength of various preparation techniques. It is clear that properly work hardening the surfaces is a vital step to produce a strong bond, however, the finer abrasive techniques produce the best results.

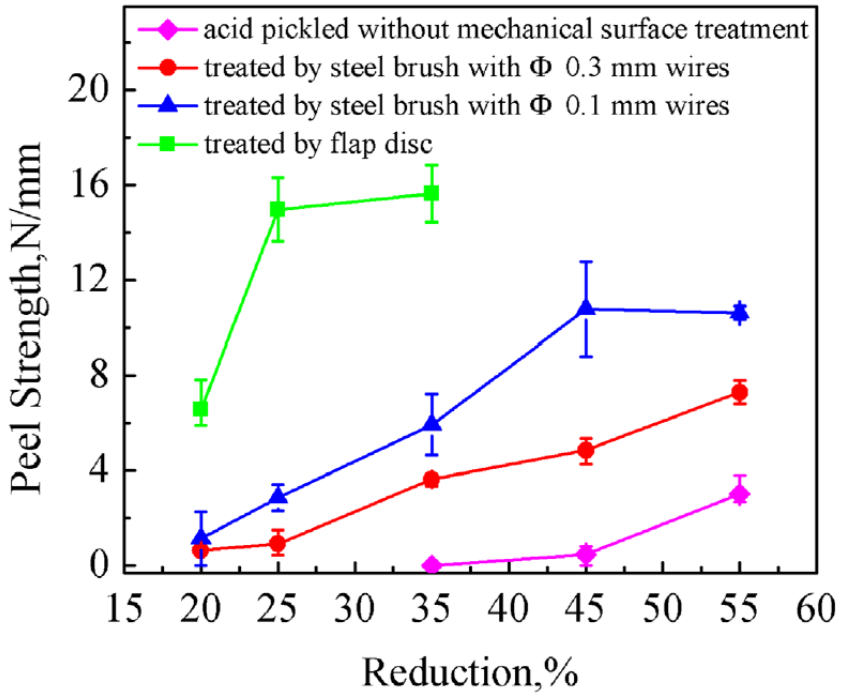

Figure 5: Effects of various surface preparation techniques on a steel-aluminum CRB material. Though work hardening is required for a strong bond, the finer abrasive techniques produce the best results [11].

Though wire brushing has traditionally been the most common way of preparing surfaces for CRB, it does have certain disadvantages, such as causing variable bond strength with a relatively large scatter [7]. It has been shown that finer abrasive techniques, such as reduced wire brush diameters, and treatment by flap disc, improve the bond strength. This is likely due to a reduction in thickness of the work hardened surface, improving its adhesion to the base material. The finer abrasive techniques also produce a smaller difference in hardness between the surface and the bulk material [11, 12]. Furthermore, it has been shown that the amount of time that is allowed to pass between wire brushing and cold roll bonding, has a significant influence on the final bond strength. Oxide layers quickly form on fresh metal surfaces, and one should strive to minimize the time between surface preparation and CRB to achieve an optimal bond strength [2, 8, 12].

2.2.3 Warm rolling

Bond strengths can be improved by heating the samples prior to roll bonding. The effect of pre heating at 200 °C - 400 °C, known as warm rolling, has been studied for steel and Aluminum [13]. Samples of stw22 steel and Al1350 aluminum were pre heated, rolled with 5 - 60 % thickness reduction, and air cooled. A peel test was performed with a 180 degree peeling direction on the aluminum layer. As well

as showing that increased thickness reduction improved the bond strength, the test also showed that the threshold reduction for bonding was reduced with higher rolling temperatures. Additionally, high bond strengths were achieved at lower levels of deformation, as seen in Figure 6. For all cases, the maximum bond strength would surpass the tensile strength of aluminum, causing the aluminum layer to tear during the peel test [13].

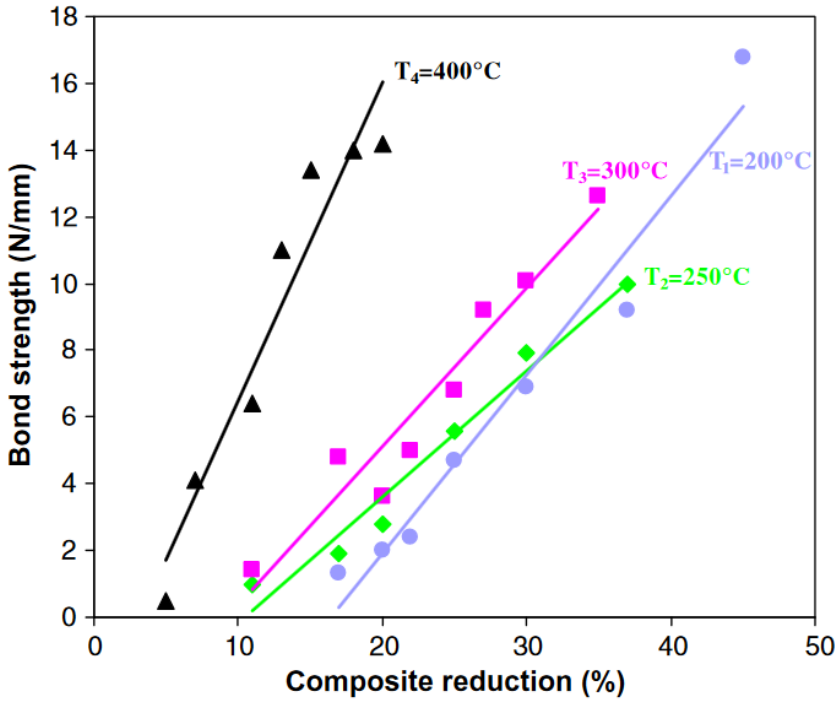

Figure 6: Warm rolling of stw22 steel and Al1350 aluminum, performed at 200 ^{o}C - 400 ^{o}C. A clear correlation is seen between increased rolling temperatures and improvements in the bond strength [13].

2.2.4 Heat treatment

CRB followed by heat treatment has been carried out for several materials in the temperature range of 50^{o}C - 900^{o}C [2]. Short term heat treatment at low temperatures, before the onset of recovery or recrystallization, has shown to improve bond strength for all cases. It has been suggested that post rolling heat treatment improves bond strength through three main mechanisms. Firstly, the heat treatment reduces hardness, thereby increasing toughness in the CRB interface. This inhibits crack propagation in the interface, thus increasing bond strength. Secondly, the elevated temperatures may allow for some diffusion and short range atomic movement to occur. Thirdly, residual stresses that are present in or near the bond, may be reduced [10].

Regions that are only partially bonded after the CRB process, may achieve complete bonding by the heat treatment. However, elevated temperatures also pose the risk of intermetallic and other brittle phases forming at the interface. Furthermore, heat

treatment at sufficiently high temperatures may result in complete failure of the bond. These properties are greatly dependent on the specific metals in question, suggesting that heat treatment parameters have to be developed for each individual metal combination, in order to achieve an optimal bond [2, 10].

It has been suggested that annealing prior to the CRB process, has an inherently greater affect on bond strength than heat treatment after CRB. Reducing hardness and increasing ductility before the CRB process, likely has the greatest influence on bond strength, regardless of how these properties are achieved [10].

2.2.5 Thermal stresses

When combining two materials at elevated temperatures, the differences in linear thermal expansion may cause issues. The thermal expansion coefficient, expressed in m/m·K, describes how much a material will expand or contract given a change in temperature. The specific values for steel and aluminum, are approximately $12.0 \cdot 10^6$ m/m·K and $23.6 \cdot 10^6$ m/m·K, respectively [14].

This large discrepancy causes significant thermal stresses in Al/steel CRB materials during changes in temperature. During cooling, the aluminum will want to contract much further than the steel, resulting in tensile forces in the aluminum and compressive forces in the steel. If the bond is too weak, these stresses could potentially cause the bond to fail by delamination. The CRB material may also have a reduced tensile strength, as the aluminum could already be close to its yield strength before stresses are applied.

2.2.6 Testing of bond strength

There are several test configurations for determining the quality of a CRB component. The bond strength may be determined by applying peeling or shearing forces, as well as qualitative evaluation by bending, torsion, fatigue, and impact testing [2]. The most widely used test for determining bond strength is the tensile shear test, as shown in Figure 7a. In this test, grooves are cut into each layer of the composite, so that the bonding interface itself will take the full tensile force. This is considered to be a very relevant test, as it determines the materials potential usefulness for subsequent forming processes such as deep drawing and stretch forming [2]. Another common test is the T-peel test, as defined by ASTM-D1876-01 [15]. Here the sample is placed in a tensile testing rig, and a force is applied to one of the sheets, as shown in Figure 7b. The average peel strength can be determined, as seen in Equation 2, by dividing the average load in Newton, by the bond width in millimeters [15].

$$Peel\ strength\ [N/mm] = \frac{Average\ peel\ force\ [N]}{Sample\ width\ [mm]} \tag{2}$$

An electrical resistivity test has recently been suggested for testing bonds of Cu/Al and Al/Steel. The difference between experimental and theoretical resistivity may be considered as the resistivity of the bond itself. This value should approach zero for an ideal bond, and the quality of the bond can thereby be evaluated [2].

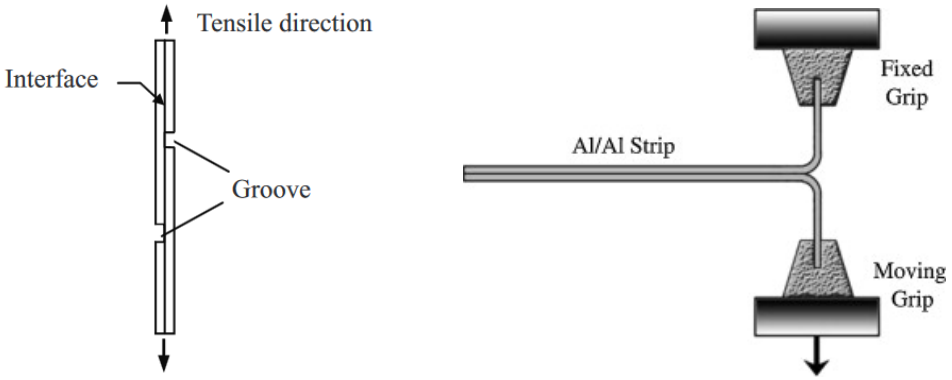

(a) Tensile shear testing [2]. (b) T-peel test [10].

Figure 7: Schematic illustration of two of the most common tests for determining bond strength in CRB materials.

2.3 Aluminum alloys

2.3.1 Precipitation hardening

Increasing the strength of a metal can be achieved through several different mechanisms. Adding solid solution alloying elements, as well as grain-refining elements, are some of the most common ways to improve mechanical properties. Precipitation hardening through a heat treatment process can also be used in some alloying systems. The requirement for such a system is that it undergoes a phase-transformation in its solid state, and that the solid solubility limit of alloying elements should decrease as temperatures decrease [16].

To achieve precipitation hardening, an applicable alloy is first heated to produce a solid solution, and quenched to produce an unstable, supersaturated state. There is now a strong driving force for precipitation to occur, a process known as ageing. Fluctuations in the concentration of alloying elements form clusters of atoms, or nucleation points, from which precipitates can grow. The size of the resulting precipitates is strongly temperature dependent, and lower temperatures result in smaller precipitates. A large number of finely dispersed particles generally produce the greatest mechanical properties in an alloy. If they are allowed to age too far, these particles will gradually be replaced by a small number of coarser particles. This state is known as over-ageing, and is associated with a reduction in hardness [16]. The different stages of the ageing process can be seen in Figure 8, where a peak in hardness is followed by a reduction in hardness in the over-aged stage.

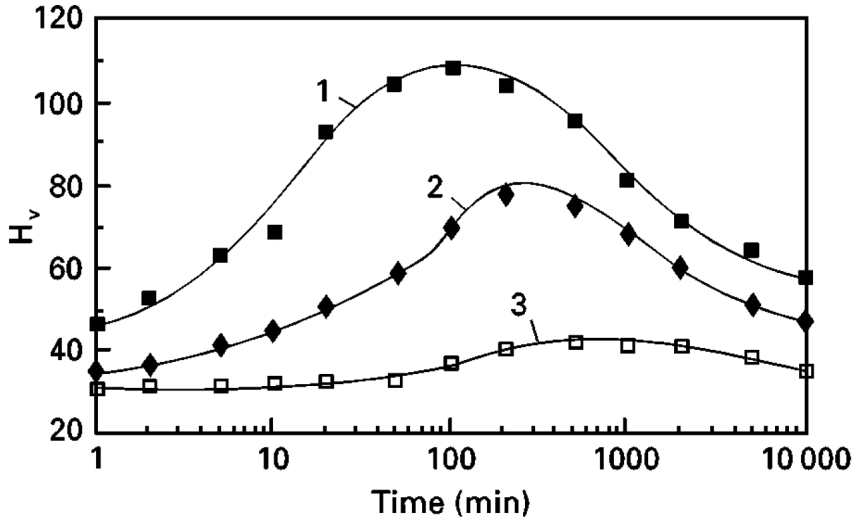

Figure 8: The ageing curves of three different Al-Mg-Si alloys being aged at 210 ^{o}C [17]. A clear peak in hardness can be observed, before the reduction in hardness associated with over-ageing

When a precipitation hardenable material is aged, a graph can be plotted, showing the different stages of ageing. The resulting curve, following a logarithmic time scale, allows for ageing to specific points on the curve. By knowing the time to achieve different levels of ageing at a specific temperature, different tempers can be accurately produced [16].

The early stages of ageing have been found to be strongly affected by the amount of vacancies in the material. Vacancies provide nucleation sites for precipitates, and it is thus favorable to produce a large number of vacancies in the material prior to the ageing process. This is achieved by rapidly quenching the alloy down to room temperature after solutionizing. Cold working the material prior to ageing has been found to reduce the amount of vacancies in the material. This is likely due to the dislocations introduced by cold working, which can act as vacancy sinks. Cold working and rapid quenching thus have opposing effects on the formation of vacancies, and subsequently on the formation of precipitates, and the hardenability of the alloy [16].

2.3.2 Al-Mg-Si alloys

Al-Mg-Si alloys are widely used in industrial applications due to the high strength they can achieve by precipitation hardening. The precipitation behavior of these alloys have been extensively studied, and has generally been considered to go through the following steps; supersaturated solid solution, formation of atomic clusters, GP-zones, metastable β", metastable β'/B', and finally stable β, as seen in Figure 9. To achieve the highest strength, the particles in the material should mainly be in the β" state, as the subsequent particles are associated with over-ageing of the material [17]. Note that some authors considers the β" phase to be a GP2-zone, preceded by GP1-zones.

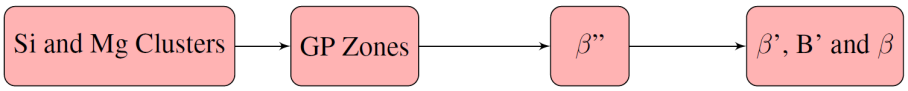

Figure 9: The sequence of precipitates and particles formed during the ageing process of a supersaturated Al-Mg-Si system [18].

The alloy is first solutionized to bring Si and Mg into solid solution. Rapidly quenching the material down to room temperature is vital to produce the supersaturated state necessary for precipitation hardening to occur. If the cooling rate is too low, precipitates will fuse into the stable β-particles, and the potential for further hardening will be lost. Quenched-in vacancies in the material provide nucleation points for precipitates during the initial steps of the ageing process. The first precipitates to form incorporate a high percentage of Al atoms and exert little strain on the surrounding matrix. The strength contribution from these precipitates is thus very limited [19]. These phases are given the general term GP-zones, and may go through several intermediate stages. They are characterized by their small size of a few nm, and a relatively large coherency with the aluminum matrix. While they are near spherical in shape during the early stages, they will grow to form needle-like structures in the later stages, like the β" particle. Both of these structures are located in the <100> directions of the Al matrix. The most developed GP-zones occur directly before the formation of β" particles.

The transition towards β" is initiated by the replacement of aluminum with silicon and magnesium atoms. The number of particles is greatly reduced, yet the hardness increases due to the large strain they exert on the Al matrix. The β" may grow to needle-shaped particles of up to 4 x 4 x 35 nm. Maximum hardness has been found to coincide with a very fine distribution of particles roughly 16 nm in length [19]. The β" particles take on a more defined structure than the GP-zones, and are believed to have a formula of Mg_5Si_6, or $(Al + Mg)_5Si_6$ [19]. At longer ageing times, the β" particles are eventually replaced by the more stable β' and β particles, resulting in a reduction in hardness.

2.3.3 Aluminum tempers

Aluminum alloys are designated according to their current temper state, presented as a code following the aluminum alloy designation [20]. The general temper class is indicated by a letter, and they are defined as follows:

F - As fabricated, with no special regard to thermal conditions or work hardening.

O - Annealed, the lowest strength temper, often used to increase workability.

H - Work hardened, increased strength, which may be combined with heat treatments.

W - Solution heat treated, applies only to alloys that age spontaneously after solution heat treating.

T - Thermally treated to produce stable tempers, which may be combined with work hardening.

The work conducted in this thesis will revolve around the thermally treated tempers, and they will thus be described more in depth. There are ten basic subdivisions to the T-temper, covering naturally and artificially aged conditions, as well as cold working. T6 is one of the most common tempers, covering products that have been solution treated, then artificially aged, to achieve the highest strength of precipitation hardenable alloys. T4 is produced in similar conditions, but is naturally aged to a stable condition. Both tempers apply only to products that have not been work hardened noticeably at any point after solutionizing. T7 applies to products that have been solution heat treated and overaged, or stabilized. T9 applies to products that have been solution heat treated, artificially aged, and work hardened to achieve higher strength. In addition to these, several more sub-categories exist, describing additional details [20].

3 Experimental

This chapter will first include a short description of the materials used in this thesis. Secondly, the sample preparation, rolling procedures, and heat treatments will be described, before the microstructural and mechanical tests that were conducted are specified.

3.1 Materials and specimen extraction

3.1.1 Materials

A large sheet of extruded AA6082 provided the aluminum for this thesis. The sheet was approximately 3 mm thick and 210 mm wide, with a chemical composition as seen in Table 1. The material was homogenized at 530 ^{o}C, before being extruded and air cooled. The sheet had since been stored in room temperature for over 10 years. The material was supersaturated with Mg and Si to allow for precipitation hardening, as well as Mn-dispersions to prevent grain growth. Also used was a large sheet of rolled, interstitial free steel. The steel sheet had a thickness of 1 mm and a width of around 1 m.

Table 1: Chemical composition of the extruded AA6082 material used in this project [21]. All values are given in weight percent.

Alloy	Mg	Si	Mn	Fe	Cu	Al
AA6082	0.67	1.04	0.54	0.20	0.003	Balance

3.1.2 Specimen extraction

Several large sections were cut from the aluminum sheet. These were fed multiple times through a rolling mill to reduce their thickness from 3 mm, to approximately 1 mm, with the rolling direction being parallel to the direction of extrusion. The resulting sheets were cut into pieces measuring 30 x 120 mm, with the longest edge in the direction of rolling. Several more samples with identical measurements were cut from the sheet of IF steel. Again the longest egde was kept parallel with the direction of rolling.

3.2 Roll bonding procedure

3.2.1 Sample preparation

Figure 10 shows a top and side view of a tree layered CRB sample. The sample preparation procedure was as follows; a hole was first drilled into each end of the sheets to allow for riveting, which was required to keep the CRB samples together during the

rolling procedure. The inner sheet was offset to the front of the sample by around 10 mm, to allow the rolling mill to grip the sample more easily. The sheets were rubbed with acetone to remove any surface contaminants, and thoroughly scratched with a steel brush, with 0.3 mm wires, to produce a work hardened surface. The surfaces were cleaned by pressurized air to remove residual surface contaminants. Three sheets were stacked on top of each other, with the outer sheets being steel and the inner sheet aluminum. Rivets were inserted to lock the samples in place, and the rivet heads were hammered flat as to not obstruct the rolling mill.

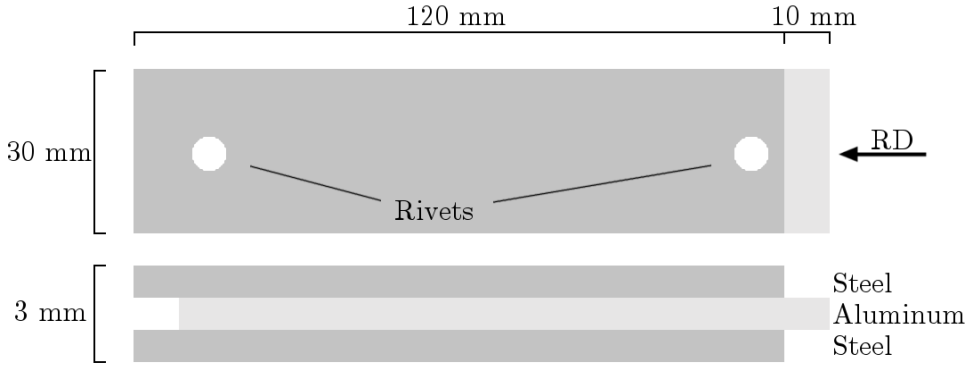

Figure 10: Top and side view of a CRB sample consisting of three sheets, each with a thickness of approximately 1 mm. The aluminum sheet is offset to the front of the sample to allow the rolling mill to grip it more easily. The location of rivets can be seen from the top view.

3.2.2 Oven calibration

After preparing the samples, whey were pre-heated in an oven to reach specific rolling temperatures. This was achieved using a small oven, of the type Scan-Form SF-2, next to the rolling mill. The oven was calibrated using both a regular k-sensor thermometer to detect the ovens temperature, and a dummy sample to estimate how long a CRB sample would take to reach the proper rolling temperature. The dummy sample was created in the same way as the actual CRB samples, as a three layered composite with aluminum as the center sheet. The dummy sample and thermometer can be seen in Figure 11. A k-sensor was placed between the aluminum and one of the steel sheets and locked in place as the sheets were riveted together. An effort was made to make sure the k-sensor was as close to the center of the dummy sample as possible, to provide the most accurate temperature reading. The time to reach specific temperatures was recorded using a thermometer. To decrease the required pre-heat time, samples were placed on top of a thick steel slab on the oven floor. The heat radiating from the steel slab was to increase the heat transfer rate to the CRB samples, compared to heating them by air alone. Tests were conducted both with and without this steel piece, to evaluate how much of an impact it made, with the results being provided in Chapter 8.4 of the appendix.

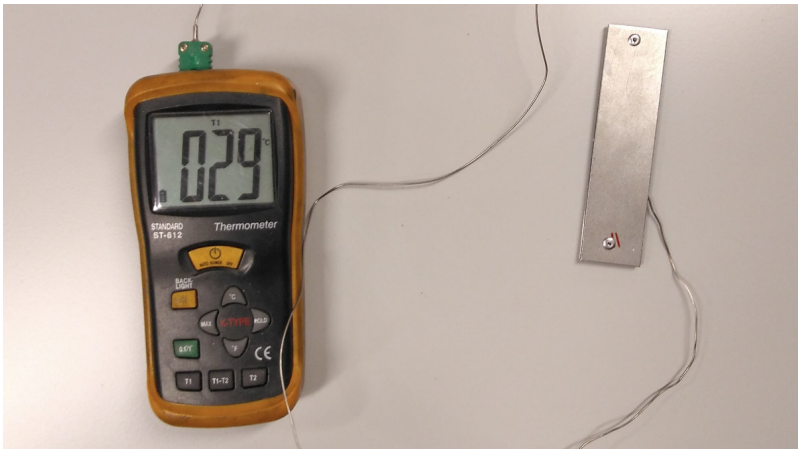

Figure 11: A thermometer used to calibrate the oven. The k-sensor is locked in place between two of the sheets in a three layered dummy CRB sample, as close to the center of the sample as possible. The required time for CRB samples to reach their pre-heat temperature could thus be estimated.

3.2.3 Rolling mill

Rolling of materials for this thesis were conducted using the rolling mill seen in Figure 12. This mill had a partially custom setup, and thus no specific values for its capabilities were known [22]. The mill was powered by a separate hydraulic engine, and the rolling speed was controlled by the Labview 2011 software. The mill had a two-high roller setup, with a roller diameter of 205 mm, and a roller circumference of 644 mm. The gap size between the rollers was manually controlled by a wheel, without any form of gauge indicating the exact gap size. There were thus an uncertainty in the gap size, in addition to a slight yielding of the mill when hard samples were rolled. The roll speed, estimated by counting revolutions per minute, was found to be 6,6 m/min.

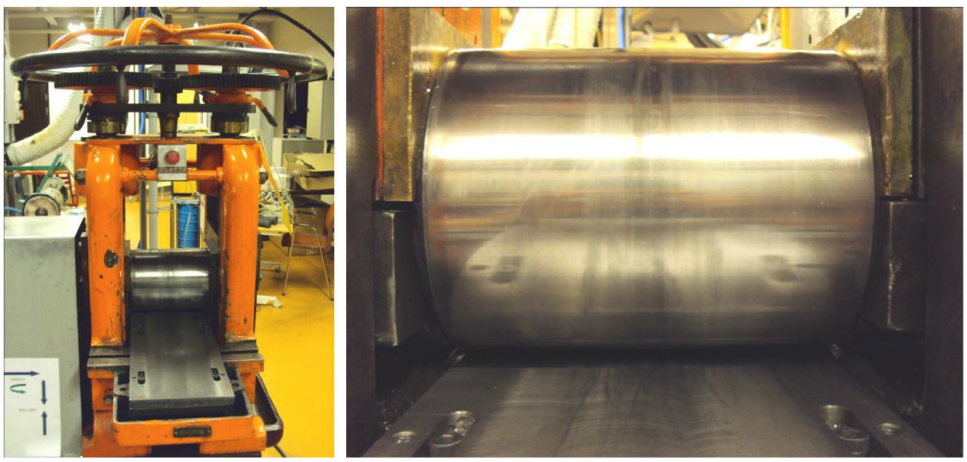

Figure 12: The rolling mill on the left, with a close up view of the top roller to the right. The lower roller is hidden by the table. The wheel for controlling gap size can be seen at the very top of the rolling mill [22].

3.3 Overview of roll bonded samples

Three main rolling procedures were tested to produce the samples, as seen in Table 2. These were chosen to gain a better understanding of how the CRB material would be affected by heat treating the aluminum at different stages before and after the CRB process. The given nomenclature indicates the production sequence of each sample; BSA implying Bonding - Solutionizing - Ageing.

BSA
The BSA rolling sequence had the samples undergo the CRB process while the aluminum was in its 1 mm thick 'as rolled' state. The samples were prepared and placed in an oven for pre-heating. After roll bonding, the CRB samples were placed in a salt bath to solutionize the aluminum, followed by an oil bath to age the aluminum to T6.

SBA
The aluminum sheets for the SBA samples were solutionized prior to the CRB process. After pre-heating and roll bonding, the samples were placed in an oil bath for ageing, with approximately 30 minutes having passed since solutionizing.

SAB
The aluminum sheets for the SAB samples were solutionized and aged to T6 prior to the CRB process. The samples were then prepared, pre-heated, and roll bonded, producing the finished samples.

Table 2: An overview of the three roll bonding sequences used.

BSA :	pre-heating	$\longrightarrow$	CRB	$\longrightarrow$	solutionizing	$\longrightarrow$	ageing to T6
SBA :	solutionizing	$\longrightarrow$	pre-heating	$\longrightarrow$	CRB	$\longrightarrow$	ageing to T6
SAB :	solutionizing	$\longrightarrow$	ageing to T6	$\longrightarrow$	pre-heating	$\longrightarrow$	CRB

A total of 16 cold roll bonded samples were produced for this thesis. They all followed the three aforementioned rolling procedures, at varying pre-heat temperatures. Each sample was heated for 10 - 15 minutes, depending on the desired pre-heat temperature, and an effort was made to roll them within a few seconds of being removed from the oven.

A pre-heat temperature of 150 ^{o}C and 200 ^{o}C was used to produce samples of all rolling procedures, as seen in Table 3. Additionally, a sample was produced at room temperature (20 ^{o}C) for the BSA sequence, and at 300 ^{o}C for the SAB sequence. Samples produced at 200 ^{o}C were quenched in water immediately after roll bonding, while the remaining samples were left to air-cool.

Table 3: The various pre-heat temperatures used to produce CRB samples

	Pre-heat temperatures			
BSA :	20 ^{o}C	150 ^{o}C	200 ^{o}C	-
SBA :	-	150 ^{o}C	200 ^{o}C	-
SAB :	-	150 ^{o}C	200 ^{o}C	300 ^{o}C

3.3.1 Solutionizing and ageing

The parameters for solutionizing and ageing were kept identical for all samples. Slight variations were however used for the applied ageing times. Solutionizing was achieved by placing the samples in a salt bath at 540 ^{o}C for 2 minutes. Ageing was conducted in an oil bath at 185 ^{o}C to reach T6. The samples were quenched in water after each step, and left in room temperature for 30 minutes between solutionizing and ageing. An ageing time of 120 minutes was used for the BSA samples, while 90 minutes was used for the SBA and SAB samples. The full heat treatment procedure is seen in Table 4. The reduced age time was chosen because of the pre-heat treatment conducted prior to roll bonding. For the SBA samples, which were solutionized prior to roll bonding, the ageing process was expected to initiate during pre-heating, thus reducing the required time of subsequent ageing. The SAB samples were at risk of over-ageing, as these samples were already at T6 prior to pre-heating. A reduced ageing time was thus used. The BSA samples were subjected to solutionizing and ageing after the CRB process was completed, and so their ageing time was not affected by the pre-heating procedure.

Table 4: The procedure for solutionizing and ageing the aluminum. The CRB process was conducted during step 3 for the SBA samples.

1	Salt bath at 540 ^{o}C for 2 minutes
2	Quenching in water
3	Resting in room temperature for 30 minutes
4	Oil bath at 185 ^{o}C for 90 or 120 minutes
5	Quenching in water

Figure 13 shows a completed CRB sample for peel testing and microstructural analysis. This sample was to be divided into two parts, indicated by the stapled line to the right in the image. The left part of this sample was used to produce a peel test specimen, while the right side was used for microstructural analysis. The sample in question had a rolling direction from right to left, with a relatively large thickness reduction, of 64 %.

Figure 13: A completed sheet of cold roll bonded IF steel and AA6082 aluminum, with a relatively large thickness reduction, of 64 %. Flattened rivets can be seen on either end of the sample, as well as the aluminum sheet sticking out on the right side.

3.4 Microstructural characterization

3.4.1 Microstructural samples

The microstructural samples were prepared by cutting pieces of the CRB material into sections of roughly 1 x 2 cm. The sections were cast in epoxy, and ground and polished down following standard procedures. The viewing direction on the samples were from a transverse direction; perpendicular to the rolling direction, and in plane with the CRB interface. It was made sure that no surfaces to be viewed originated from the outer edges of the CRB sheets, to avoid edge effects from the CRB process. The final step of surface preparation consisted of polishing with either 1 μm diamond suspension, or 0,05 μm colloidal silica in a vibration polisher. Three of the finished samples can be seen in Figure 14.

Figure 14: Three of the finished microstructural samples. The section at the center of each sample is the actual CRB specimen, while the outer pieces are IF steel meant to stabilize the samples during grinding and polishing. The black plastic clips were used to hold each sheet in place during epoxy casting.

3.4.2 Optical microscopy

The microstructure of several aluminum specimens were studied by anodizing and applying polarized light in an optical microscope. Samples of the 1 mm thick aluminum sheets were examined both before and after solutionizing, to study the potential for recrystallization to occur. Additionally, specimens were collected from samples of each of the three rolling procedures, produced with a pre-heat temperature of 200 ^{o}C. These were delaminated to extract the aluminum sheet from the

center of the material. This was achieved by mounting the samples in a vice, and hammering a knife in between the individual sheets to separate them. It was necessary to remove the surrounding steel layers as the large difference in galvanic potential between the two metals would inhibit anodization.

Each section was cast in epoxy and ground and polished down to 1 μm. To make the samples electrically conductive, a wooden screw was inserted from the back of each sample, as seen in Figure 15. The screw was in electrical contact with the specimen inside the epoxy, allowing the anodizing circuit to be completed. The samples were anodized for 90 seconds in Barker's reagent, at 20 V of applied current. Images were taken with an optical microscope equipped with polarizer and analyzer.

Additional images were taken of the completed CRB samples at 50X magnification by unpolarized light. This was conducted in order to study the percent reduction that the steel and aluminum sheets had experienced. By measuring the thickness of each sheet relative to the initial thickness, the percent reductions could be calculated.

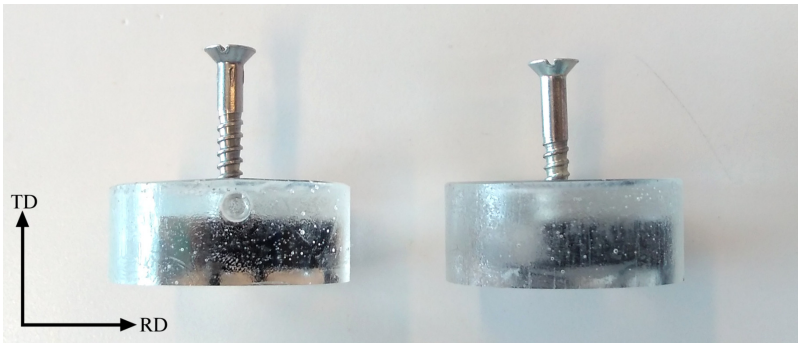

Figure 15: Two samples prepared for anodizing. A wooden screw was inserted from the back of each sample, contacting the specimen to be anodized. This ensured that electric contact could be achieved with the specimen, required for anodizing to take place.

3.4.3 Scanning electron microscopy

Scanning electron microscopy (SEM) was used to study the CRB interfaces, with special regard to intermetallic phases. Six samples were studied, as seen in Table 5. Two different BSA-150 samples were chosen to study the microstructure at different stages of heat treatment; both directly after solutionizing, and after ageing for 2 hours to reach T6. This was done to see if ageing would produce any notable differences in the interface compared to solutionizing alone. Samples produced with a pre-heat temperature of 200 ^{o}C were studied for all rolling parameters, as well as at 150 ^{o}C for the SBA samples. SAB-150 samples were not studied as the bond strength of these samples were deemed too low for the material to be of any use.

Table 5: The various samples that were studied by SEM analysis.

Sample	Condition
BSA-150$_{sol}$	Solutionized after CRB
BSA-150	Aged to T6 after CRB
BSA-200	Aged to T6 after CRB
SBA-150	Aged to T6 after CRB
SBA-200	Aged to T6 after CRB
SAB-200	Aged to T6 prior to CRB

Additionally, a point scan by energy-dispersive X-ray spectroscopy (EDS) was carried out to study the change in chemical composition across the CRB interface. 12 points were scanned, covering approximately 4 μm, in a direction perpendicular to the interface. The scan was performed on the BSA-150$_{sol}$ sample, that had been solutionized after the CRB process. An acceleration voltage of 10 kV was used, and signals produced by aluminum and iron were recorded.

Each sample was cast in epoxy and ground and polished following standard procedures. The final step of polishing consisted of vibration polishing with 0.05 μm colloidal silica for 17 - 19 hours, to produce a highly polished surface. Finally, the samples were covered by aluminum foil and carbon tape to make them electrically conductive, as required for SEM analysis. Three of the finished samples can be seen in Figure 16.

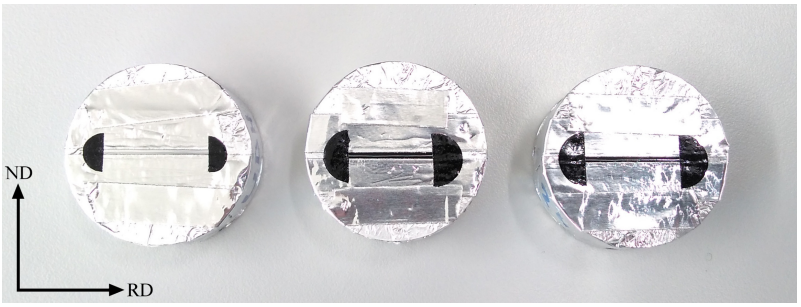

Figure 16: Epoxy samples covered by aluminum foil and carbon tape for SEM analysis. The horizontal slit visible on each sample is the actual CRB specimen.

The microscopes used were Zeiss Supra 55 VP and Zeiss Ultra 55 LE Field Emission SEMs. EDS analysis were performed by Quantax Esprit 1.9 software. Images were taken with the secondary electron and in-lens detectors, at magnifications from 1000X to 10.000X. An acceleration voltage of 10 kV was used, aperture size of 30 μm, and with a working distance of around 10 mm.

3.5 Mechanical characterization

3.5.1 Ageing curves

Three ageing curves were produced to examine the ageing potential at different conditions. The first was used to study the unprocessed, extruded material, the second was for sheets that had been reduced to 1 mm by cold rolling, and the third was to study the required ageing time for the cold roll bonded BSA samples.

Five sections of the extruded raw material were solutionized and aged according to Table 4, however, solutionizing was conducted for 10 minutes rather than 2 minutes. An oil bath was used to age the samples at 185 ^{o}C at the following hold times; 10, 30, 120, 240, and 360 minutes, before quenching in water. Hardness measurements were conducted both before and after solutionizing, and after ageing of each sample. These measurements were conducted from the normal direction of each sample, and thus casting the samples in epoxy was not required. A load of 5 kg with 10 seconds of hold time was utilized for these measurements.

The second ageing curve was created from sheets that had been reduced from 3 mm to approximately 1 mm by cold rolling. These samples were solutionized and aged after the thickness reduction. This was necessary to find the ageing curve for the SAB samples, that were hardened to T6 prior to the CRB process. The same parameters and hold times as for the previous ageing curve was used, however, solutionizing at 540 ^{o}C was conducted for the standard 2 minutes. Hardness measurements were conducted with the same parameters as previously specified.

The third ageing curve was produced from a BSA-150 sample, which was solutionized and hardened to T6 after the CRB process. Sections were cut from the sample, measuring approximately 1 x 2 cm. These were solutionized at 540 ^{o}C for 2 minutes, and aged in an oil bath at 185 ^{o}C at the following hold times; 30, 60, 90, 120, 180, and 240 minutes. The sections were cast in epoxy, ground and polished down to avoid any edge effects from the CRB procedure, and micro hardness measurements were conducted from the transverse direction. A load of 300 grams with 10 seconds of hold time were utilized for these measurements.

3.5.2 Hardness measurements

Several hardness measurements were conducted in relation to the ageing curves. Additional measurements were conducted on all but the BSA-20 sample. The samples were cast in epoxy, and measurements were taken from a transverse direction, in plane with the CRB interface. Indents were taken as close to the center of the aluminum as possible. Measurements were taken with a Leica VMHT MOT micro hardness tester, and a load of 300 grams with 10 seconds of hold time were utilized. Five measurements were conducted on each sample.

3.5.3 Peel testing

A total of 13 samples were produced for peel testing; three from each CRB procedure with a pre-heat temperature of 200 ^{o}C, two BSA-150, and two SBA-150 samples. Due to material constraints, only four samples were produced with a pre-heat temperature of 150 ^{o}C. No SAB-150 peel samples were produced as their bond strength was deemed too low.

Peel testing works by measuring the force required to delaminate one sheet from the three layered composite. To allow for delamination to initiate, the rear end of each CRB sample was prepared without scratch brushing. This ensured that the ends were weakly bonded, allowing them to be pulled apart easily before mounting the samples in the peel testing rig. A section of approximately 50 mm had to be delaminated, as the testing rig required some material to grip the samples securely.

The finished peel testing samples were roughly 250 mm long, as seen in Figure 17. This included the peel testing region itself, stretching approximately 200 mm from one end of the sample to the rivet, and the unbonded region, covering the remaining 50 mm. The edges running alongside the samples were trimmed off by abrasive jet machining, reducing their width from 30 mm to 20 mm. This removed any curvature in the samples, and ensured that potential edge effects introduced during the CRB process did not interfere with peel testing results.

Figure 17: One of the finished peel testing samples. The sample has been machined down to a width of 20 mm, and a length of approximately 250 mm. A flattened rivet is visible on the left side of the sample.

Peel testing was conducted using a custom peel testing rig, that allowed samples to be delaminated from a 90 degree peel direction. The testing rig was loosely based off the ASTM-D3167-10 standard [23], however, several simplifications were made to make both the rig and peel testing specimens easier to produce. The test rig consisted of two rollers with a diameter of 20 mm, mounted 50 mm apart, center to center. The rollers were 80 mm wide and equipped with ball bearings. They were mounted on top of a small table, measuring 150 x 280 mm, for the samples to slide along during testing. The height of the rollers above the table could be adjusted by inserting shims underneath the roller mounts, to suit samples of different thicknesses. The two rollers and the table were meant to counter the twisting motion that a three-layered composite would otherwise experience during peel testing. A schematic drawing of the rig is seen in Figure 18, while the finished rig is seen in Figure 19.

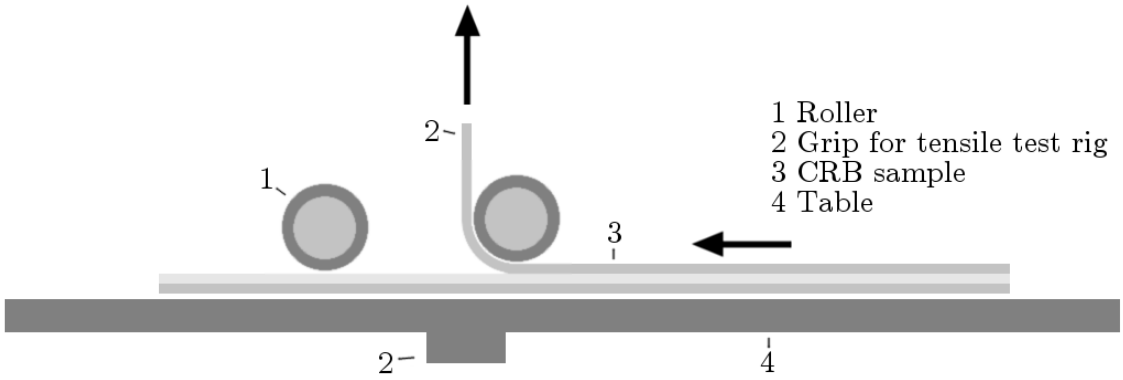

Figure 18: A schematic drawing of the tensile test rig. The rig is kept stationary while the top steel layer is pulled upwards. As the sample delaminates, it is pulled towards the left.

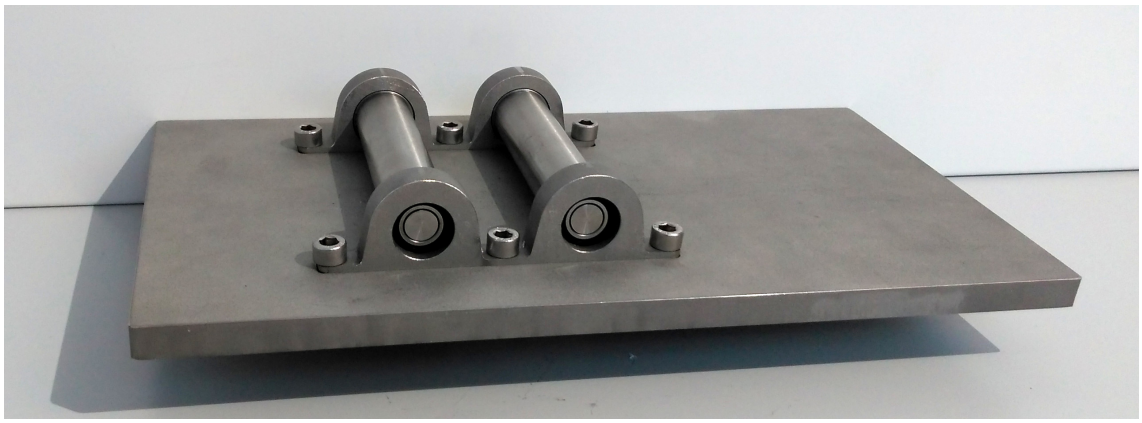

Figure 19: The finished peel test rig. The table measures 150 x 280 mm, and the rollers are 50 mm apart. Samples are fed in from the right, one layer is pulled upwards while the two remaining layers exit to the left of the rig.

To guide the samples into the rollers at a straight angle, additional guide blocks were clamped onto the table, roughly 20 mm apart. The peel testing rig was mounted in a regular tensile testing machine, as seen in Figure 20. The tensile testing machine gripped the steel layer at the top, and locked onto a mount underneath the table. The table remained stationary, while the top steel layer was pulled upwards.

A Zwick Roell Zwickiline Z2.5 tensile testing machine, controlled by Testxpert II software, was used to conduct the peel tests. The software was first zeroed with the weight of the test rig, including clamp and guide blocks. A peeling speed of 25 mm/min was used, and the force in newton, versus relative peel distance, was recorded. By dividing the average force required for peeling by the width of the peel specimen, the bond strength was given in N/mm, as seen in Equation 2. The peel samples used some time to reach stable measured values, and thus the first few centimeters of the peel test regions were disregarded. Similar discrepancies were found to occur near the end of each specimen, and so this region was disregarded as well.

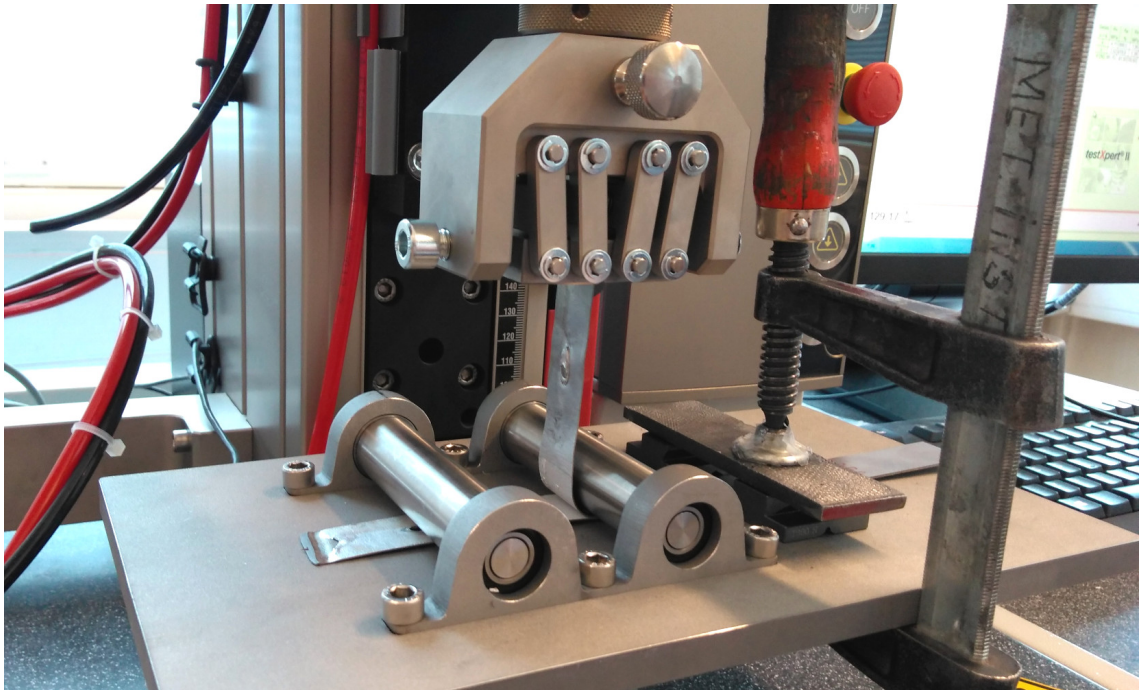

Figure 20: The peel test rig mounted in a tensile test machine. Guide blocks were clamped onto the table to ensure that samples were fed through at a straight angle. The tool for gripping the steel layer is seen directly above the rollers.

SEM analysis

After completing the peel tests, sections were cut from each of the various CRB samples, to study their fracture surface by SEM. Sections were extracted from the steel sheets that had been peeled away from the CRB samples. Additional samples were gathered from the opposing fracture surface; the aluminum layer on the remaining CRB specimen. The steel fracture surfaces from the BSA, SBA, and SAB -200 samples were studied, as well as the aluminum fracture surfaces from the BSA and SBA -150 samples, and the SAB-200 sample.

Pieces measuring roughly 1 x 2 cm were extracted, as seen in Figure 21. The fracture surfaces were cleaned in methanol by an ultrasonic cleaner, but no further sample preparations were conducted. The samples were examined by the Zeiss Ultra Field Emission SEM previously specified. An EDS area scan was performed on each sample, to detect the chemical composition at the fracture surface. Scanning was performed at 1000X magnification, and the signal was analyzed by the Quantax Esprit 1.9 software. The aperture size was 120 μm, the working distance was roughly 10 mm, and high current mode was activated. Experiments were conducted with acceleration voltages from 5 to 15 kV, to study how this would affect the penetration depth, and thus the signal received by the EDS scan. On the steel fracture surfaces, a low acceleration voltage of 5 kV was used to reduce the beam's penetration depth, thus allowing a thin layer near the surface to be viewed. This acceleration voltage was too low to excite iron atoms, and only the aluminum signal was recorded. On

the opposing fracture surfaces, with aluminum as the substrate, acceleration voltages were increased to 10 kV, allowing iron on the aluminum surface to be detected.

The resulting EDS maps from the steel fracture surfaces were analyzed to determine the amount of residual aluminum left on the steel fracture surface. Lines were drawn across the images in the rolling direction, and the percentage of the surface covered by aluminum was measured along these lines.

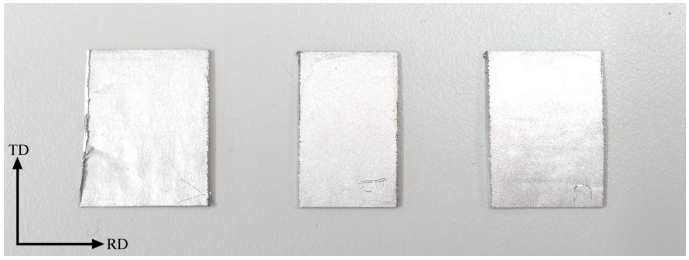

Figure 21: Pieces of the steel layer peeled away from the CRB samples. These sections were cleaned by an ultrasonic cleaner before the EDS scans were performed.

4 Results

This chapter will first provide a quick presentation of results from the cold roll bonded samples that were produced. Next the microstructural and mechanical characterization of the initial material is provided, followed by a presentation of each individual CRB rolling procedure.

4.1 Cold roll bonding

Three main rolling procedures were tested, with several different pre-heat temperatures. Table 6 shows results from each individual rolling procedure and pre-heat temperature, as well as the achieved thickness reductions. Chapter 8.2 of the appendix includes images of each sample, used to calculate the percent thickness reduction of each sheet in the CRB materials. Table 6 also includes comments, describing how well each sample appeared to be joined together, immediately after roll bonding. 'Poor joint' indicates that the CRB samples could easily be pulled apart by hand. Areas of delamination were also commonly found on these samples. The bond strength was deemed too low for these CRB materials to be of any use, and thus no further experiments were conducted. 'Sound joint' indicates a sample where no delamination was visible, and where the sheets could not be pulled apart easily by hand. These samples were regarded as being sufficiently strong for further investigation to take place. A table containing information about each individual peel sample, is provided in Chapter 8.1 of the appendix.

Table 6: All CRB procedures tested, including percent reductions of aluminum and steel, as well as total thickness reductions. A short comment describes how well each sample was joined together, immediately after roll bonding.

Sample	Al reduction	St. reduction	Total reduction	Comment
BSA-20			61 %	Poor joint
BSA-150	69 %	57 %	58 %	Sound joint
BSA-200	62 %	65 %	61 %	Sound joint
SBA-150	57 %	63 %	64 %	Sound joint
SBA-200	64 %	64 %	65 %	Sound joint
SAB-150			62 %	Poor joint
SAB-200	59 %	62 %	59 %	Sound joint
SAB-300			43 %	Sound joint

All samples produced with a pre-heat temperature of 200 ^{o}C achieved a sound joint. At 150 ^{o}C, all but the SAB-150 samples achieved a sound joint, this despite the large thickness reduction. Two SAB-150 samples were produced, with a thickness reduction of 59 and 62 %, and both showed signs of delamination and a very poor joint. The bond strength was deemed too low for these samples to be of any use for

further investigations, and they were thus discarded. A sample was subsequently produced with a pre-heat temperature of 300 ^{o}C, and a sound joint was achieved. As this was the only sample at this temperature, it was excluded from most tests, though hardness measurements were conducted.

The first few samples produced for this thesis were cleaned with acetone as a final step of sample preparation, prior to riveting and roll bonding. None of these samples achieved any form of bonding during the CRB process. Tests were conducted using pressurized air to remove debris from the surface instead, and bonding was achieved. Pressurized air was thus used for all subsequent samples produced, though no further investigations were conducted to determine how large an influence acetone has during the final steps of sample preparation.

4.2 Initial material

4.2.1 Optical microscopy

The microstructure of the 1 mm thick aluminum sheets were studied to see the influence of solutionizing. Images were produced by anodizing the samples and studying them in an optical microscope. Figure 22 shows two images of the same material, the left image shows the aluminum after reduction to 1 mm, while the right image shows the material after subsequent solutionizing at 540 ^{o}C for 2 minutes. After reduction to 1 mm, the material had a typical structure as expected from extrusion and cold rolling, with needle shaped grains elongated in the rolling direction. After solutionizing, the material had recrystallized, resulting in larger grains of a fairly uniform structure, with most of the morphology from the rolling procedure removed.

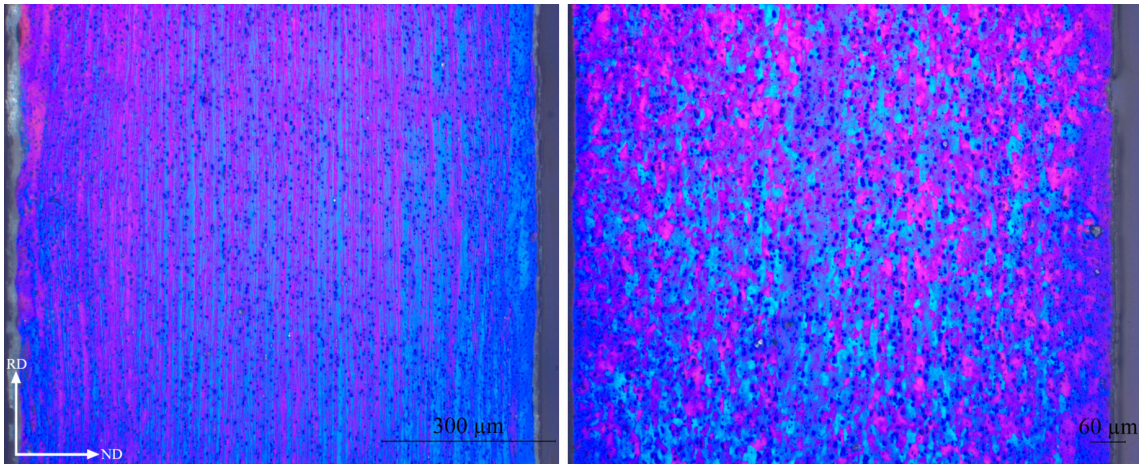

Figure 22: Images of the 1 mm thick aluminum sheets at 100X. The left image shows the material directly after cold rolling, while the right image shows the material after solutionizing. The needle shaped grains have recrystallized to form a fairly uniform grain structure.

4.2.2 Mechanical characterization

Two ageing curves were produced from the aluminum sheets, one from the 3 mm thick extruded raw material, and one after reducing it to 1 mm by cold rolling. The ageing curve from the extruded raw material is seen in Figure 23, and suggests that T6 is reached after approximately 4 hours of ageing at 185 ^{o}C. Figure 24 shows the resulting ageing curve from the material that was reduced to 1 mm by cold rolling. T6 was reached after approximately 2 hours, significantly faster than for the raw material.

The extruded raw material, prior to solutionizing, was found to have a hardness of 82,5 HV, while the hardness dropped to 57,0 HV after solutionizing. After ageing to T6, a hardness of 122 HV was achieved for the raw material, while the 1 mm thick material reached a hardness of 116 HV.

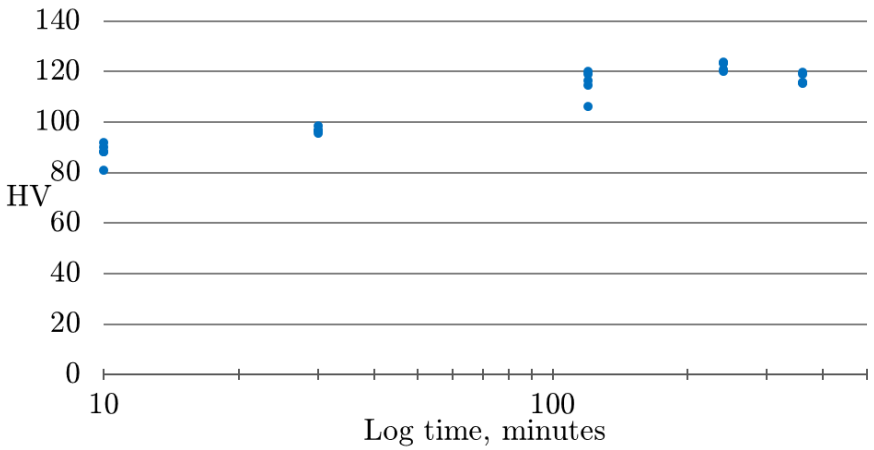

Figure 23: Ageing curve produced from the extruded raw material, after ageing at 185 ^{o}C. T6 is reached after approximately 4 hours, with a hardness of 122 HV.

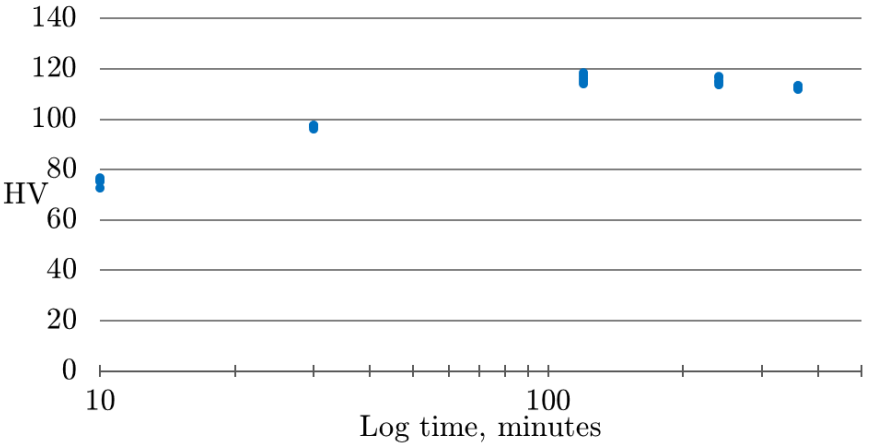

Figure 24: Ageing curve produced from the material reduced to 1 mm by cold rolling. T6 is reached after approximately 2 hours, with a hardness of 116 HV.

4.3 BSA samples

pre-heating	⟶	CRB	⟶	solutionizing	⟶	ageing to T6

4.3.1 Optical microscopy

The microstructure of the aluminum layer in the CRB samples were studied by delaminating the samples, extracting the aluminum layer, anodizing, and applying polarized light in an optical microscope. Figure 25 shows the microstructure of a BSA-200 sample. As solutionizing and ageing was conducted after the rolling procedure, the aluminum had recrystallized to form a fairly uniform microstructure, where most of the morphology introduced by cold rolling has been removed.

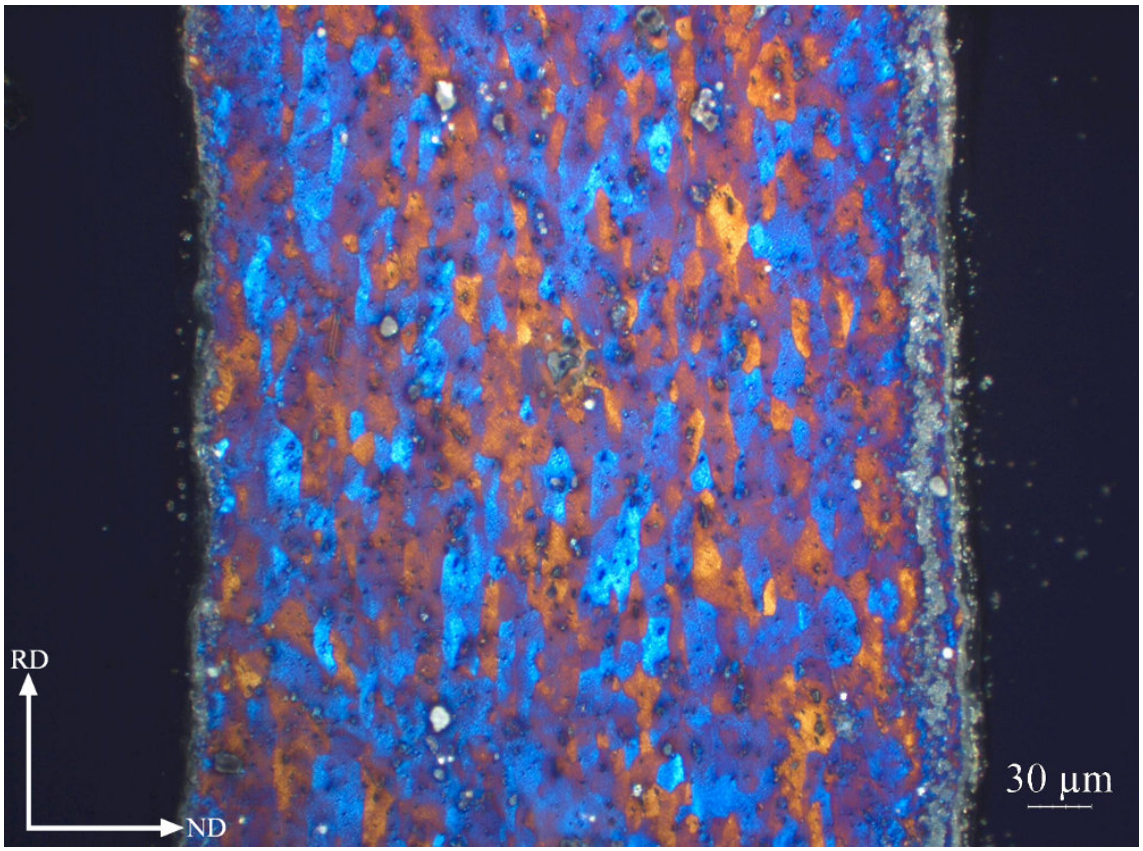

Figure 25: BSA-200 at 200X. The aluminum has recrystallized after the CRB process, resulting in a fairly uniform distribution of large grains.

4.3.2 Scanning electron microscopy

The following SEM images were produced to examine the changes in the CRB interface at different conditions. Figure 26 shows the BSA-150$_{sol}$ sample, where only solutionizing, and no artificial ageing, had taken place. Figure 27 and 28 shows a BSA-150 sample after ageing to T6, at 1000X and 5000X magnification, respectively. Both samples show similar intermetallic layers, roughly 1 μm thick, which appear to have grown primarily into the aluminum. A more uneven interface was seen between the aluminum and the intermetallic layer, than between the intermetallic layer and the steel.

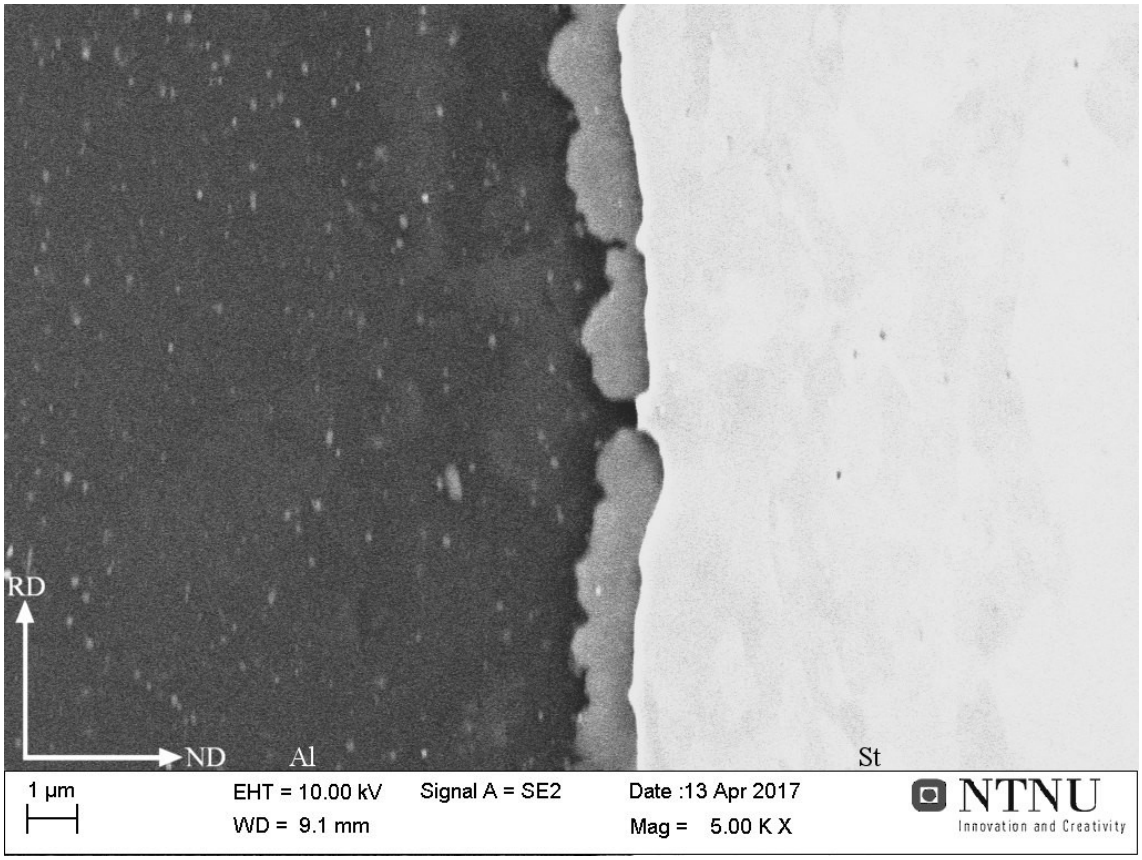

Figure 26: BSA-150$_{sol}$ at 5000X, with aluminum on the left and steel on the right. A layer of intermetallic phases covers most of the CRB interface, though a bare spot is visible at the center of the image. Several particles are visible in the aluminum

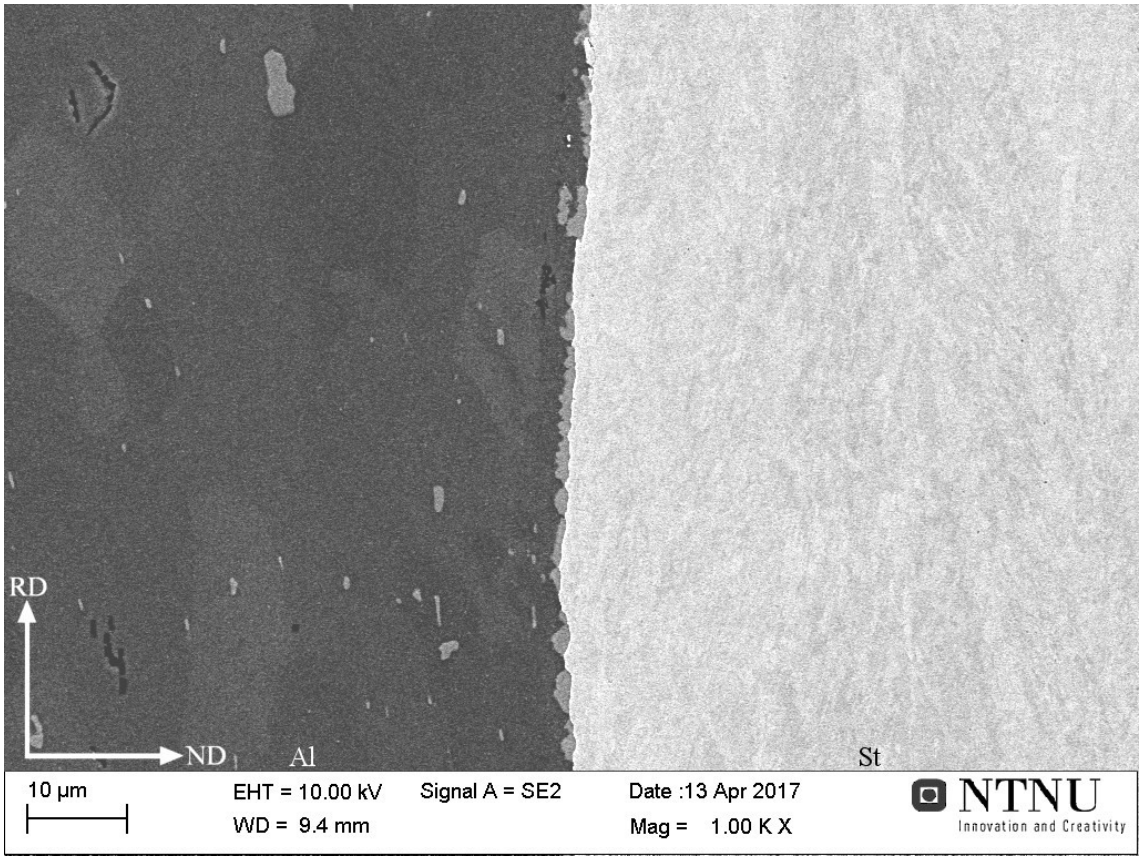

Figure 27: BSA-150 at 1000X, with aluminum on the left and steel on the right. An uneven layer of intermetallic phases can be seen covering the CRB interface. Several particles are visible in the aluminum, as well as grains in the steel.

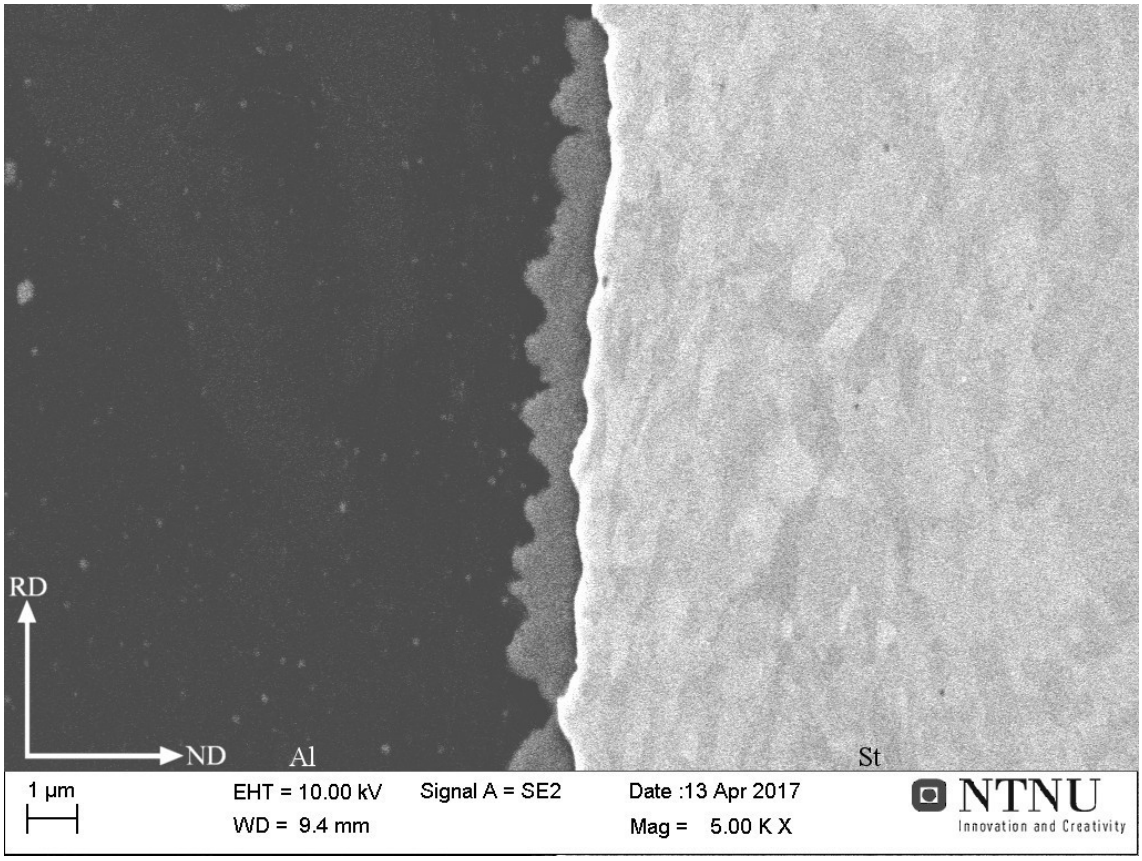

Figure 28: BSA-150 at 5000X, with aluminum on the left and steel on the right. A layer of intermetallic phases can be seen covering the CRB interface. Several particles are visible in the aluminum, as well as grains in the steel.

Figures 29 and 30 shows a BSA-200 sample at 1000X and 5000X magnification, respectively. The images show similar thickness and distribution of intermetallic phases as for the sample produced at 150 ^{o}C. Again an uneven layer is found at the CRB interface, roughly 1 μm thick. Figure 30 shows a close up view of an area where the intermetallic phases appear to have fractured. Several cracks are seen, mostly running in the rolling direction, through the center of the intermetallic region. The fractures appear brittle, as no plastic deformation is visible. Several areas where mechanical interlocking has occurred, are visible on both images.

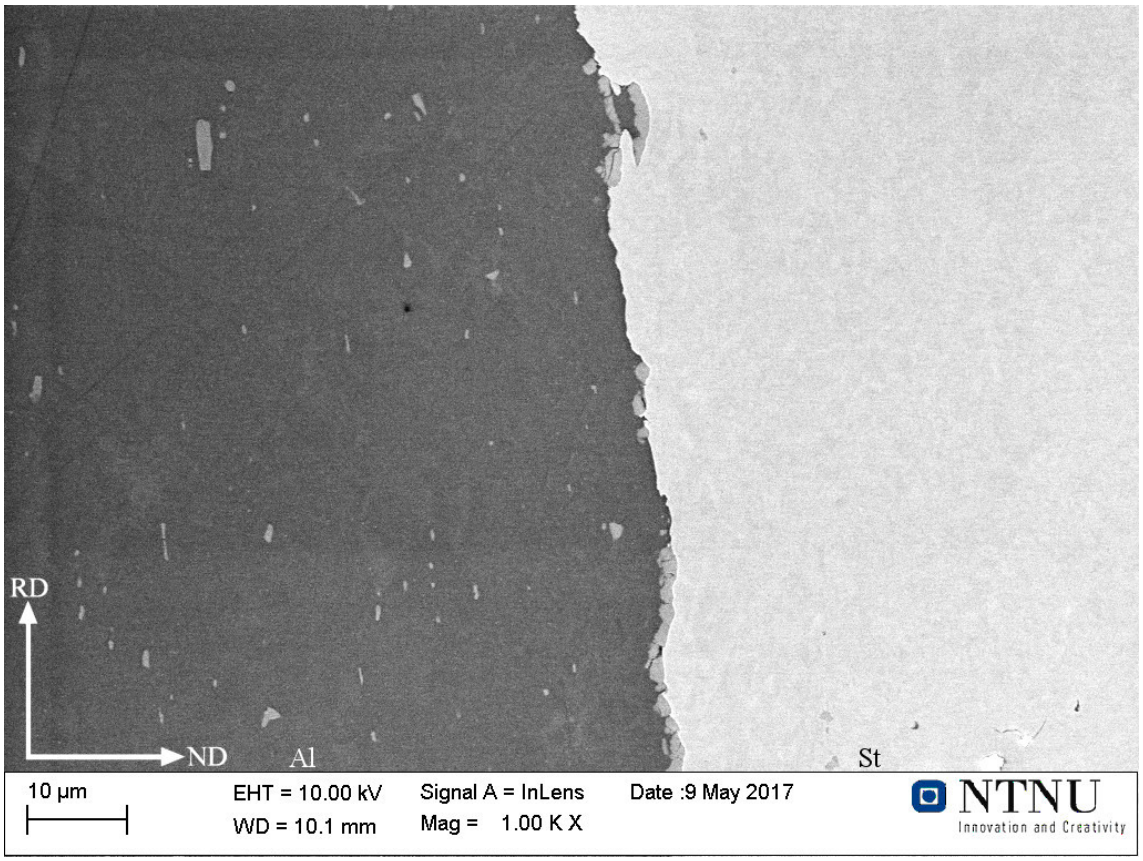

Figure 29: BSA-200 at 1000X, with aluminum on the left and steel on the right. An uneven layer of intermetallic phases can be seen covering the CRB interface. Several particles are visible in the aluminum, as well as grains in the steel.

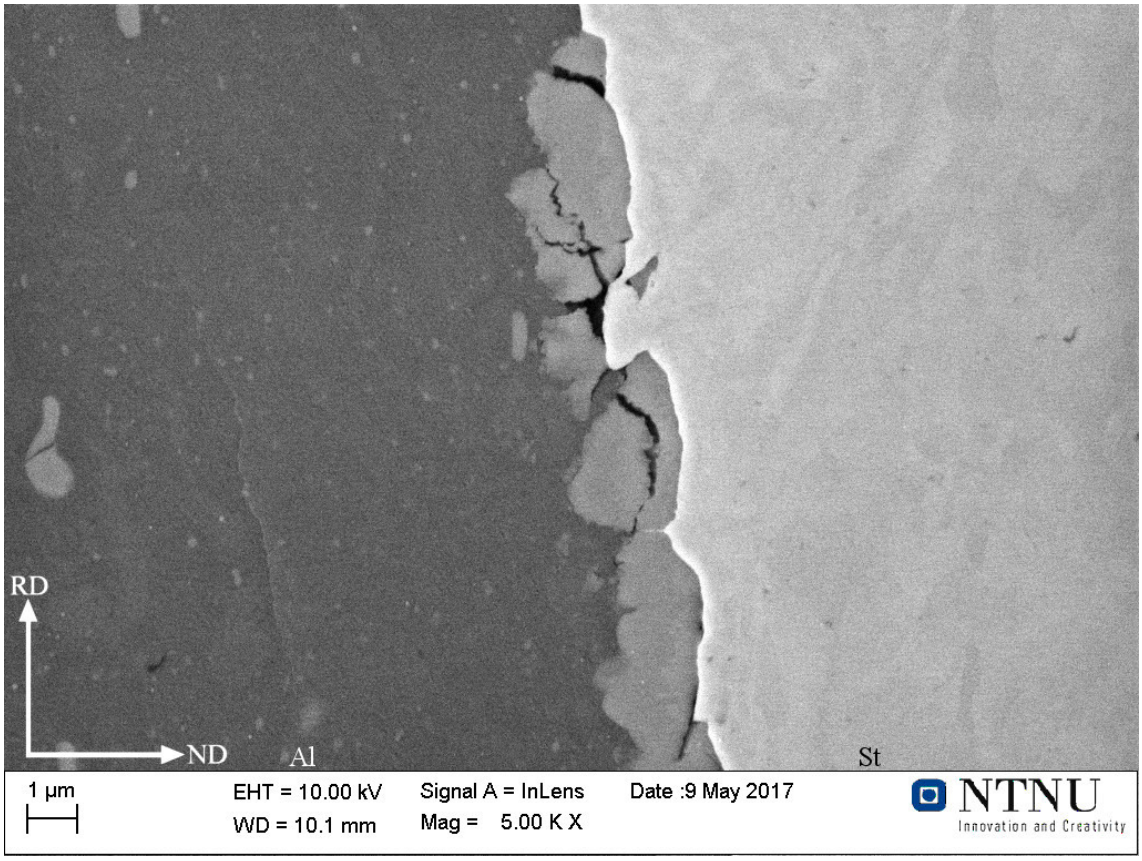

Figure 30: BSA-200 at 5000X, with aluminum on the left and steel on the right. A layer of intermetallic phases are visible on the CRB interface, containing multiple cracks in the rolling direction. Several particles are visible in the aluminum, as well as grains in the steel.

EDS point scan

An EDS point scan was performed on the BSA-150$_{sol}$ sample. 12 points were scanned in a direction perpendicular to the CRB interface, as seen in Figure 31. The scan was performed at 15.000X magnification, covering approximately 4 μm across the interface. Though the EDS signal suggested a number of different elements to be present, only the aluminum and iron signals were recorded, as seen in Figure 32. The chart shows the chemical composition at different data points across the interface. The first and last four data points all show areas where only one of the elements are present, with a sharp transition to the intermetallic region. The data points from the intermetallic phase shows a high aluminum content, at roughly 75 - 85 at.%, with the remaining 15 - 25 % being iron. A reduction in aluminum content is observed closer to the iron phase.

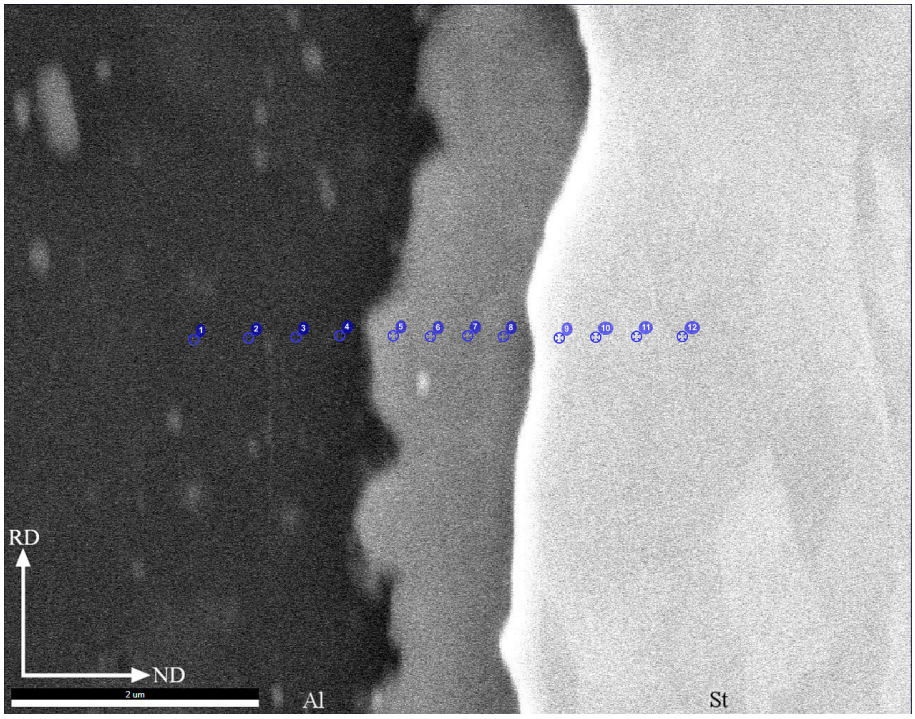

Figure 31: BSA-150$_{sol}$ at 15.000X, with aluminum on the left and steel on the right. 12 points are marked across the interface, indicating the location of each EDS point.

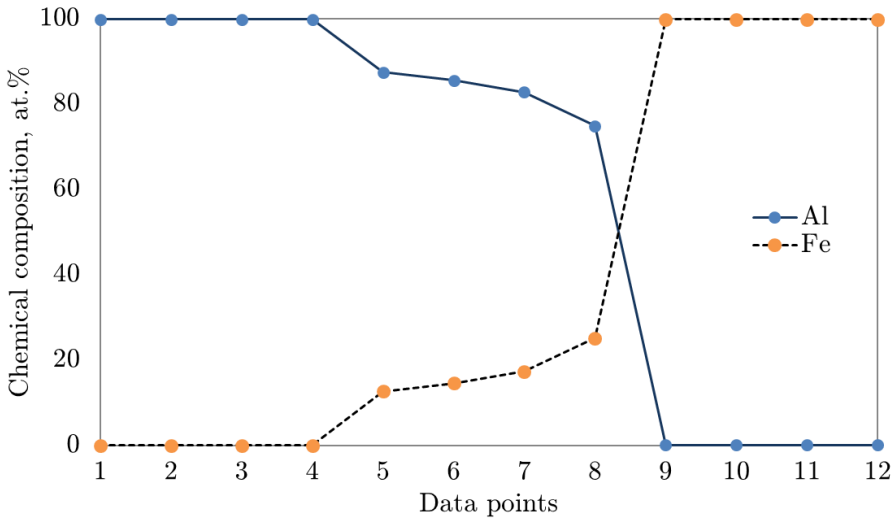

Figure 32: The resulting chemical composition across the EDS data points, measured in atomic percentage. A sharp transition is seen between each metal phase and the intermetallic region. The intermetallic region contains roughly 75 - 85 at.% aluminum.

EDS map of peel test surfaces

EDS was used to study the chemical composition of the fracture surfaces produced by peel testing. Experiments were conducted with an acceleration voltage of 5, 10, and 15 kV, to study how the difference in penetration depth would affect the results. Figure 33 shows two images from a steel fracture surface, where only the aluminum signal is recorded. The left image was produced at 5 kV, while the right image was produced at 15 kV. A stronger aluminum signal can be seen in the left image, and 5 kV was thus chosen as the standard for the subsequent images.

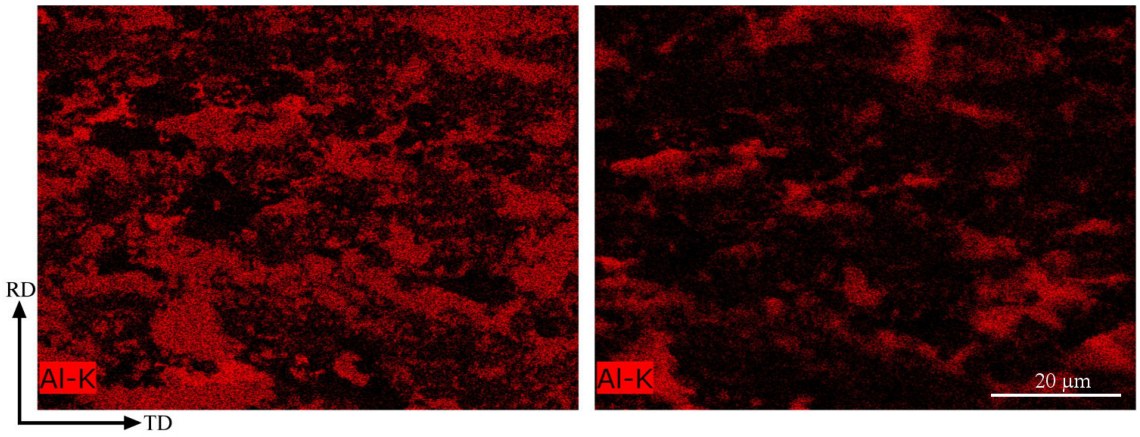

Figure 33: BSA-200 at 1000X. The images show only the aluminum signal from the sample. The left image was produced at 5 kV, while the right image was produced at 15 kV. An improvement in aluminum signal strength is observed in the left image.

Figures 34 and 35 shows the EDS images from the BSA-150 and the BSA-200 samples, respectively. The images were taken from the steel layers that were peeled away from each CRB sample. They were produced by the secondary electron detector, with an overlay of the aluminum signal from the EDS scan. Both samples appear to have a large amount of aluminum stuck to the steel substrate, though the distribution is fairly uneven. Aluminum appears in small patches on the steel surface, as well as larger flakes of aluminum, especially pronounced in the BSA-150 sample. Both fractures appear to have been brittle, indicated by the lack of plastic deformation.

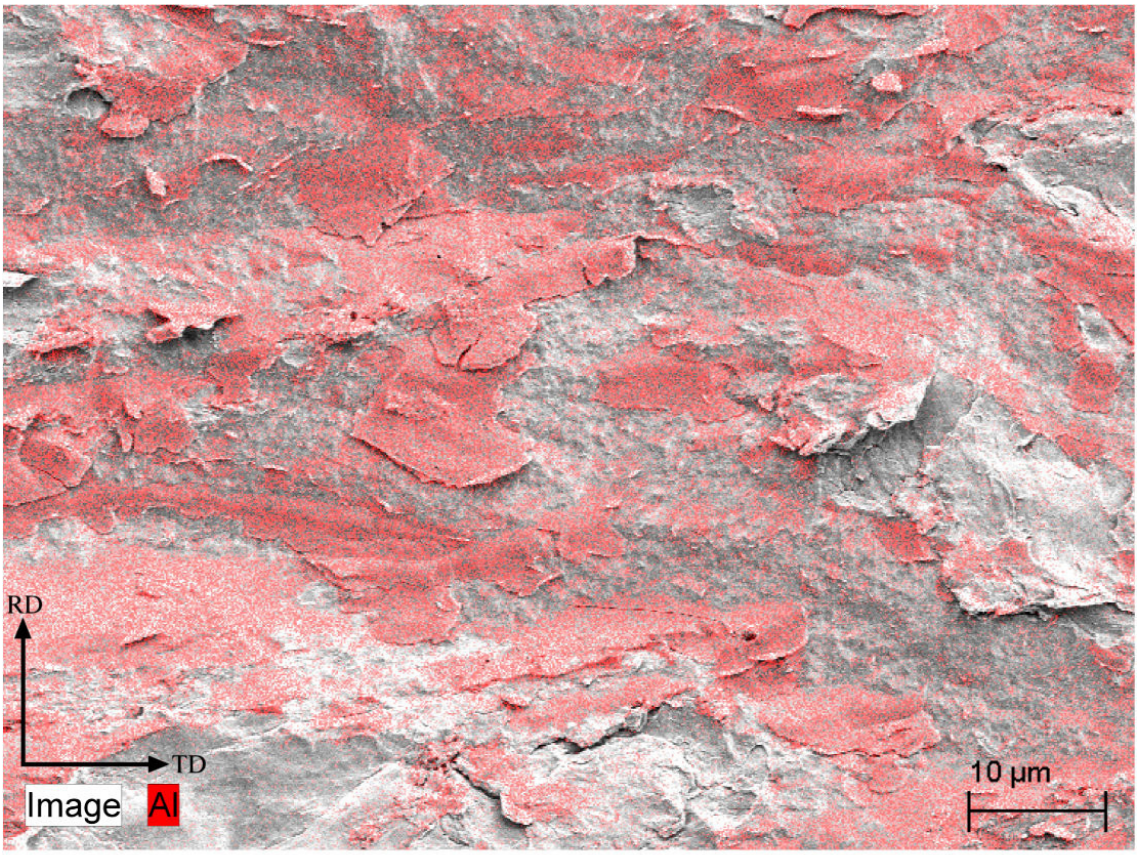

Figure 34: BSA-150 at 1000X, with 5 kV of acceleration voltage. The image shows the steel surface peeled away from the CRB sample, with an overlay of the aluminum signal from an EDS scan. Aluminum appears in patches on the steel substrate, as well as larger flakes.

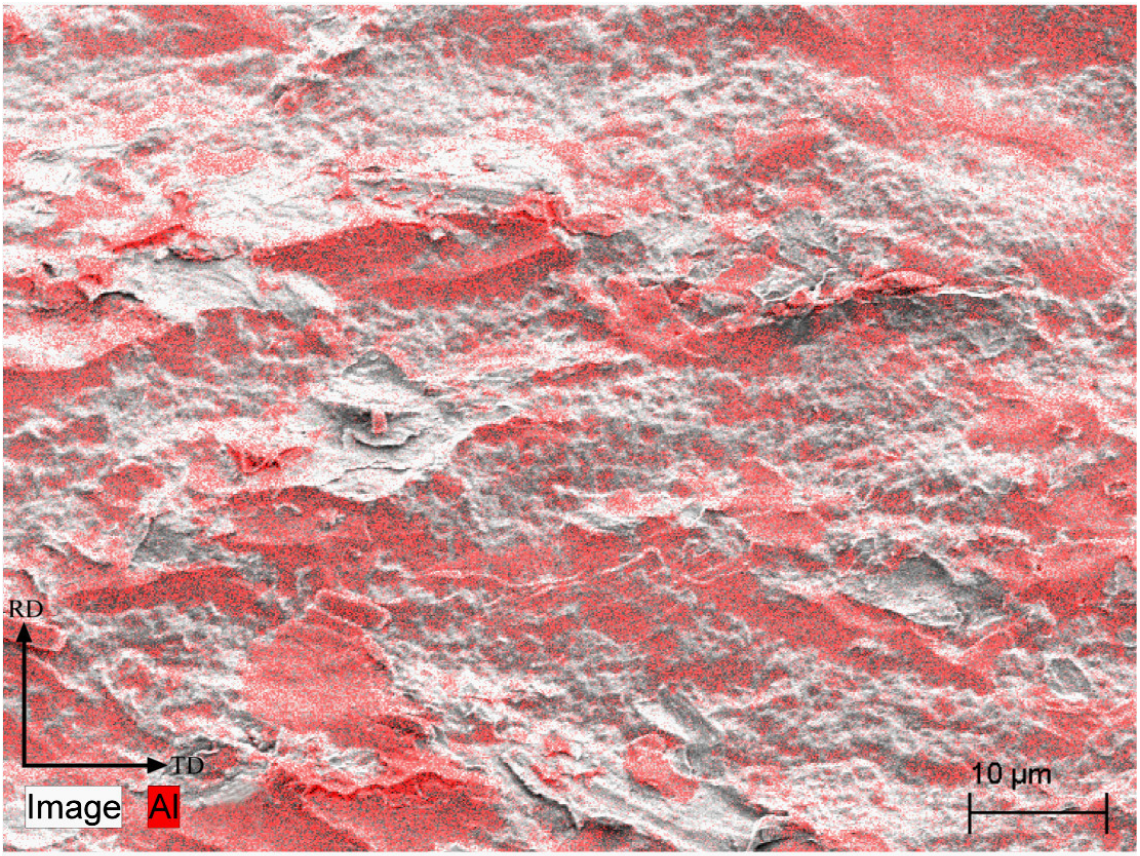

Figure 35: BSA-200 at 1000X, with 5 kV of acceleration voltage. The image shows the steel surface peeled away from the CRB sample, with an overlay of the aluminum signal from an EDS scan. Aluminum appears in patches on the steel substrate.

Figure 36 shows a scan of the opposite fracture surface; the aluminum layer on the remaining CRB specimen. Only iron was recorded in this scan, to detect the relative amounts left on the aluminum surface. This image was produced with an acceleration voltage of 10 kV rather than 5 kV, as required to excite the iron. The image shows a thin layer of evenly distributed iron, indicated by the green tint covering the image, as well as a few particles with higher concentrations of iron. Also visible are a few areas that appear void of any iron, and where the aluminum appears plastically deformed.

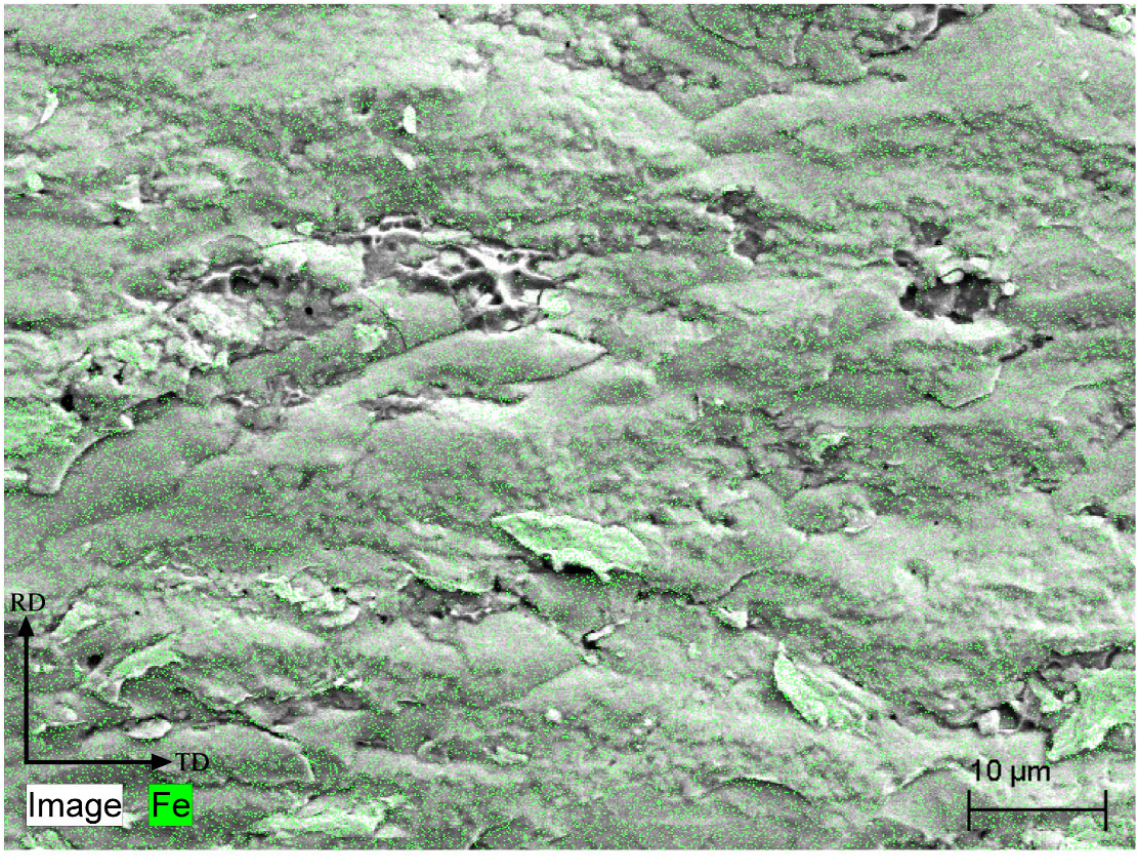

Figure 36: BSA-150 at 1000X, with 10 kV of acceleration voltage. The image shows the aluminum fracture surface, with an overlay of the iron signal from the EDS scan. An even distribution of iron is indicated by the green tint covering the image. A few particles with higher concentrations of iron are visible, as well as areas void of iron, and where the aluminum appears plastically deformed.

4.3.3 Mechanical characterization

Hardness

Figure 37 shows the ageing curve from a BSA-150 sample. The sample reached T6 after approximately 2 hours, significantly faster than what was found for the extruded raw material. An average hardness of 123 HV was found after 2 hours of ageing. Similarly, a hardness of 122 HV was achieved for the BSA-200 samples.

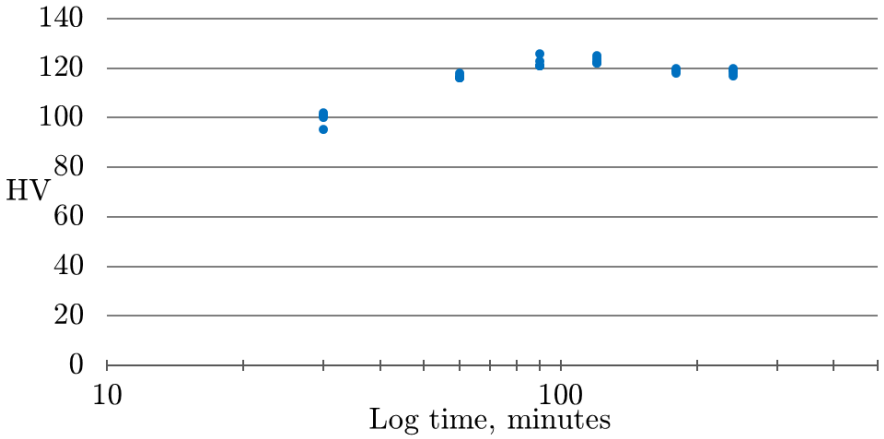

Figure 37: Ageing curve produced from a BSA-150 sample, after ageing at 185 ^{o}C. T6 is reached after approximately 2 hours, with a hardness of 123 HV.

Peel strength

Peel testing was conducted with a peel testing rig mounted in a tensile testing machine. The force required to peel off a steel layer, as well as the relative peel distance, was plotted in a graph, as seen in Figure 38 and 39. These graphs show results from the BSA-150 and BSA-200 samples, respectively. A set distance at the beginning and end of each sample was disregarded, as most peel specimens required some time to reach a stable value. This effect was more pronounced on the SBA and SAB samples. The graphs show raw data from the peel testing, and a stapled line has been added to show the overall average values. The average peel strengths were found to be 20,7 N and 28,8 N, for the BSA-150 and BSA-200 samples, respectively. When divided by the width of the test specimens, 20 mm, bond strengths of 1,0 N/mm and 1,4 N/mm were found.

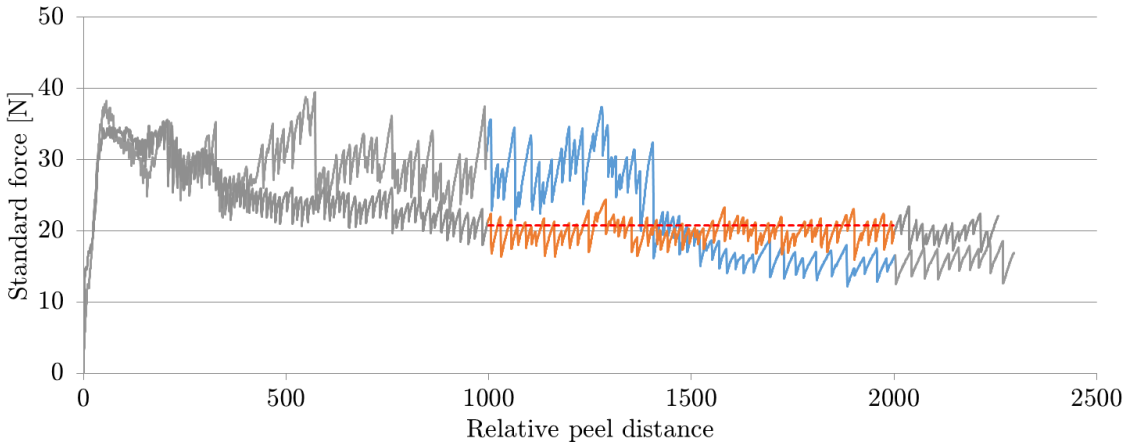

Figure 38: Peel test results for the BSA-150 samples. An average force of 20,7 N was required to delaminate the samples, giving a bond strength of 1,0 N/mm.

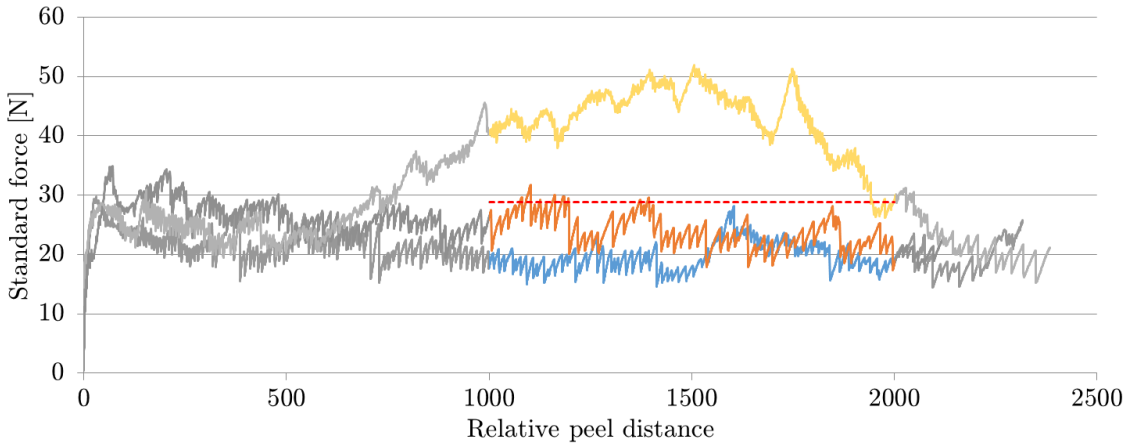

Figure 39: Peel test results for the BSA-200 samples. An average force of 28,8 N was required to delaminate the samples, giving a bond strength of 1,4 N/mm.

4.4 SBA samples

solutionizing	$\longrightarrow$	pre-heating	$\longrightarrow$	CRB	$\longrightarrow$	ageing to T6

4.4.1 Optical microscopy

The microstructure of the aluminum in an SBA-200 sample can be seen in Figure 40. These samples were solutionized prior to the CRB process, and thus they had recrystallized, followed by cold rolling. The resulting grains are elongated in the rolling direction, and show a fairly uneven grain structure.

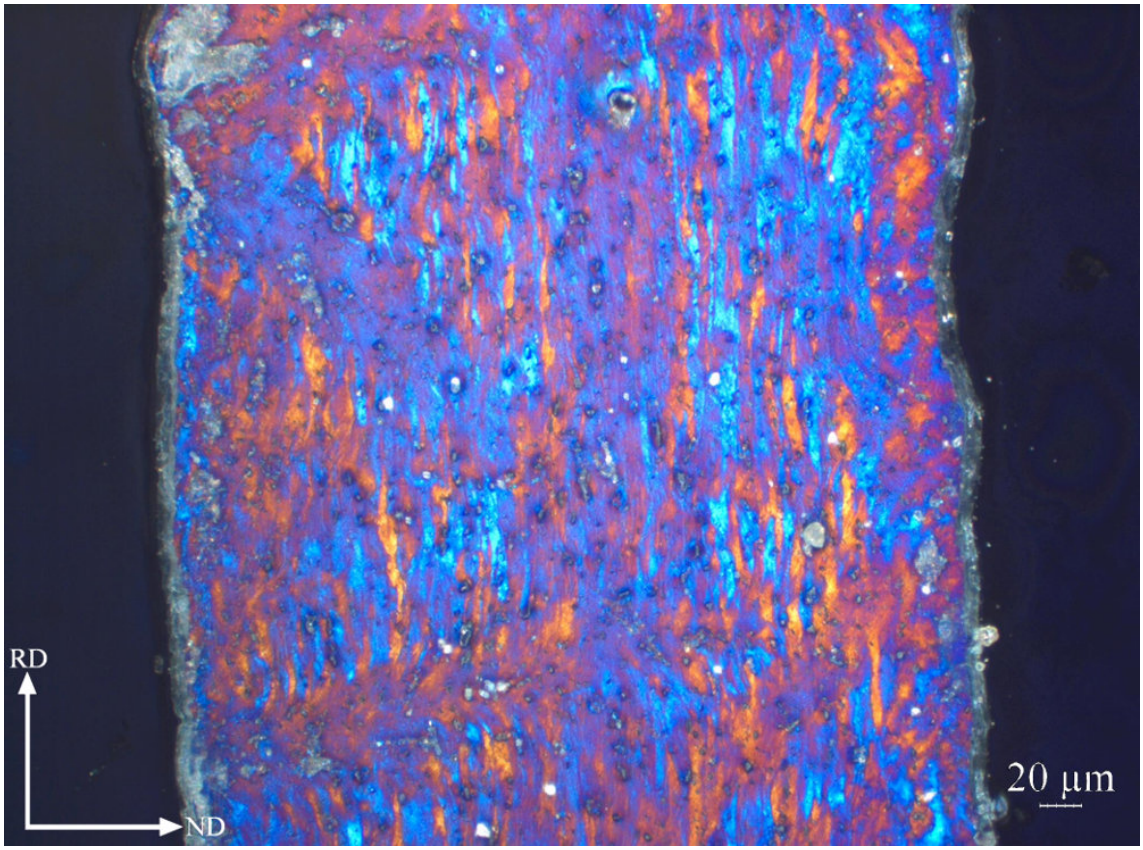

Figure 40: SBA-200 at 200X. The aluminum has recrystallized prior to the CRB process, producing larger grains that are elongated in the rolling direction.

4.4.2 Scanning electron microscopy

SEM images of an SBA-150 sample are provided in Figure 41 and 42, at 1000X and 10.000X magnification, respectively. The images show an interface with a sharp transition between the two metals. Few features are visible at the interface, though a few areas with mechanical interlocking can be seen. Figure 42 shows a feature on the steel interface which may have broken away from the matrix, or which may have been a loose steel fragment embedded at the interface during the CRB process. No intermetallic phases are visible

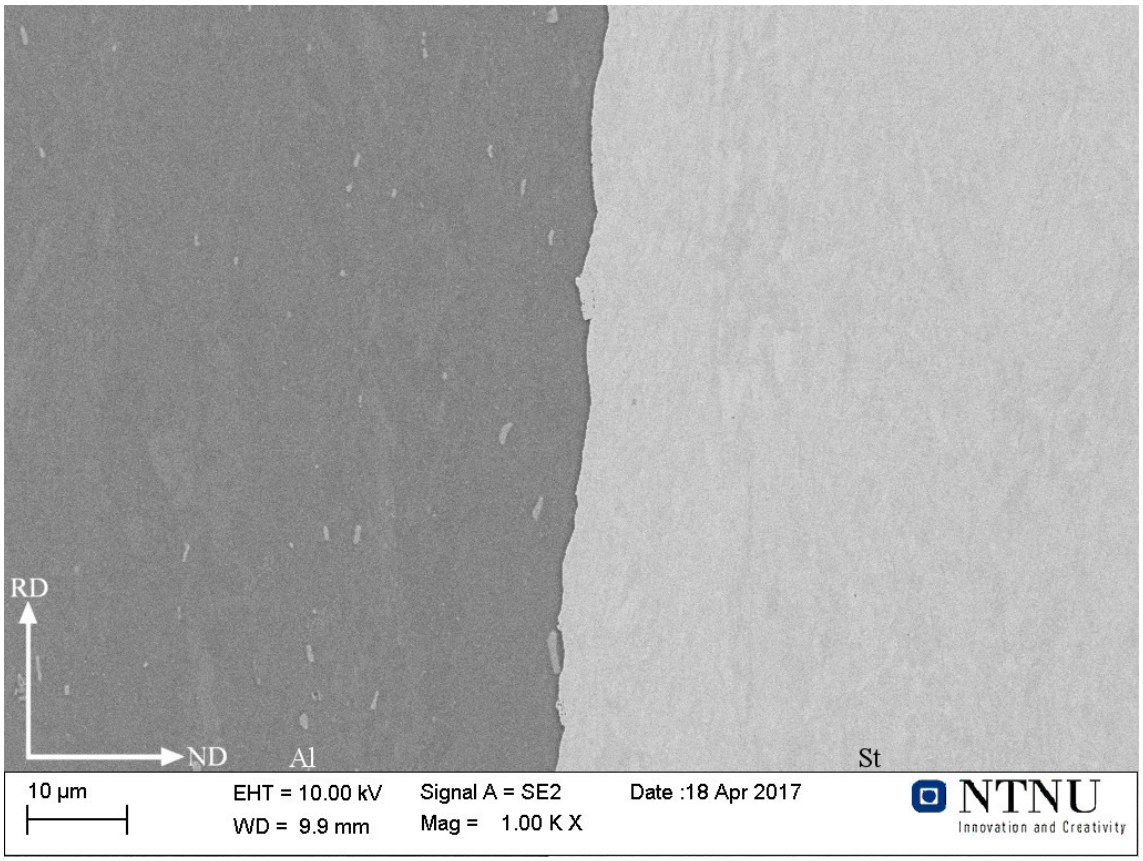

Figure 41: SBA-150 at 1000X, with aluminum on the left and steel on the right. A sharp transition is seen between the two metals, as well as a few points of mechanical interlocking.

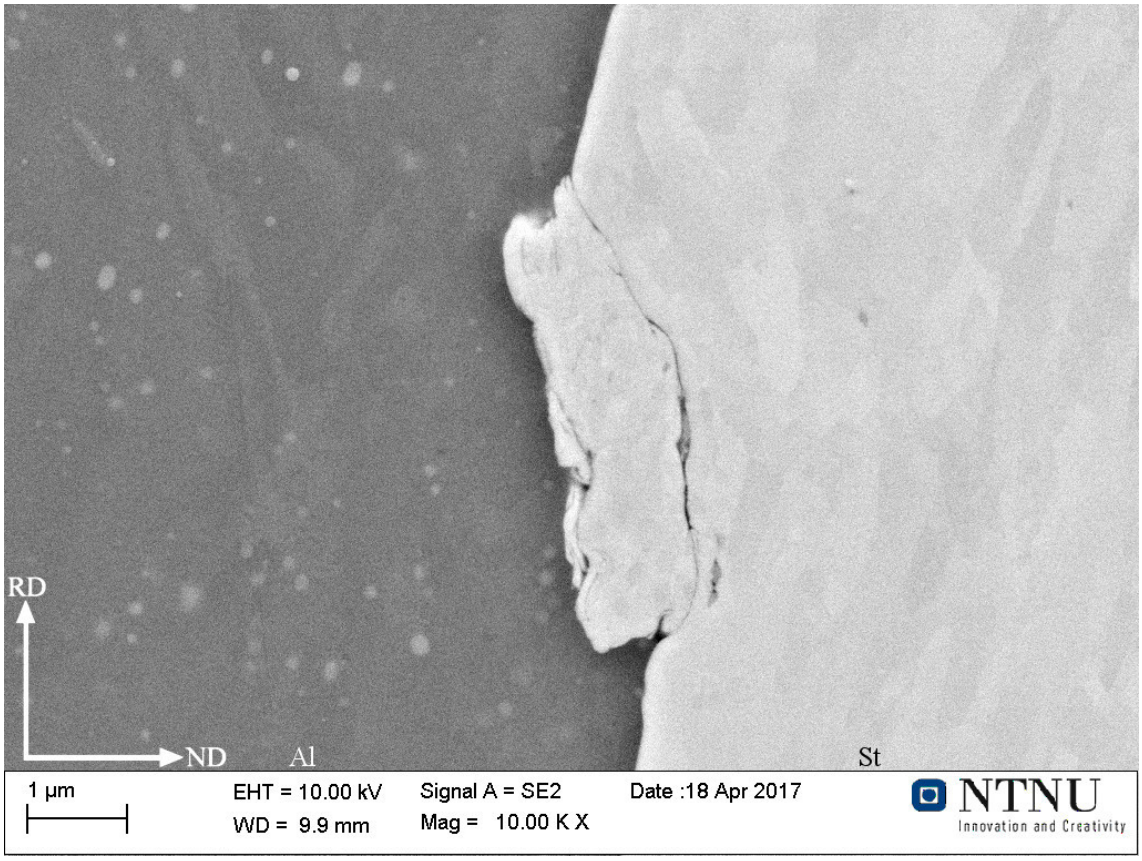

Figure 42: SBA-150 at 10.000X, with aluminum on the left and steel on the right. A large steel particle is visible at the interface, which may have broken off from the steel matrix, or which may have been a loose fragment embedded at the interface during the CRB process.

Images of SBA-200 are provided in Figure 43 and 44, at 1000X and 10.000X magnification, respectively. A sharp transition is seen with few visible features on the interface. At 10.000X magnification, a few jagged edges are visible on the steel side of the interface, likely pieces of the fractured oxide layer. No intermetallic phases are visible

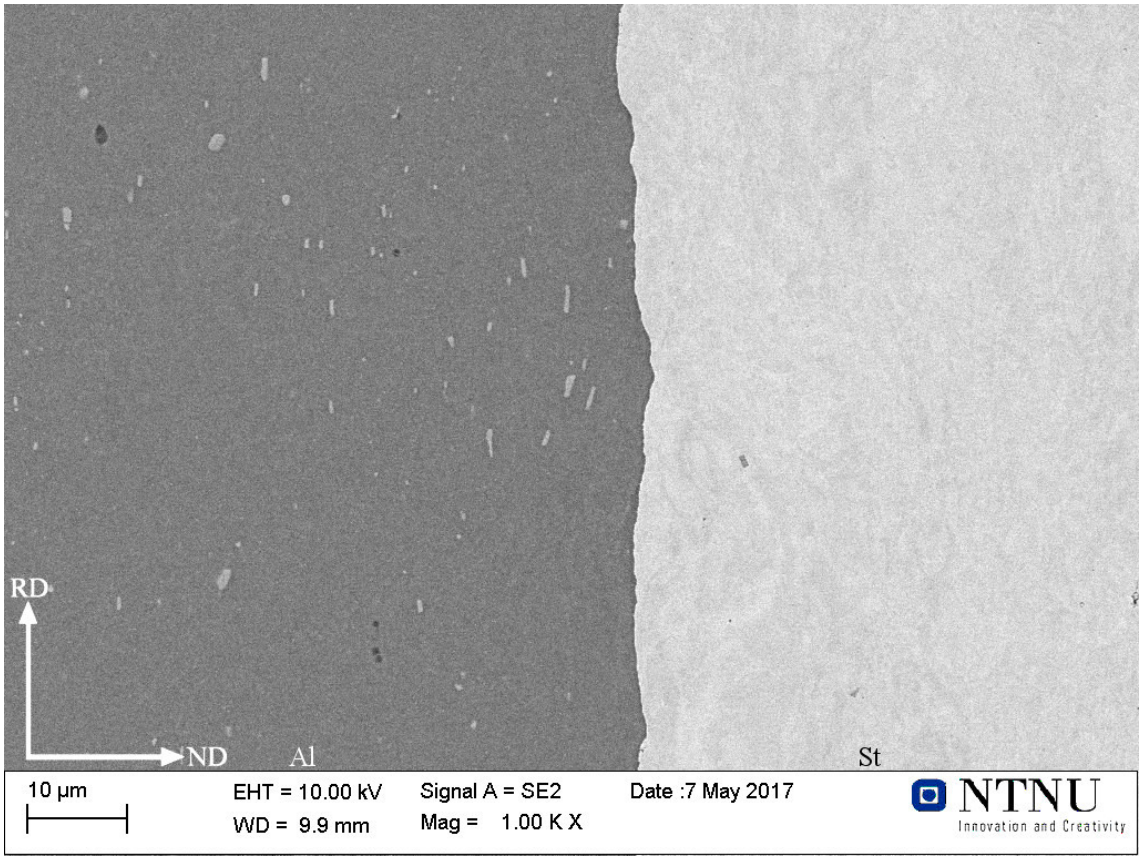

Figure 43: SBA-200 at 1000X, with aluminum on the left and steel on the right. A sharp transition is seen between the two metals, with few notable features. Several particles are visible in the aluminum.

Figure 44: SBA-200 at 10.000X, with aluminum on the left and steel on the right. Several jagged edges are seen sticking out from the steel side of the interface, which may be pieces of the fractured oxide layer. A few grains are visible in the aluminum, as well as several particles.

EDS map of peel test surfaces

The SBA-150 and SBA-200 samples are seen in Figures 45 and 46, respectively. The images were captured from the fracture surface of the steel layers that were peeled away from the CRB samples. Both samples show a clearly defined structure, where a flat steel substrate is covered by ridges of aluminum. The aluminum is gathered in bands stretching in a transverse direction across the surface. These ridges appear to have undergone severe plastic deformation, and show typical signs of a ductile fracture, indicated by dimples and sharp peaks in the aluminum. Measurements were conducted to determine the percent of the steel fracture surfaces covered by aluminum. 38 and 42 % of the SBA-150 and SBA-200 fracture surfaces were found to be covered by aluminum, respectively. Measurements are provided in Chapter 8.3 of the appendix.

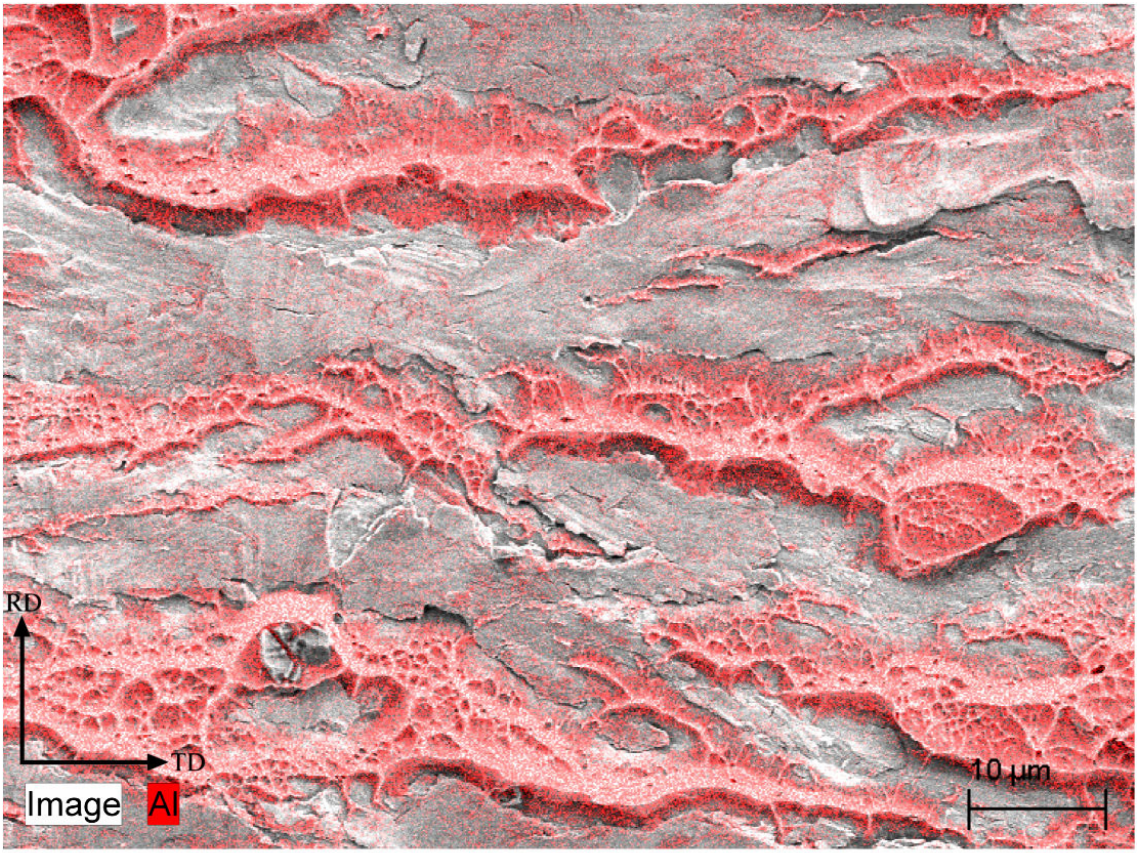

Figure 45: SBA-150 sample at 1000X, with 5 kV of acceleration voltage. A clear steel substrate is seen covered by ridges of aluminum in a transverse direction. The aluminum appears severely plastically deformed, indicated by dimples and sharp peaks in the aluminum.

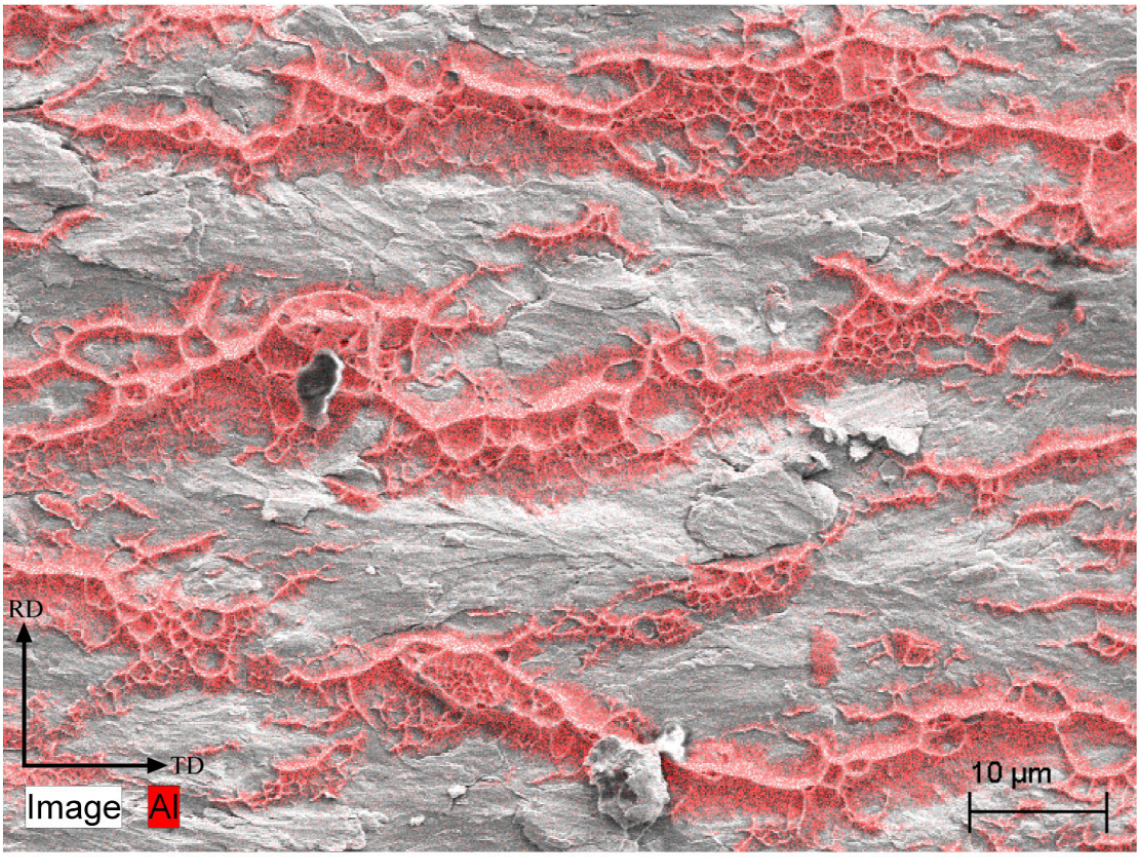

Figure 46: SBA-200 sample at 1000X, with 5 kV of acceleration voltage. A clear steel substrate is seen covered by ridges of aluminum in a transverse direction. The aluminum appears severely plastically deformed, indicated by dimples and sharp peaks in the aluminum.

Figure 47 shows a scan of the aluminum fracture surface. The iron signal from the EDS scan was recorded and indicated by the green color. The image shows a highly deformed aluminum surface with a large amount of dimples, indicating a ductile fracture. Only small amounts of iron are visible on the fracture surface, though a few iron-rich particles are seen embedded in the aluminum.

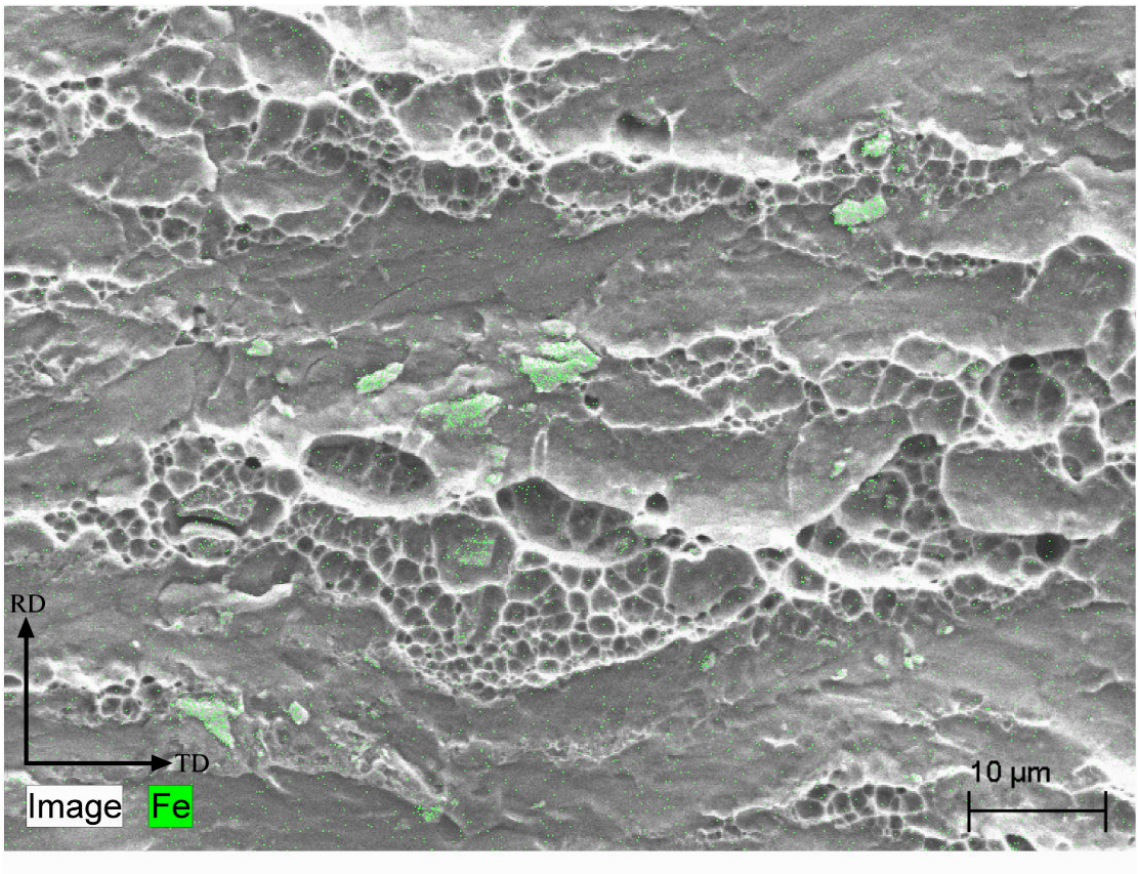

Figure 47: SBA-150 sample at 1000X, with 10 kV of acceleration voltage. The image shows the aluminum fracture surface, with iron indicated by the green color. The fracture surface appears ductile, and embedded with a few iron-rich particles.

4.4.3 Mechanical characterization

Hardness

Five hardness measurements were conducted each on an SBA-150 and an SBA-200 sample. The SBA-150 sample was found to have a hardness of 122 HV in T6, while SBA-200 achieved a hardness of 124 HV. Both samples achieved values of hardness as expected from the aluminum in T6 condition.

Peel strength

Peel test results for the SBA-150 and SBA-200 samples are provided in Figure 48 and 49, respectively. The graphs show the raw data from the peel tests, and an overall average value is shown by the stapled line. The average forces required for delamination were found to be 51,8 N and 59,4 N. When divided by the width of the samples, a bond strength of 2,6 N/mm and 3,0 N/mm were found for the SBA-150 and SBA-200 samples, respectively.

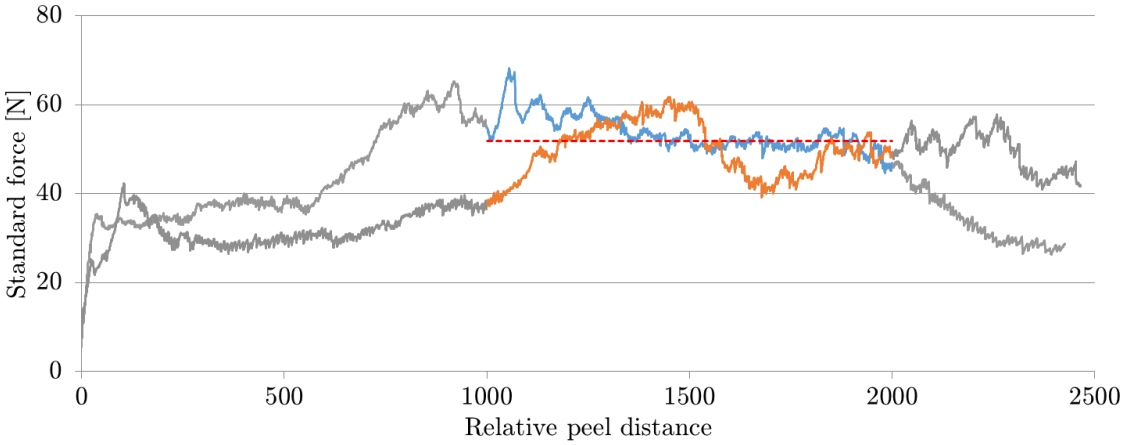

Figure 48: Peel test results for the SBA-150 samples. An overall average force of 51,8 N was required to delaminate the samples, indicated by the dotted line. This gives a bond strength of 2,6 N/mm.

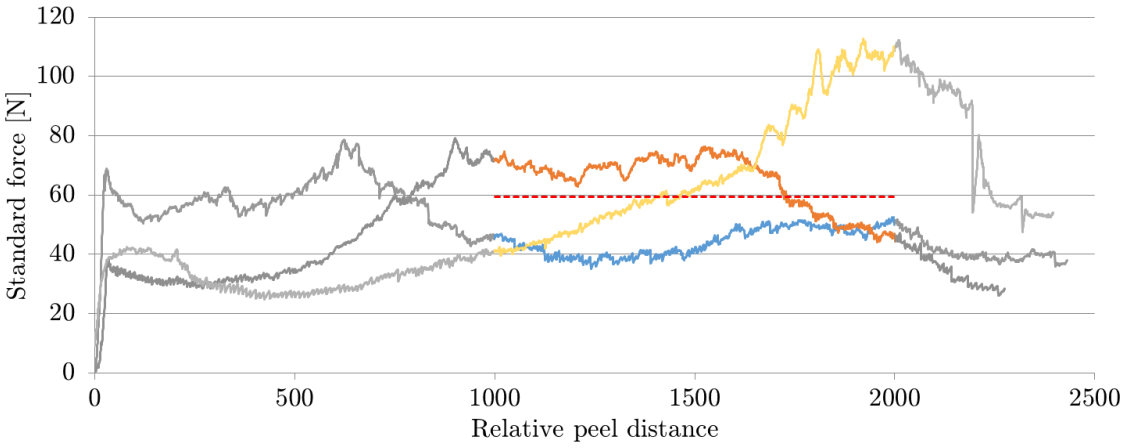

Figure 49: Peel test results for the SBA-200 samples. An overall average force of 28,8 N was required to delaminate the samples, indicated by the dotted line. This gives a bond strength of 3,0 N/mm.

4.5 SAB samples

solutionizing	⟶	ageing to T6	⟶	pre-heating	⟶	CRB

4.5.1 Optical microscopy

The microstructure of an SAB-200 sample can be seen in Figure 50. This sample was solutionized and aged prior to the CRB process. It is evident that the aluminum has recrystallized during solutionizing, resulting in large grains, elongated by the subsequent roll bonding procedure.

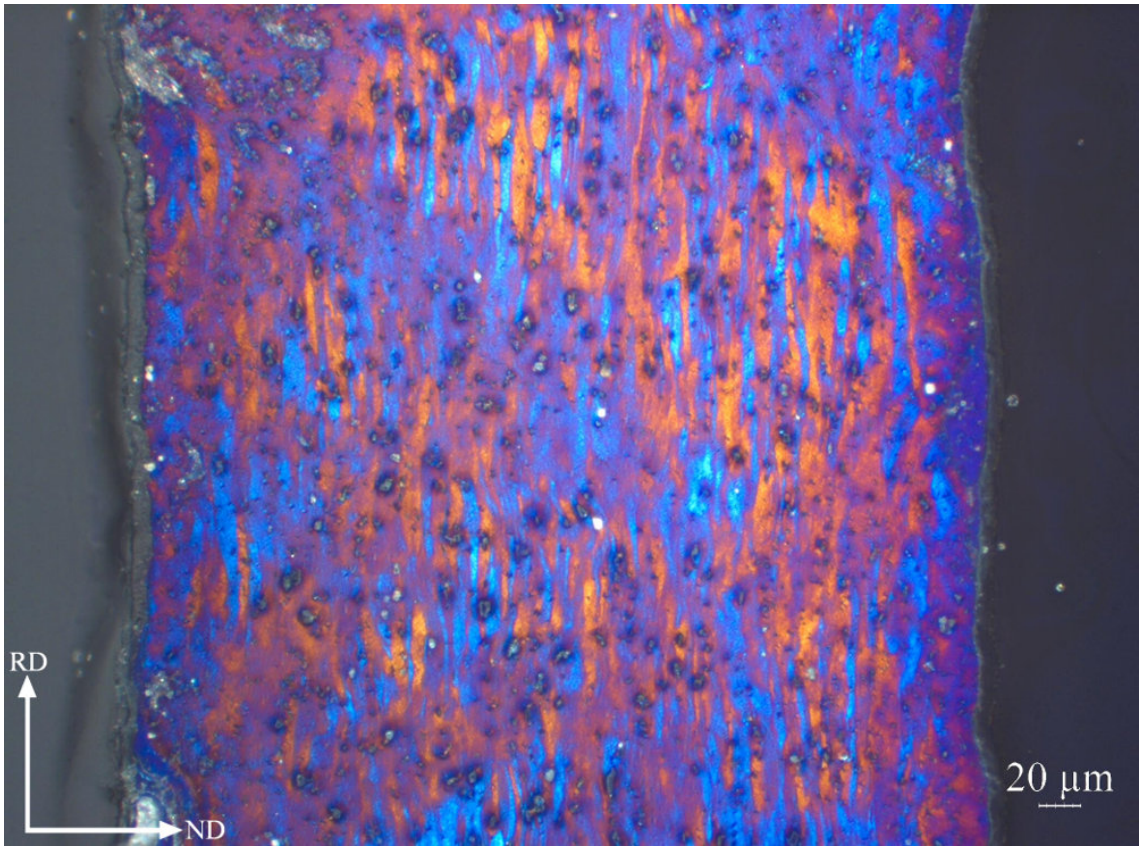

Figure 50: SAB-200 at 200X. The aluminum has recrystallized, resulting in large grains, elongated by the roll bonding procedure.

4.5.2 Scanning electron microscopy

Figure 51 and 52 shows an SAB-200 sample at 1000X and 10.000X magnification, respectively. Images of the SAB-150 samples are not provided, as these samples were not deemed sufficiently strong to conduct any further research. Figure 51 shows a fairly uneven bond, with several features protruding from the surfaces, providing mechanical interlocking. Figure 52 shows a steel fragment at the bond, as well as a large particle embedded in the aluminum surface. Cracks are also seen underneath the steel surface, aligned in the direction of rolling. Again areas of mechanical interlocking are visible. No intermetallic phases are visible in these images.

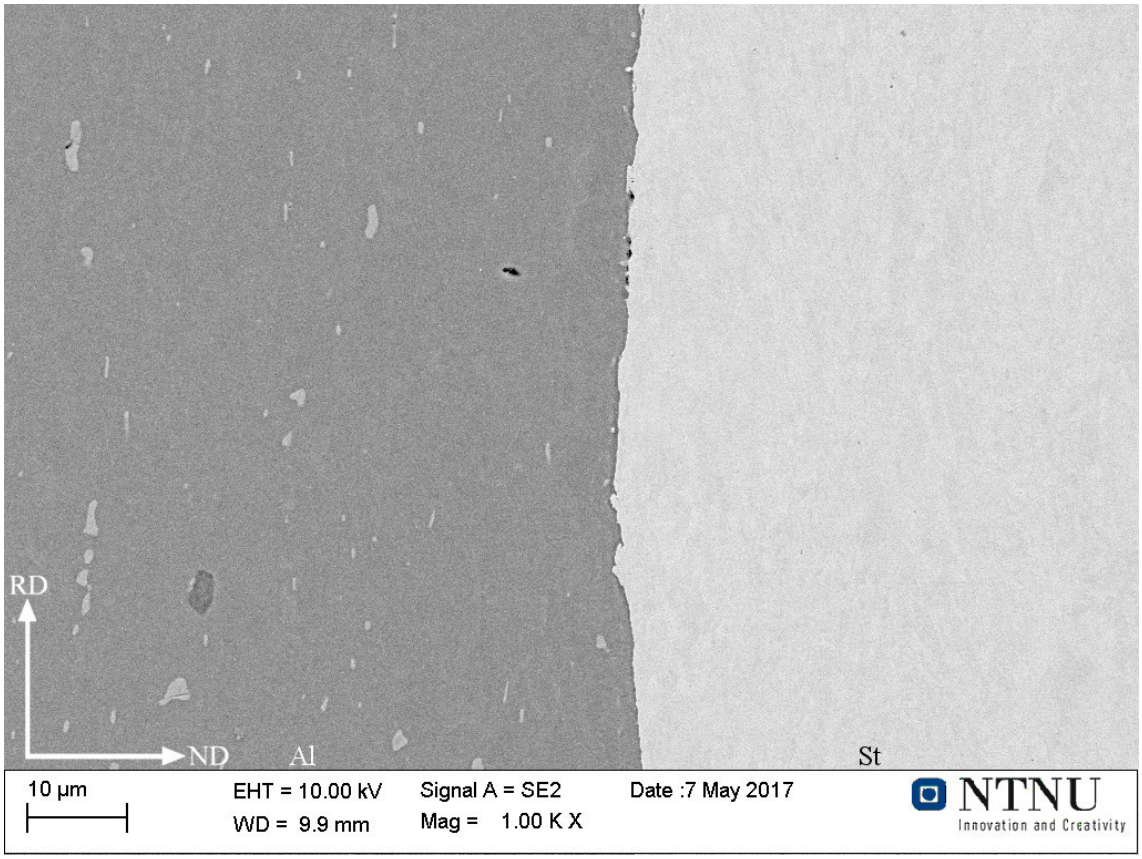

Figure 51: SAB-200 at 1000X, with aluminum on the left and steel on the right. A fairly uneven bond is seen, with several features protruding from the surfaces. Several particles are visible in the aluminum.

Figure 52: SAB-200 at 10.000X, with aluminum on the left and steel on the right. A large steel fragment is seen at the CRB bond, as well as a large particle embedded in the aluminum surface. Cracks are seen underneath the steel surface, following in the direction of rolling.

EDS map of peel test surfaces

Figure 53 shows a fracture surface from the steel layer of an SAB-200 sample. Ridges of aluminum can be seen stretching across the steel substrate, mainly in a transverse direction. Severe plastic deformation and a ductile fracture is indicated by dimples and sharp peaks on the aluminum ridges. 39 % of the steel fracture surface was found to be covered by aluminum. Measurements are provided in Chapter 8.3 of the appendix. Figure 54 shows a scan of the aluminum fracture surface. The iron signal from the EDS scan was recorded and indicated by the green color. The fracture surface appears very ductile, and contains only a small amount of iron. A few small iron-rich particles are visible.

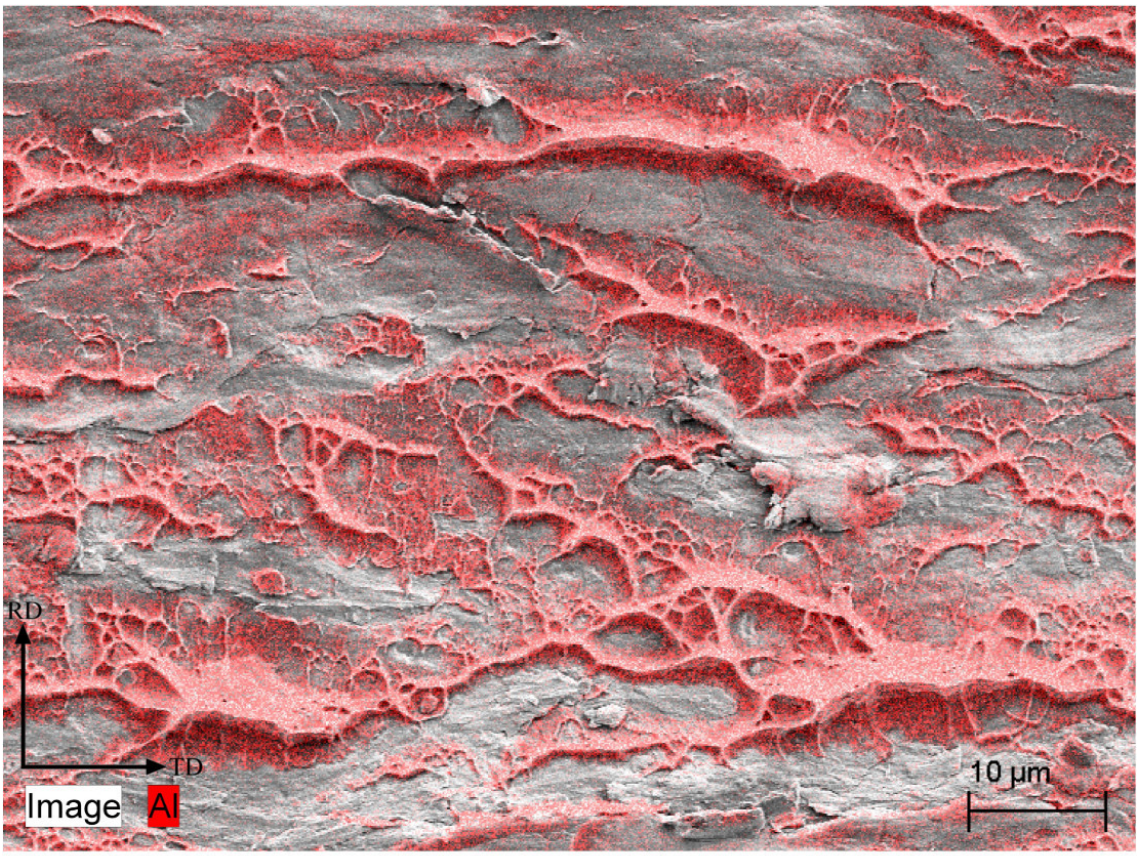

Figure 53: SAB-200 at 1000X, with an acceleration voltage of 5 kV. A steel substrate can be seen covered by ridges of aluminum in a transverse direction. Large plastic deformation is visible in the aluminum.

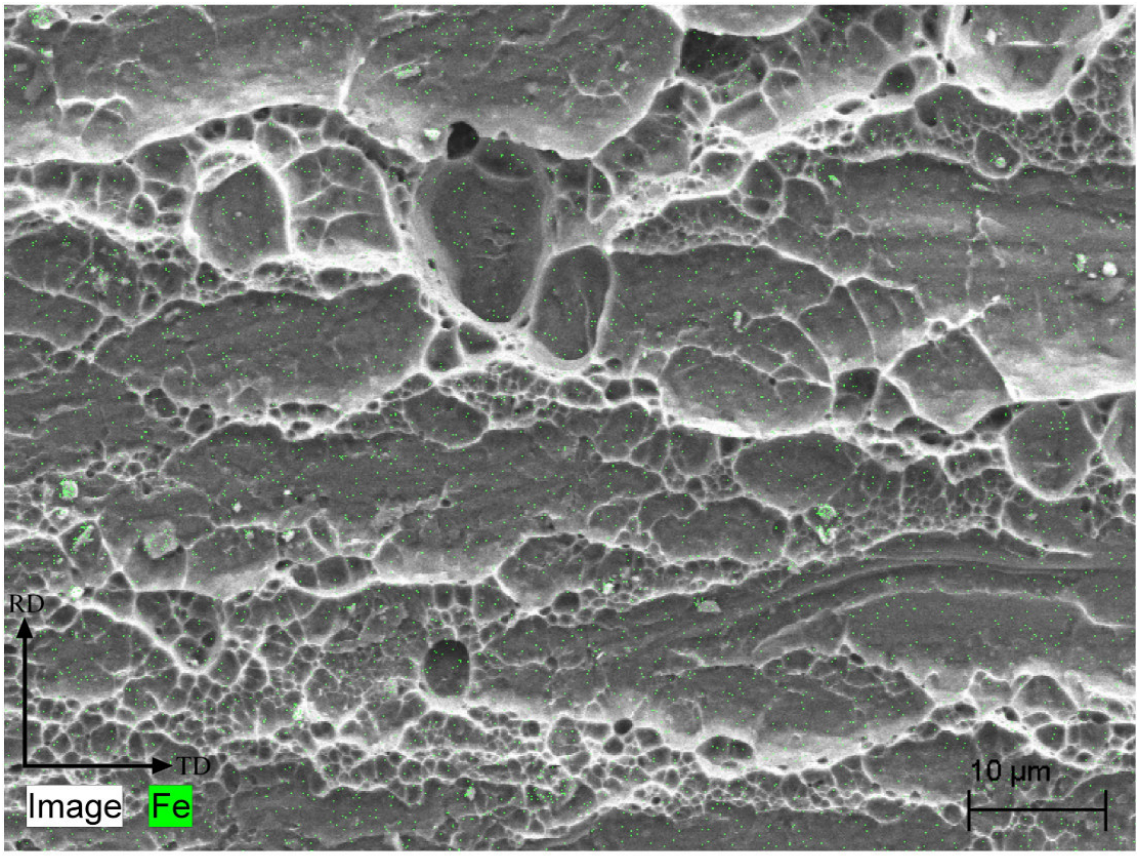

Figure 54: SAB-200 at 1000X, with an acceleration voltage of 10 kV. The image shows the aluminum fracture surface, with iron indicated by the green color. The fracture surface contains very little iron, though a few small iron-rich particles are visible.

4.5.3 Mechanical characterization

Hardness

Hardness measurements were conducted on one of the SAB-200 samples, and on the SAB-300 sample. The SAB-200 sample was found to have a hardness of 136 HV, while the SAB-300 sample had a hardness of 80 HV. Both were aged to T6 prior to the CRB process. The SAB-300 sample had lost all its achieved artificial age hardness, by the time the roll bonding process was completed.

Peel strength

Peel test results for the SAB-200 samples are provided in Figure 55. The graph shows the raw data from peel testing, with an overall average required delamination force of 65,6 N, indicated by the stapled line. When divided by the width of the specimens, a average bond strength of 3,3 N/mm was found.

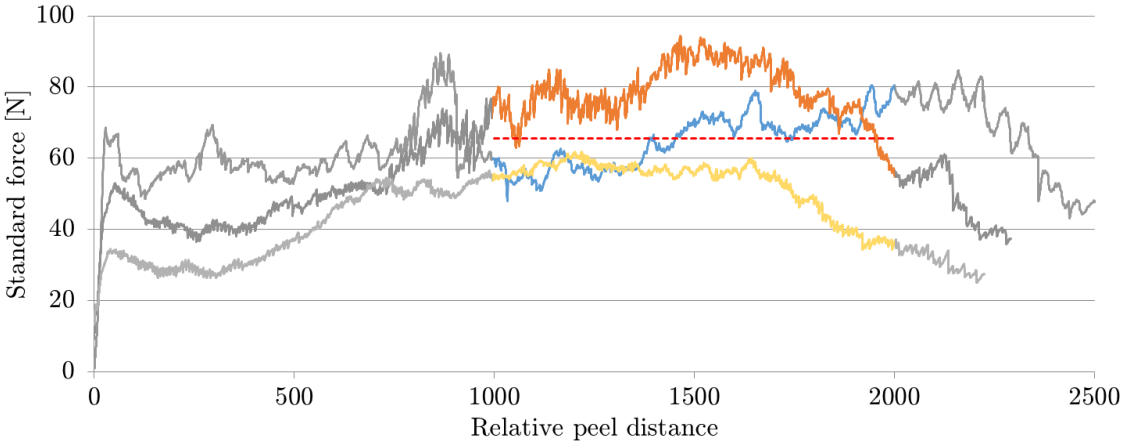

Figure 55: Peel test results for the SAB-200 samples. An average force of 65,6 N was required to delaminate the samples, giving a bond strength of 3,3 N/mm.

5 Discussion

This chapter will include three main topics of interest. First, the influence of the various heat treatment procedures on the samples will be discussed, as producing a composite with the aluminum in T6 condition was one of the main objectives of this thesis. Next, the formation of intermetallic phases are considered, as this has a significant influence on the CRB bond. Finally, the bond strength and bonding mechanisms are discussed.

5.1 The effects of heat treatment

Three different heat treatment sequences were tested for use with cold roll bonding. This was conducted in order to study which parameters produce the best bonding between steel and aluminum. Furthermore, as AA6082 aluminum is commonly aged to T6 condition for industrial applications, achieving this was one of the main goals. Buchner et al. [24] achieved good results by roll bonding an AA6xxx aluminum alloy and IF steel, followed by heat treatment. They further indicated that the optimal heat treatment procedure may be annealing, followed by roll bonding, and then ageing to T6, to optimize both formability and strength of the material [24]. It was thus expected that the BSA and SBA samples would yield good results, while little was known of what to expect for the SAB samples.

A comparison of hardness measurements from the aluminum layer of each sample is provided in Figure 56. All samples, except for the SAB-300 sample, reached hardness values as expected for the AA6082 alloy in T6 condition [25, 26]. Pre-heating the samples at 150 ^{o}C and 200 ^{o}C does not appear to have affected the precipitation hardening of the samples in any negative way. At 300 ^{o}C however, severe over-ageing occurred. Solutionizing of the aluminum was conducted at 540 ^{o}C for 2 minutes. Though this is a very short amount of time [27, 28], it does appear to have solutionized the aluminum sufficiently, as appropriate hardness values were achieved by ageing. Insufficiently solutionized samples were expected to produce lower hardness values, as some ageing potential would be lost [16].

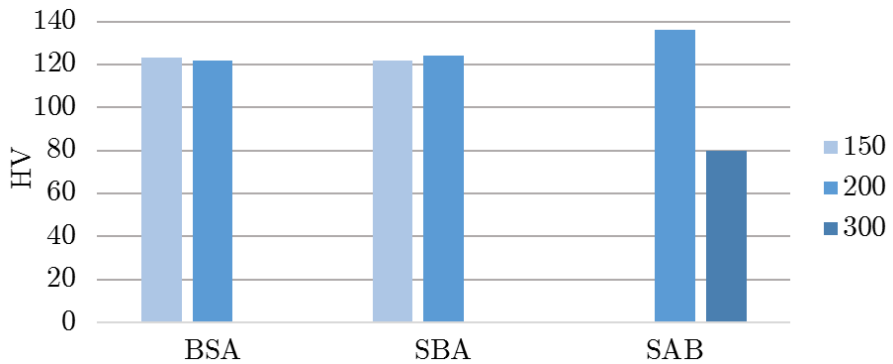

Figure 56: Average hardness values of aluminum in the various CRB samples. Five measurements were taken per sample.

The BSA and SBA samples were subjected to ageing after the CRB procedure. It has been found that post-CRB heat treatment at low temperatures can improve the bond strength of the material [2, 29]. This is likely due to short-range atomic movement that may complete bonding in areas where only partial bonding has taken place [2]. It is hard to evaluate what sort of influence this may have had on the BSA samples, as the solutionizing step was first conducted, causing intermetallic phases to grow. The SBA samples are expected to have gained some bond strength during the ageing step [2].

The SBA samples were roll bonded while in their solutionized state, which may reduce the ageing potential of the material [16]. Cold working reduces ageing potential by introducing dislocations, which can act as vacancy sinks. Vacancies provide nucleation sites for precipitates, and optimizing the number of vacancies is thus favourable to produce a large number of finely dispersed precipitates [16]. The fact that the SBA samples still achieved appropriate hardness values, is likely due to work hardening [28]. Dadbakhsh et al. [28] showed that plastic deformation between the solutionizing and ageing steps, can improve the hardness of AA6082 alloys. The obtained hardness values were strongly dependant on the ageing temperature, where lower temperatures produced greater hardness, as less static recovery took place. With an ageing temperature of 185 ^{o}C, the aluminum likely experienced a slight improvement in hardness due to work hardening [28].

The two SAB samples produced vastly different results. The aluminum in the SAB-200 sample reached an average hardness of 136 HV, much greater than what could be achieved by ageing alone [25, 26]. This effect was due to work hardening during the roll bonding procedure [28]. Conversely, the SAB-300 sample was reduced to 80 HV by the time the CRB process was completed. This is likely due to the high pre-heat temperature, which may have been elevated even further by the adiabatic heating experienced as it deformed [22]. Additionally, after roll bonding, the SAB-300 sample was left to air-cool, presumably recovering from any work hardening achieved [28, 30], while the samples rolled at 200 ^{o}C were quenched in water.

5.2 Intermetallic phases

Intermetallic phases were of particular interest due to the large influence they may have on the properties of a steel-aluminum bond [5]. These phases were expected to form on the BSA samples, due to the high temperature applied during solutionizing [29]. The intermetallic phases were however not expected to affect the bond strength in any significant way. Buchner et al. [24] conducted mechanical tests after similar heat treatment procedures, and no detrimental effects were found to be associated with the thin intermetallic layers formed. The SBA and SAB samples were not expected to form any measurable amount of intermetallic phases, due to the low temperatures they were subjected to after roll bonding [29].

An EDS point scan, as seen in Figure 31, was carried out to study the change in chemical composition across the CRB interface of the BSA-150$_{sol}$ sample. An acceleration voltage of 10 kV was applied. This was roughly the lowest applicable voltage that would still excite iron atoms sufficiently [31]. At this voltage, the spatial resolution in aluminum may be as low as 1,09 μm, due to the substantial penetration depth of the electron beam [31]. Though the spatial resolution potentially was poor, it does not appear to have interfered with the results. One would expect this interference to manifest itself as blurred transitions between the different phases, as the points closest to the interface would detect both sides of the interface at once [32]. Instead, sharp transitions were observed, suggesting that a fairly accurate representation of the chemical composition in each point was found, rather than a larger area around them.

Several brittle intermetallic phases may form between steel and aluminum. This applies to the aluminum-rich phases in particular, such as Fe_2Al_5 and $FeAl_3$ [4]. The fact that iron is prone to diffuse into aluminum, and not the other way around, ensures that aluminum-rich phases are likely to form [4]. The EDS point scan revealed that the intermetallic phases in the BSA-150$_{sol}$ sample had a chemical composition of roughly 75 - 85 at.% aluminum. The region at around 75 % aluminum is where the $FeAl_3$ phase is most likely to form, and it is thus very likely that this phase was present in the BSA samples. As for the SBA and SAB samples, no intermetallic phases were found to be present when studying the samples at 10.000X magnification, though intermetallic layers may still have existed with a thickness below the resolution of the SEM. With the applied magnification and imaging parameters, this resolution was at around 11 nm. As diffusion rates are strongly temperature dependent, it does seem unlikely that intermetallic layers of any measurable thickness would form in the SBA and SAB samples by the temperatures applied [29].

Several authors have stated that thin intermetallic layers do not impact the strength of a steel-aluminum bond [5, 24]. Specifically, intermetallic layers of up to 10 μm have been said to still correspond in strength to that of the aluminum matrix, while layers above this thickness quickly reduce the bond strength [5]. This is in contrast to the results presented, as the phases formed appeared brittle, though they were merely 1 μm thick. Figure 30 in particular, shows a brittle intermetallic layer, where several cracks are present. As the intermetallic layer was developed during solutionizing, the cracks presumably formed due to thermal stresses, caused by the large difference in thermal expansion coefficients between the two metals [29].

5.3 Bond strength

The most important factor when producing cold roll bonded composites, is the achieved bond strength, as this governs the potential suitability of the material for industrial applications. The bond strength of each sample was tested using a peel testing rig, measuring how much force was required to delaminate one of the sheets from the composite. Both the measured force, and the resulting fracture surfaces, could then be evaluated.

The peel test rig was loosely based off the ASTM-D3167-10 standard [23]. However, several simplifications were made to make both the test rig, and specimens, easier to produce. The results obtained can thus not be compared directly to the work conducted by others. Peel test results are in general hard to compare across different experimental setups, as results will be influenced by factors such as thickness and stiffness of the layer being peeled off. Despite this, the peel tests still provided valuable data, and accurate comparisons can be made among the different samples produced for this thesis.

A large deviation was seen in peel strengths between the three rolling procedures, as seen in Figure 57. The BSA samples produced poor results, with an average bond strength of 1,0 and 1,4 N/mm for the BSA-150 and BSA-200 samples, respectively. A large improvement was found for the SBA-150 and SBA-200 samples, at 2,6 and 3,0 N/mm, respectively. The SAB-200 samples provided the highest values, at 3,3 N/mm.

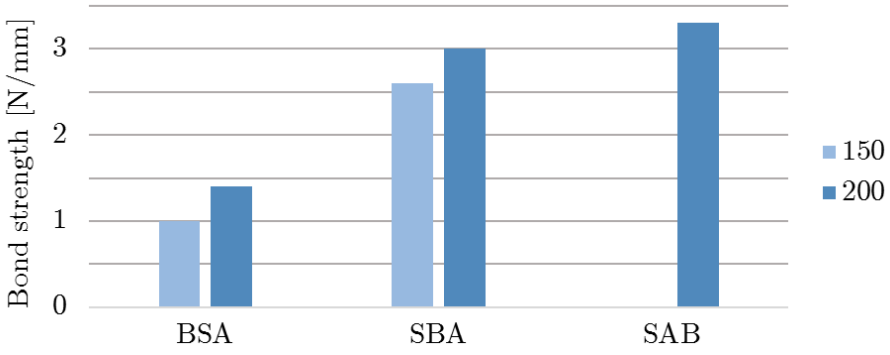

Figure 57: Overall average bond strength results for various CRB procedures.

The peel test results show a clear tendency for samples produced with a higher pre-heat temperature to achieve greater bond strengths. This is consistent with literature, and as expected for cold roll bonding [2, 24]. Despite this, the samples with the highest average bond strengths, only achieved an average of 3,3 N/mm. These are low values, especially considering the relatively large thickness reductions achieved. Typical values of bond strengths at 50 - 60 % reduction, is 6 - 10 N/mm [11, 33], while values as high as 16 and 20 N/mm have been achieved for Al-Al and

Al-304L bonds, respectively [29]. Note that these values were produced using slightly different versions of the peel test rig, and results are thus not expected to coincide fully.

Figure 58 shows a close-up view of the SBA-200 sample at 10.000X, taken from Figure 44. Arrows have been added, pointing to fragments on the bonding interface that are likely pieces of the fractured, work hardened, steel surface layer [11, 34]. During the CRB process, the work hardened surface layers are expected to have fractured, and virgin material extruded through the cracks [34]. Once opposing virgin metal surfaces come into contact, additional pressure causes the actual metallic bond to form [35]. The fracture surfaces, seen in Figure 59, indicates a bond consistent with the work conducted by others [15, 29], and with the film theory in general [34]. Areas of mechanical interlocking were also found to be present at the CRB interfaces, as seen in Figure 58 and 60, which may provide an additional strengthening mechanism for the bond [24].

Due to the large difference in hardness between the two metals, it is likely that the steel surface merely cracked, and that virgin aluminum was extruded into the fractured steel surface [29]. This should apply to the SBA samples in particular, which were roll bonded while the aluminum was in its solutionized state, and thus very soft. Buchner et al. [24] showed that preheating the steel and not the aluminum prior to CRB, increased the bond strength. They further suggested that this was due to the more equal hardness between the two metals, and thus a greater surface expansion of the steel. Optical microscopy images of the samples, provided in Chapter 8.2 of the appendix, indicates that the percent reduction of Aluminum and steel was fairly even for most samples, hence the surface expansion of each metal was fairly equal as well. Consequently, the surface expansion of steel does not seem to be the limiting factor of bonding [24].

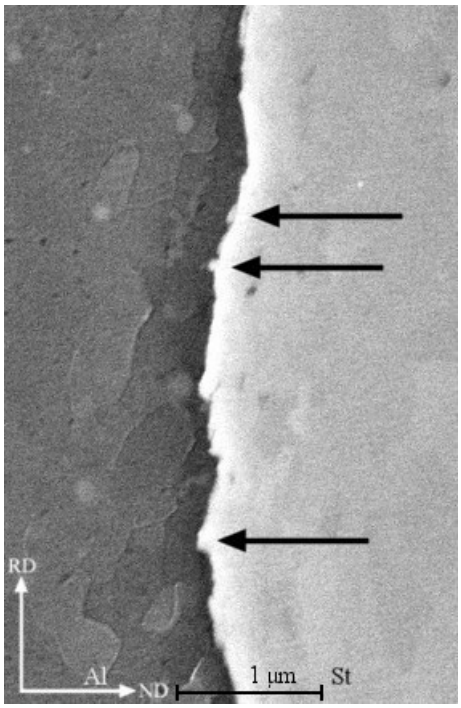

Figure 58: Close-up view from Figure 44, showing an SBA-200 sample at 10.000X. Arrows indicate pieces of the fractured surface layers.

Figure 59 shows EDS scans from the steel and aluminum fracture surfaces of various samples. While the fracture surfaces of the BSA samples have been largely governed by the formation of intermetallic phases, the SBA and SAB samples both show a different mechanism of bonding. Large amounts of aluminum were left on the steel substrates, mainly located in bands stretching in a transverse direction across the surfaces. These stretch lips, as named by A. Lilleby [36], indicates areas where actual bonding has taken place between the two metals.

While the stretch lips have a thin peak caused by a ductile fracture point, the actual region of bonding was likely larger, indicated by the footprint of each stretch lip [22]. By measuring the fraction of the surface covered by stretch lips, the percent of the surface area where actual bonding had taken place, could be estimated. Five lines along the rolling direction were measured. 42 % of the SBA-200 sample was found to be covered by stretch lips, and 39 % of the SAB-200 sample. 38 % was found for the SBA-150 sample, slightly less than for the sample pre-heated to 200 ^{o}C, and likely a reason for the reduced bond strength. Calculations are provided in Chapter 8.3 of the appendix. It could be argued that a large portion of the aluminum left on the SBA and SAB fracture surfaces are merely residual pieces of aluminum not contributing to bond strength. The fact that dimples and ductile fracture points are found in most of the aluminum observed on these samples, suggests that it was bonded to the steel surface with a local bond exceeding the tensile strength of the aluminum matrix. The SAB-200 samples reached a slightly higher peel strength value than the SBA-200 samples, and this may in part be due to the greater strength of the aluminum in the SAB-200 samples. This is indicated by the hardness values, and would suggest that more force would be required to tear off the bonded regions from the aluminum surface in the SAB-200 samples.

The BSA samples likely had an initial bond very similar to what was found for the other two CRB procedures. However, due to the solutionizing step conducted after the CRB process, the interface was altered, namely by the formation of a 1 μm thick intermetallic layer. A large number of small islands of intermetallic regions appear to have formed, which corresponds well with the SEM images taken from the transverse direction, where patches of intermetallic phases are visible. The formation of intermetallic phases thus appear fairly uneven, as large areas of the interface still remain unaffected, as seen in Figure 27 and 29. As the crack induced by peel testing propagated through the CRB interface, it likely experienced no resistance in areas between these intermetallic islands, as the metals were not bonded together. This might be a contributing reason for the low peel strength values observed for the BSA samples. A homogeneous layer of intermetallic phases covering the entire interface, would likely have reduced the local stress concentrations, producing a stronger bond.

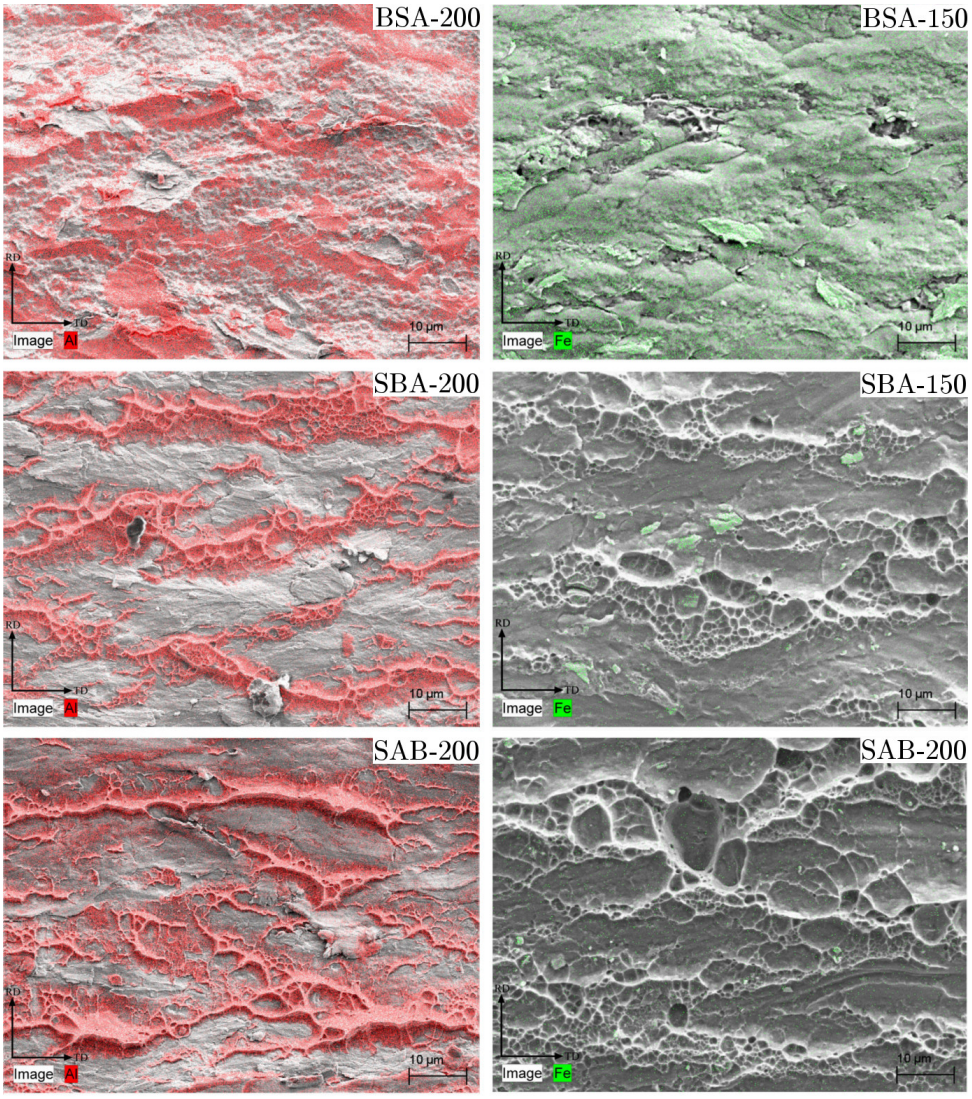

Figure 59: EDS maps at 1000X magnification. The images on the left shows the steel fracture surface of the BSA, SBA, and SAB -200 samples, in descending order. The images on the right shows the aluminum fracture surface on the BSA-150, SBA-150, and SAB-200 samples, in descending order. The red color indicates aluminum, while the green color indicates iron.

The EDS map from the BSA-200 sample, shows a large amount of aluminum left on the steel fracture surface. The aluminum fracture surface, taken from the BSA-150 sample, appears to have an even distribution of iron covering the entire surface, in addition to a few iron-rich particles. This is in contrast to the SBA and SAB samples, which show aluminum fracture surfaces practically void of any iron, except for a few iron-rich particles embedded in the surface. By comparing images of the steel and aluminum fracture surfaces from the BSA samples, it seems as though the fracture has occurred near the center of the intermetallic region, as a mixture of both elements are found on each surface. Akramifard et al. [29] have stated that crack propagation mainly follows the boundary between aluminum and the intermetallic layer, ensuring that the majority of the intermetallic region is left on

the steel fracture surface after debonding [29]. This does not appear to be the case for the BSA samples. Figure 30 shows several fractures in the intermetallic phase, mainly following the center of the region. The fracture may have occurred further into the intermetallic phase due to the chemical composition of the region, which proved to be very aluminum-rich, or simply because of how thin the intermetallic layer was compared to what others have studied [5, 29].

The SAB-150 sample did not achieve a sufficiently strong bond during the CRB process. There may be several contributing reasons for this, mainly related to the T6-condition that the aluminum was in prior to roll bonding. To initiate bonding, an increase in hardness must be introduced to the surface layer [2]. The difference in hardness between this layer and the matrix, is what allows the surface to fracture during roll bonding [2]. As the aluminum was already in its hardened state, the plastic deformation induced by wire brushing may not have work hardened the surface sufficiently. The difference in hardness may have been too limited, and the surface layer may not have fractured adequately, thus inhibiting bonding. The threshold reduction, Rt, defined as the minimum percentage reduction that consistently produces a sound joint, is reduced as rolling temperatures increase [2]. Rt likely exists somewhere above 60 % reduction with a pre-heat temperature of 150 ^{o}C, while it is reduced to below the investigated reductions, for pre-heat temperatures of 200 ^{o}C. Although Rt for the SAB samples may have been higher than for the other two rolling procedures, once proper bonding was achieved, it produced the highest values found in this thesis. This is consistent with literature, as bond strength has been found to increase rapidly as soon as the threshold reduction is surpassed [2, 15].

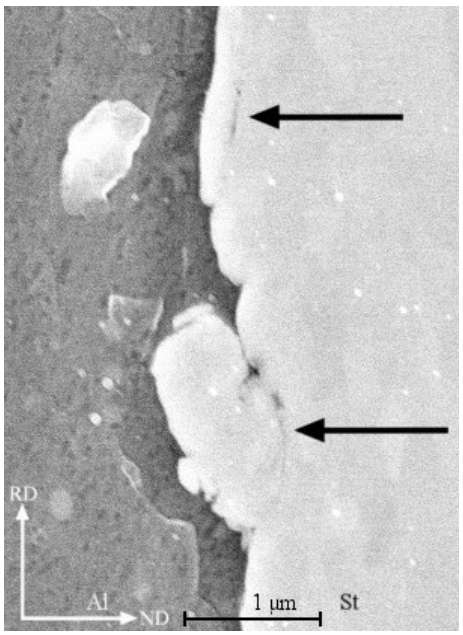

Figure 60: Close-up view from Figure 52, showing a SAB-200 sample at 10.000X. Arrows indicate the location of cracks underneath the work hardened surface.

Wang et al. [11] tested the effects of various surface preparations methods in relation to bond strength, namely wire brushing with 0,1 and 0,3 mm wires, and flap disc. They concluded that the reduction in peel strength associated with wire brushing with 0,3 mm wires, was due to the much greater work hardening experienced at the surface layer of the steel. This resulted in fractures between the work hardened surface layer and the matrix. Images they provided of the aluminum fracture surfaces, showed a large amount of steel embedded in the aluminum surface, as the steel surface had broken off from the matrix. SEM images provided in this thesis show similar cracks underneath the steel surface, namely in Figure 42 and 52. Figure 60 is a close-up view from Figure 52, of the SAB-200 sample. Arrows indicate the location of cracks underneath the surface. EDS scans from the aluminum fracture surface, as

seen in Figure 54, show very little steel embedded in the surface. It thereby seems unlikely that cracks below the work hardened steel surface is the primary reason for the poor bond strengths, as very little steel appears to have been removed from the steel matrix.

6 Conclusion

Three different thermomechanical production procedures have been investigated for an AA6082 - IF steel cold roll bonded composite material. The materials were investigated by microscopy, hardness measurements, and peel testing, to evaluate the quality of the bonds obtained. Conclusions from this work are summarized as follows:

- Roll bonding with the aluminum in T6 condition resulted in the greatest bond strengths, though this procedure also had the highest threshold reduction.
- Roll bonding followed by solutionizing at 540 ^{o}C for 2 minutes, produced an intermetallic layer roughly 1 μm thick. This layer caused a severe reduction in bond strength, as measured by peel testing.
- Ageing samples at 185 ^{o}C for 90 minutes did not produce any intermetallic phases that were measurable by the tests applied.
- For samples with an intermetallic layer, the fracture during peel testing was found to propagate inside the intermetallic region, rather than following the boundary between the aluminum and the intermetallic layer.
- Conducting the roll bonding process while the aluminum was in its solutionized state, did not affect the overall hardness achieved. Though some ageing potential may have been lost, hardness was gained by work hardening of the aluminum.
- Increasing the pre-heat temperature lead to an improvement in bond strength for all samples investigated.
- With a pre-heat temperature of 150 - 200 ^{o}C, reduced ageing times should be used for samples which are partially or fully heat treated prior to the CRB process. For samples which are heat treated after the CRB process, full ageing times apply.
- Roll bonding with a pre-heat temperature of 150 and 200 ^{o}C, did not cause any negative effects in the samples in relation to precipitation hardening of the aluminum. With a pre-heat temperature of 300 ^{o}C, all effects of artificial age hardening were lost.
- In areas where proper bonding were achieved, the local bond strength surpassed the strength of aluminum, causing pieces of the aluminum surface to be ripped off during delamination. Despite this, the overall bond strengths remained low.
- Preparing samples by wire brushing with 0,3 mm wires, did not cause the steel surface layer to break away from the steel matrix.
- The bonding mechanism was found to be in agreement with the film theory.

7 Further work

The following are recommendations for further work that could be conducted in order to gain a deeper understanding of the topics investigated:

- The effects of acetone versus pressurized air as the final step of sample preparation prior to CRB, should be investigated further.
- Samples could be produced using the production parameters presented, but with milder forms of work hardening techniques. Work hardening by wire brushing with finer wires, with a flap disc, or with a belt grinder, could be investigated.
- Low peel strength values were found for all samples produced for this thesis. More experiments should be conducted with cold roll bonding of AA6082 aluminum and IF steel, to see if these materials have a low potential for bonding in general.
- Other mechanical tests, such as tensile shear, and bend testing, could be conducted to evaluate the bond strengths by other loading mechanisms. This would be particularly interesting in regard to samples with intermetallic phases, to see if peel testing loads the specimen in a way that makes the intermetallic phases especially prone to failure. Buchner et al. [24] found no detrimental effects of intermetallic phases by shear and bend testing.
- The BSA samples, which developed intermetallic phases, should also be peel tested directly after the roll bonding process. Though the aluminum would not be artificially aged to T6, valuable results could still be obtained to determine the detrimental effects of intermetallic phases on peel strength.
- The most promising samples; SBA and SAB, should be investigated further to find the optimal production parameters, and to find out which is best suited for subsequent forming in mechanical design.
- Experiments could be conducted where the SBA samples are aged at a lower temperature, as this is expected to improve the hardness of the aluminum [28], and potentially also improve the bond strength [2].

Acknowledgement

I would like to thank my main supervisor, Ida Westermann, and my co-supervisors, Bjørn Holmedal and Siri Marthe Arbo, for all the great help and feedback they provided while I was working on this thesis. An extra thanks to Siri Marthe Arbo for all the hours she spent with me in the laboratory producing samples for this thesis.

Furthermore, I want to thank Pål Skaret for his help with sample production and mechanical testing, Trygve Lindahl Schanche for his help with sample preparation and optical microscopy, Yingda Yu for his help with scanning electron microscopy, and Øystein Gjervan Hagemo, for producing the peel test rig and machining samples.

References

[1] M. F. Ashby. Materials Selection in Mechanical Design, fourth edition. *Elsevier Ltd. 2011.*

[2] Long Li, Kotobu Nagai, Fuxing Yin. Progress in cold roll bonding of metals. *Science and Technology of Advanced Materials, 2008, Vol.9(2), Available from: http://iopscience.iop.org/article/10.1088/1468-6996/9/2/023001/meta;jsessionid=74BC9498D95DB7C7602955C781341470.c6.iopscience.cld.iop.org*

[3] D.R. Lesuer, C.K. Syn, O.D. Sherby, J. Wadsworth, J.J. Lewandowski, W.H. Hunt. Mechanical behaviour of laminated metal composites. *Int Mater Rev 1996;41:169.*

[4] S. Kobayashi, T. Yakou. Control of intermetallic compound layers at interface between steel and aluminum by diffusion-treatment. *Materials Science and Engineering: A, Volume 338, Issues 1–2, 15 December 2002, Pages 44–53*

[5] K.G. Kosch, B.A. Behrens. Challenges in Compound Forging of Steel-Aluminum Parts. *EPD Congress 2012, Metallurgy of Non-Ferrous Metals, Chapter 20, p.169-176*

[6] R. Cao, J. H. Sun, J. H. Chen, P. C. Wang. Cold Metal Transfer Joining of Aluminum AA6061 T6 to Galvanized Boron Steel. *Journal of Manufacturing Science & Engineering, 136(5), Aug 06, 2014. Available from: http://manufacturingscience.asmedigitalcollection.asme.org/article.aspx?articleid=1889283*

[7] F.C. Campbell. Joining : Understanding the Basics. *ASM International, 2011, ch 6.*

[8] Roohollah Jamaati and Mohammad Reza Toroghinejad. The Role of Surface Preparation Parameters on Cold Roll Bonding of Aluminum Strips. *Materials Science and Engineering: Volume 527, Issue 9, 15 April 2010. Available from: http://www.sciencedirect.com/science/article/pii/S0921509309012702*

[9] H. A. Mohamed and J. Washburn. Mechanism of solid state pressure welding. *1975, Available from: https://app.aws.org/wj/supplement/WJ_1975_09_s302.pdf*

[10] R. Jamaati, M. R. Toroghinejad. Cold roll bonding bond strengths: review. *Materials Science and Technology, 27:7, 1101-1108, 2011*

[11] C. Wang, Y. Jiang, J. Xie, D. Zhou, X. Zhang. Effect of the steel sheet surface hardening state on interfacial bonding strength of embedded aluminum–steel composite sheet produced by cold roll bonding process. *Materials Science & Engineering A 652 (2016) 51–58*

[12] Chunyang Wang, Yanbin Jiang, Jianxin Xie, Dejing Zhou, Xiaojun Zhang. Effect of the steel sheet surface hardening state on interfacial bonding strength of embedded aluminum–steel composite sheet produced by cold roll bonding process. *Materials Science and Engineering: A, Volume 652, 15 January 2016, available from: http://www.sciencedirect.com/science/article/pii/S0921509315306298*

[13] M. Soltan Ali Nezhad, A. Haerian Ardakani. A study of joint quality of aluminum and low carbon steel strips by warm rolling. *Materials and Design, Volume 30, Issue 4, April 2009, available from: http://www.sciencedirect.com/science/article/pii/S0261306908003063*

[14] W. D. Callister. Materials Science and Engineering. *John Wiley & Sons, Inc. 7th edition, 2007, ch 19.*

[15] Roohollah Jamaati, Mohammad Reza Toroghinejad. Investigation of the parameters of the cold roll bonding (CRB) process. *Materials Science and Engineering: AVolume 527, Issue 9, Available from: http://www.sciencedirect.com/science/article/pii/S0921509309012702*

[16] R. E. Smallman, A. H. W. Ngan. Modern Physical Metallurgy, eight edition. *Elsevier Ltd. 2013, ch 13, available from: http://www.sciencedirect.com/science/book/9780080982045*

[17] M.Takeda,F.Ohkubo,T.Shirai. Stability of metastable phases and microstructures in the ageing process of Al–Mg–Si ternary alloys. *Journal of Materials Science 1998, Volume 33, Issue 9, pp 2385–2390, available from: http://link.springer.com/article/10.1023/A:1004355824857*

[18] A. Earnshaw, N. Greenwood. Chemistry of the Elements, 2nd edition. *Butterworth-Heinemann, 1997. p. 216–267, available from: http://www.sciencedirect.com/science/article/pii/ B9780750633659500134*

[19] C.D. Marioara, S.J. Andersen, J. Jansen, H.W. Zandbergen. Atomic model for GP-zones in a 6082 Al–Mg–Si system. *Acta Materialia, 2001, Vol.49(2), pp.321-328, available from: http://www.sciencedirect.com/science/article/pii/S1359645400003025*

[20] J.G. Kaufman. Introduction to Aluminum Alloys and Tempers. *ASM International, 2000, ch 2, available from: http://ebookcentral.proquest.com/lib/ntnu/detail.action?docID=3002316*

[21] Ø. Ryen. Work Hardening and Mechanical Anisotropy of Aluminium Sheets and Profiles. *Master's thesis, NTNU, 2004*

[22] S. Lauvdal. Experimental Studies of Cold Roll Bonded Aluminum Alloys. *Master's thesis, NTNU, 2011*

[23] ASTM-D3167-10. Standard Test Method for Floating Roller Peel Resistance of Adhesives. *ASTM International, West Conshohocken, PA, 2010, available from: https://www.astm.org/Standards/D3167.htm*

[24] M. Buchner, B. Buchner, B Buchmayr, H. Kilian, F. Riemelmoser. Investigation of different parameters on roll bonding quality of aluminum and steel sheets. *Int. Journal of Material Forming, 2008, Vol.1, pp.1279-1282*

[25] O. Sulen. A TEM Study of Weakly Overaged Precipitates in AA 6082. *Master's thesis, NTNU, 2016*

[26] Ø. Ryen, B. Holmedal, K. Marthinsen, T. Furu. Precipitation, strength and work hardening of age hardened aluminium alloys. *Materials Science & Engineering, 2015, Vol.89. Available from: http://iopscience.iop.org/article/10.1088/1757-899X/89/1/012013/pdf*

[27] N. Kumar, S. Goel, R. Jayaganthan, H. G. Brokmeier. Effect of Solution Treatment on Mechanical and Corrosion Behaviors of 6082-T6 Al Alloy. *Metallography, Microstructure, and Analysis, October 2015, Volume 4, Issue 5, pp 411–422, available from: https://link.springer.com/article/10.1007/s13632-015-0219-z*

[28] S. Dadbakhsh, A. Karimi Taheri, C.W. Smith. Strengthening study on 6082 Al alloy after combination of aging treatment and ECAP process. *Materials Science & Engineering A, 15 July 2010, Vol.527(18-19), pp.4758-4766. Available from: http://iopscience.iop.org/article/10.1088/1757-899X/89/1/012013/pdf*

[29] H.R. Akramifard, H.Mirzadeh, M.H.Parsa. Cladding of aluminum on AISI 304L stainless steel by cold roll bonding: Mechanism, microstructure, and mechanical properties. *Mat. Science and Engineering: A, Vol. 613, 2014, P. 232–239, available from: http://www.sciencedirect.com/science/article/pii/S0921509314008375*

[30] N. Kumar, R jayaganthan, H. G. Brokmeier. Effect of deformation temperature on precipitation, microstructural evolution, mechanical and corrosion behavior of 6082 Al alloy. *Transactions of Nonferrous Metals Society of China, Volume 27, Issue 3, March 2017, Pages 475–492. Available from: http://www.sciencedirect.com/science/article/pii/S1003632617600554*

[31] B. Hafner. Energy Dispersive Spectroscopy on the SEM: A Primer. *Characterization Facility, University of Minnesota*

[32] J. Hjelen. Scanning elektron-mikroskopi. *SINTEF, Avdeling for metallurgi, Metallurgisk institutt, NTH, 1986*

[33] B. Wu, L. Li, C. Xia, X. Guoc, D. Zhou. Effect of surface nitriding treatment in a steel plate on the interfacial bonding strength of the aluminum/steel clad sheets by the cold roll bonding process. *Mat. Science & Engineering A, 2017, Vol.682, pp.270-278, available from: http://www.sciencedirect.com/science/article/pii/S0921509316314046*

[34] N. Bay. Mechanisms Producing Metallic Bonds in Cold Welding. *Weld. Res. Suppl. 5 137, 1983, available from: https://app.aws.org/w/r/wj/supplement/WJ_1983_05_s137.pdf*

[35] M. Samandari, K. Abrinia, A. Akbarzadeh, H. A. Bulaqi, G. Faraji. Properties and Mechanism of Al/St Bimetal Tube Bonding Produced by Cold Spin-Bonding (CSB) Process. *Trans Indian Inst. Met. 2017*

[36] A. Lilleby. Experimental and Finite Element Studies of Cold Pressure Welding of Commercial Purity Aluminium by Divergent Extrusion. *Doctoral thesis, NTNU, 2009*

8 Appendix

8.1 Peel test samples

Table 7: Complete list of all peel test samples produced for this thesis, including percent total thickness reductions. The resulting lengths were measured on the steel sheets, with an initial length of 120 mm.

Sample	CRB temp.	Init. thickness	Res. thickness	Reduction %	Res. length
BSA_1	150 ^{o}C	2,95 mm	1,10 mm	63 %	298 mm
BSA_2	150 ^{o}C	2,95 mm	1,06 mm	64 %	310 mm
SBA_1	150 ^{o}C	2,95 mm	1,03 mm	65 %	305 mm
SBA_2	150 ^{o}C	2,95 mm	1,03 mm	65 %	305 mm
BSA_1	200 ^{o}C	2,95 mm	1,07 mm	64 %	300 mm
BSA_2	200 ^{o}C	2,93 mm	1,15 mm	61 %	270 mm
BSA_3	200 ^{o}C	2,95 mm	1,05 mm	64 %	310 mm
SBA_1	200 ^{o}C	2,95 mm	1,02 mm	65 %	315 mm
SBA_2	200 ^{o}C	2,95 mm	1,04 mm	65 %	315 mm
SBA_3	200 ^{o}C	2,95 mm	1,04 mm	65 %	312 mm
SAB_1	200 ^{o}C	2,95 mm	1,07 mm	64 %	300 mm
SAB_2	200 ^{o}C	2,95 mm	1,20 mm	59 %	260 mm
SAB_3	200 ^{o}C	2,92 mm	1,12 mm	62 %	280 mm

8.2 Thickness reductions

The following are images of samples used to calculate the percent thickness reduciton of each metal. All calculations assume an initial thickness of 1 mm for the steel, and 0,9 mm for the aluminum.

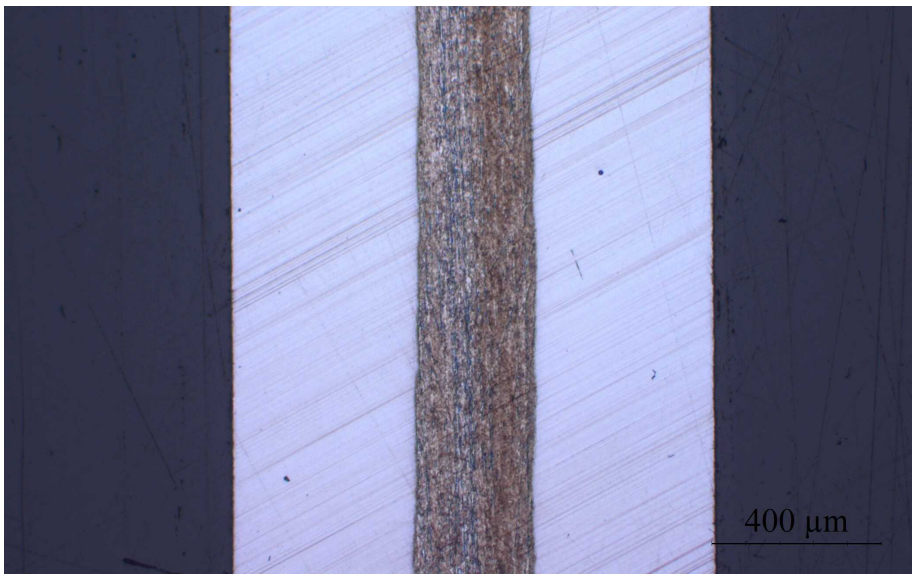

Figure 61: BSA-150 at 50X. The aluminum was reduced to 0,28 mm, while the steel was reduced to an average of 0,43 mm, giving a percent reduction of 69 % and 57 %, respectively.

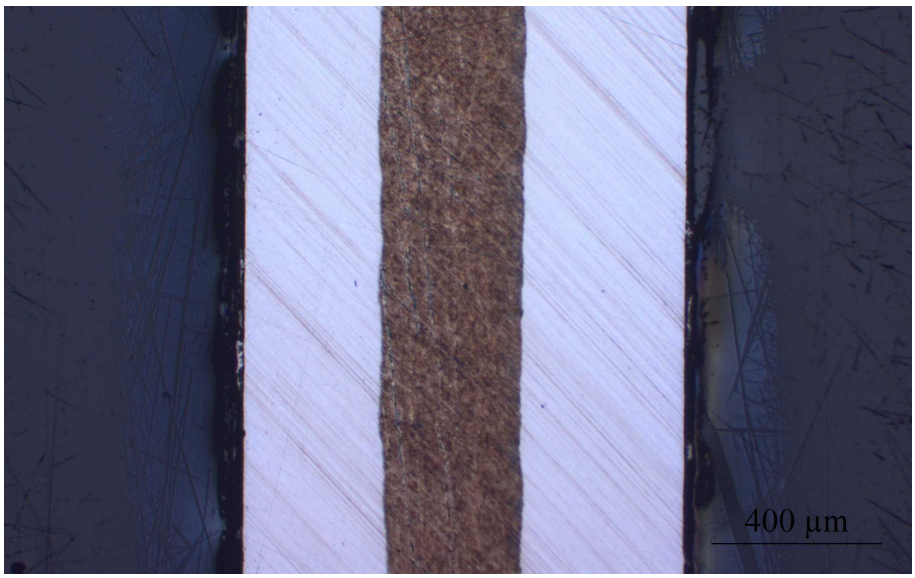

Figure 62: BSA-200 at 50X. The aluminum was reduced to 0,34 mm, while the steel was reduced to an average of 0,35 mm, giving a percent reduction of 62 % and 65 %, respectively.

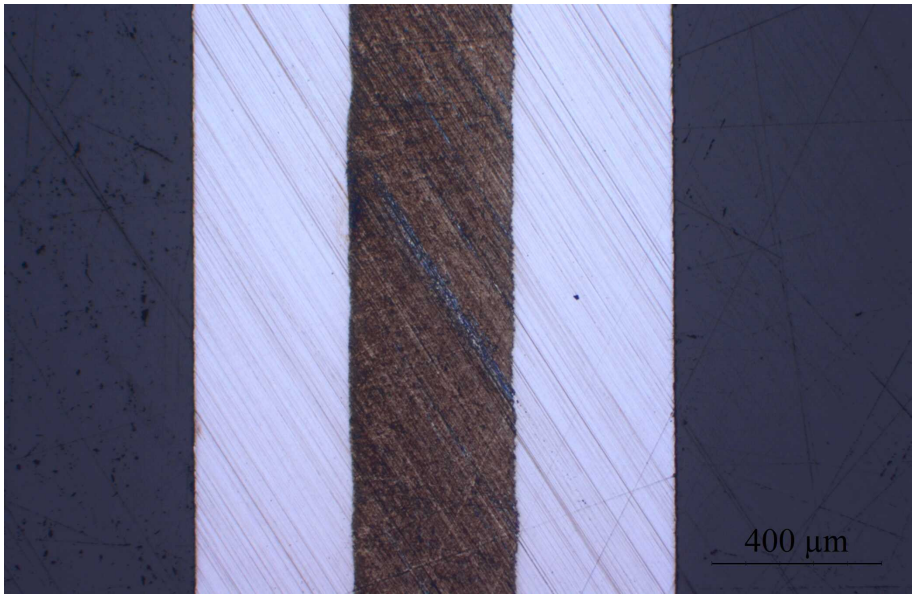

Figure 63: SBA-150 at 50X. The aluminum was reduced to 0,39 mm, while the steel was reduced to an average of 0,37 mm, giving a percent reduction of 57 % and 63 %, respectively.

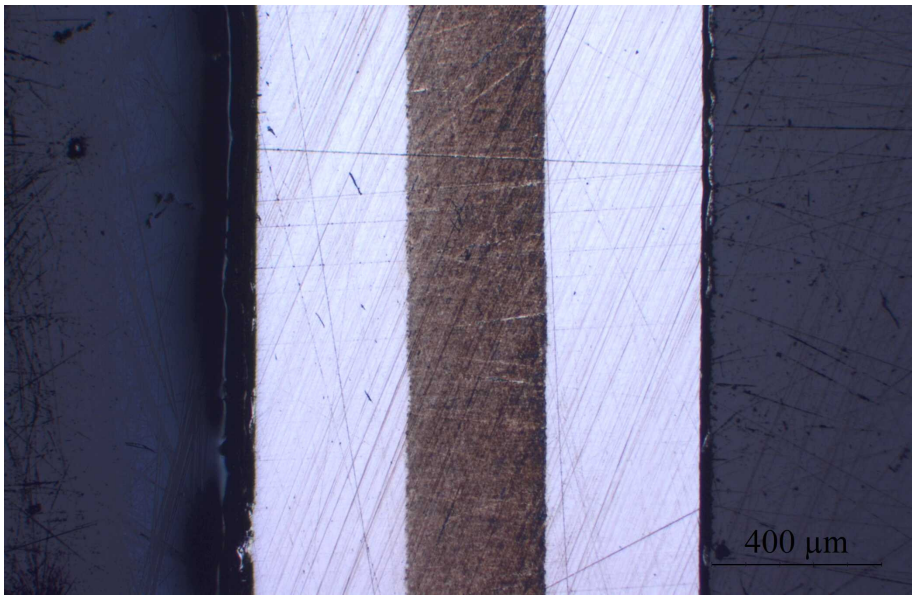

Figure 64: SBA-200 at 50X .The aluminum was reduced to 0,33 mm, while the steel was reduced to an average of 0,36 mm, giving a percent reduction of 64 % and 64 %, respectively.

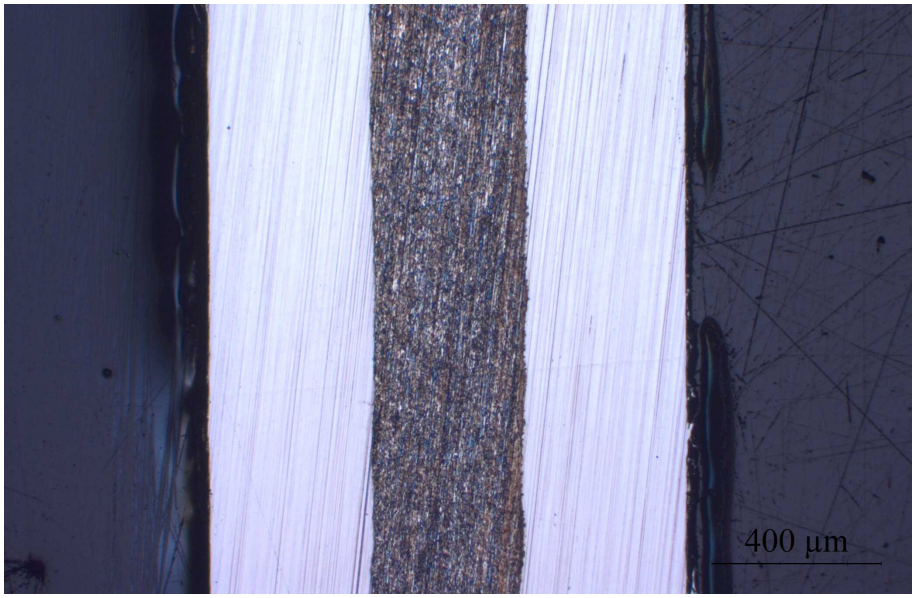

Figure 65: SAB-200 at 50X. The aluminum was reduced to 0,37 mm, while the steel was reduced to an average of 0,38 mm, giving a percent reduction of 59 % and 62 %, respectively.

8.3 Residual aluminum on the fracture surfaces

Measurements were conducted to estimate the percent of the steel fracture surface covered by aluminum. Five lines were drawn on each EDS scan, and the amount of aluminum relative to steel was measured following the lines.

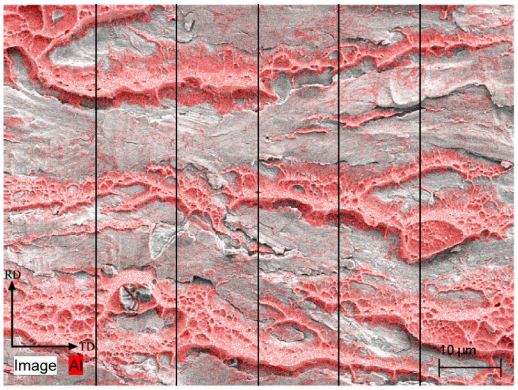

Figure 66: EDS scan of the SBA-150 sample at 1000X. The average percentage of aluminum on the steel substrate was found to be 38 %.

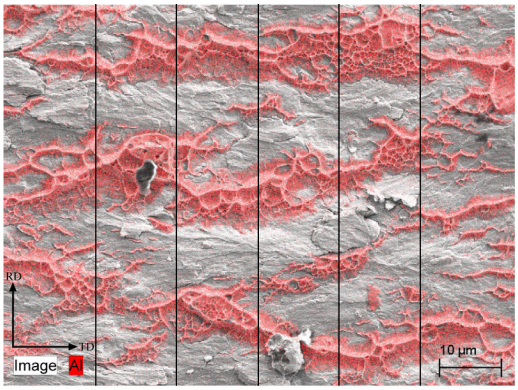

Figure 67: EDS scan of the SBA-200 sample at 1000X. The average percentage of aluminum on the steel substrate was found to be 42 %.

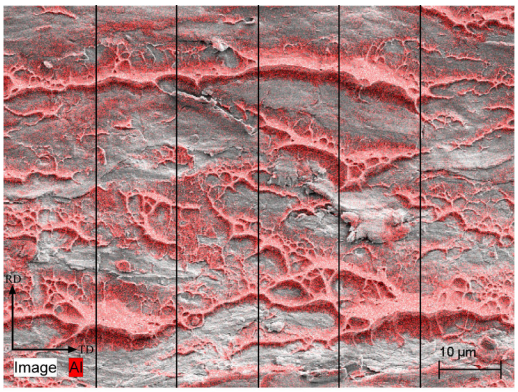

Figure 68: EDS scan of the SAB-200 sample at 1000X. The average percentage of aluminum on the steel substrate was found to be 39 %.

8.4 Oven calibration

A small portable oven next to the rolling mill, of the type Scan-Form SF-2, was used to heat the samples prior to roll bonding. Calibrations of this oven are provided as they may prove valuable for future work.

With the built-in thermometer on the oven measuring 220 ^{o}C, the actual temperature, measured by two external k-sensors, was 235 - 245 ^{o}C.

Samples were heated both with and without a thick steel slab on the oven floor, meant to increase heat transfer rate. The heating rate, both with and without the steel slab, can be seen in Figure 69.

Various parameters for reaching specific temperatures:
oven thermometer measuring 185 ^{o}C, 10 minutes without the steel slab = 150 ^{o}C
oven thermometer measuring 220 ^{o}C, 9 minutes with the steel slab = 200 ^{o}C
oven thermometer measuring 300 ^{o}C, 14 minutes with the steel slab = 300 ^{o}C

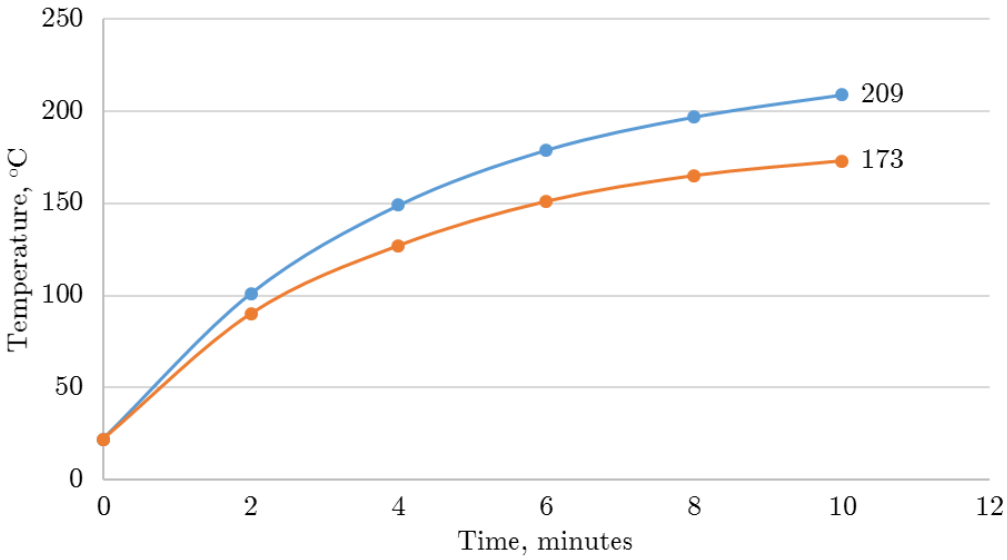

Figure 69: Heating of the dummy sample, with and without placing it on a steel slab on the oven floor. The oven was set as 220 ^{o}C (235 - 245 ^{o}C actual temperature). When using the steel slab, the sample reached a temperature 36 ^{o}C higher than without it, after 10 minutes of heating.

8.5 Blueprint of the peel test rig

The following is the original blueprint of the peel test rig. It was produced, according to this blueprint, at the mechanical workshop at NTNU.